Department für Ökologie und Ökosystemmanagement

Fachbereich für Limnologie

A method for mapping submerged macrophytes in lakes using hyperspectral remote sensing

Nicole Pinnel

Summary

This study describes the development of a hyperspectral remote sensing method to map and monitor submerged aquatic vegetation, meeting examination and assessment criteria for adoption in the European Water Framework Directive.

Identifying macrophyte species using objective remote sensing methods can be a consistent and reliable means to map large areas of lakeshores for monitoring purposes, but only if the spectral properties of *in situ* species are distinct. To determine this, the spectral signatures of eight common aquatic macrophyte species (*Chara aspera*, *C. contraria*, *C. intermedia*, *C. tomentosa*, *Nitellopsis obtusa*, *Najas marina*, *Potamogeton pectinatus*, *P. perfoliatus*) were investigated to establish whether or not they contain sufficient information for species differentiation. To assess the range of spectral variability that may be found in each species, reflectance spectra of homogeneous macrophyte patches were measured with a submersible spectroradiometer in 2003 and 2004 at Lake Constance and Lake Starnberg, Germany.

Seasonal variation was found in magnitude and shape of the reflectance spectrum in all species, but highest variation occurred in tall growing species (*P. pectinatus*), showing 3 % increased reflectance, a shift of reflectance maximum to longer wavelengths and a distinct second reflectance shoulder centred around 650 nm in senescent species. This effect can mainly be attributed to chlorophyll breakdown. Small growing species (*C. contraria*) showed less variation in reflectance values ($< 2\,\%$ absolute) and wavelengths.

Local variations in macrophyte reflectances were observed, mainly due to species richness differences between lakes and differences in macrophyte patch densities. Highest difference was found in green reflectance peak of *P. pectinatus*, which reflected on average twice as much light at Lake Constance (8 %) than at Lake Starnberg (4 %). In contrary *C. aspera* reflected only half of the light at Lake Constance (6 %) as compared to Lake Starnberg (12 %). Lake-specific spectral differences suggest that unique statistical analyses must be performed for each new data set. Daily variation could not be observed, and was considered to be less ($< 2\,\%$) than within-species variation for both, tall and short growing species.

The second goal of this study was to create an automated macrophyte classification method to use on hyperspectral airborne data. In a first step, locations and widths of wavebands were visually identified that can be applied in routine analyses. It was shown that derivative analysis improved separability of seven macrophyte species in visible wavelengths from 90 % to 98 %. In these wavelength ranges *in situ* spectra were influenced by canopy structure and absorption of chlorophylls and accessory photosynthetic pigment.

A genetic algorithm (GA) technique was then used to identify important wavebands for classification. The advantage of this multivariate method is the automated selection of wavelength combinations while optimising separability. For Lake Constance and Lake Starnberg, four wavelengths were chosen between $445-665$ nm. These selected wavelengths for Lake Constance were 510 nm in reflectance, 530 nm and 625 nm in the 1st order, and 535 nm in the 2nd order derivative of reflectance. For Lake Starnberg, somewhat different wavelength locations were selected: 445, 520, 625 and 665 nm in the 1st derivative. The GA-selected wavelengths were consistent with the visually-selected wavelengths identified using derivative analyses and coincide with major reflection and absorption peaks of the macrophyte photosynthetic pigments. Most selected wavelengths were below 625 nm, where the water column attenuates less of the reflected signal, suggesting that accurate spectra discrimination might be possible up to 2 - 4 m water depth. Statistical tests such as unsupervised classifications (Principal Component Analysis) and distance measure (Jeffries-Matusita) indices were used to confirm species separation. Cross-validation by linear discriminant analysis, a supervised classification approach, confirmed that *in situ* spectra could be used to discriminate between seven species with > 98 % accuracy using as few as four optimally-positioned bands. At Lake Constance classification accuracy ranged from 68.2 % (*Chara tomentosa*) to 98.2 % (*Potamogeton perfoliatus*), whereas species at Lake Starnberg could be correctly classified between 90.1 % (*Chara contraria*) and 99.6 % (*Potamogeton pectinatus*). The results of this study demonstrate that it is possible to accurately detect and delineate submerged macrophytes using a hyperspectral remote sensing technique, and that the potential for species separation using advanced data-analysis techniques exists.

This field-based study was tested on airborne hyperspectral remote sensing data from HyMap acquired during HyEurope flight campaigns in 2003 and 2004. The images were corrected for atmospheric, air-water interface, and water column effects using the Modular Inversion & Processing System (MIP). Atmospheric correction accuracy was less than 0.3 % absolute reflectance. Despite the dominance of the water column optical properties in the surface reflectance signal, the inversion process using MIP resulted in obtaining benthic albedo spectra of up to 0.5 % absolute reflectance difference compared to *in situ* spectra for

transmissions higher than 50%, a result found to be acceptable for differentiating similar substrates, such as macrophyte species.

After pre-processing, the hyperspectral data were classified to bottom cover classes by linear spectral unmixing. The result contains percent cover classes for short-growing macrophytes (e.g. Characeae), tall-growing macrophytes (e.g. *P. pectinatus*), and bottom sediments. A subsequent classification of pixels more than 70% vegetation cover was performed on species level, producing a detailed macrophyte distribution map (in 4×4 m^2 pixel resolution) to 4.5 m water depth.

The physics-based approach promotes automatisation and the removal of subjectivity from the classification process, allowing improved transferability to additional sampling locations and extension of the monitoring season. HyMap sensor was well suited for littoral vegetation mapping. However the maximal spatial pixel resolution provided by the HyMap sensor was 4×4 m^2, which might be limitation in macrophyte species recognition, especially in smaller lakes where patch size and inhomogeneity requires higher spatial resolution.

The quality of aquatic macrophyte species discrimination was dependent on species diversity, species composition and homogeneity within the patch, patch size and density. Classification results of HyMap imagery showed that some species were difficult to be accurately discriminated by remote sensing instruments, primarily due to spectral overlap with other species (e.g. *C. aspera, C. contraria*), or lack of field data (e.g. *C. intermedia, N. obtusa*). Although difficulty in differentiating the morphologically similar *Chara* species was expected, the results support the merit in further investigations of hyperspectral remote sensing of submerged aquatic vegetation.

Given that the reflectance spectra of many macrophyte species are statistically distinct, with high-quality radiometric calibration of hyperspectral imagery, it is also anticipated that more macrophyte species can be accurately identified during classification applications. However, further research is required on high spectral resolution reflectance properties of aquatic macrophytes and expansion of spectral libraries remains a priority.

Successful results of a semi-automated, airborne remote sensing approach for the reconstruction of submerged aquatic vegetation show promising potential for shallow water targets in littoral and coastal environments. The methods presented herein form a basis for future development of a precise automated routine. Consequently, hyperspectral remote sensing could become an economical and accurate monitoring technology for assessing the quality of inland waters, benefiting the management of this precious natural resource, and in monitoring the success of natural ecosystem restoration, rehabilitation, and conservation efforts.

Zusammenfassung

In der vorliegenden Arbeit wurde eine operationelle Methode zur Kartierung von Unterwasserpflanzen mit Hilfe von spektral und räumlich sehr hochauflösenden Fernerkundungsdaten entwickelt. In Zukunft soll es damit möglich sein, die Überwachungs- und Bewertungskriterien der Europäischen Wasserrahmenrichtlinie zu erfüllen.

Die Identifizierung von Unterwasserpflanzen (submersen Makrophyten) auf der Basis von Fernerkundungsdaten kann eine zuverlässige Methode zur großflächigen Kartierung der Litoralzone von Seen sein. Dies ist jedoch nur dann möglich, wenn die vorhandenen Arten in ihren spektralen Signaturen unterscheidbar sind. In der vorliegenden Arbeit wurden die spektralen Eigenschaften von acht häufig auftretenden Makrophytenarten (*Chara aspera, C. contraria, C. intermedia, C. tomentosa, Nitellopsis obtusa, Najas marina, Potamogeton pectinatus, P. perfoliatus*) untersucht. Um ein Maß für die spektrale Variabilität einer Art zu erhalten, wurde in den Jahren 2003 und 2004 im Rahmen von Feldmessungen am Bodensee und am Starnberger See die Reflexion einzelner homogener Makrophytenpolster mit einem Unterwasserspektrometer (RAMSES) bestimmt. Dabei wurden bei allen Arten saisonale Unterschiede in der Amplitude sowie in der Form der Reflexionsspektren festgestellt. Die größten Unterschiede traten bei hochwüchsigen Pflanzen auf. So wurde bei älteren *P. pectinatus* Pflanzen eine durchschnittlich 3 % höhere Reflexion (absolut) im grünen Wellenlängenbereich, eine Verschiebung des Reflexionsmaximum zu längeren Wellenlängen, sowie ein ausgeprägtes zweites Reflexionsmaximum bei 650 nm beobachtet. Diese Veränderungen werden hauptsächlich durch den Alterungsprozess der Pflanzen und den damit verbundenen Abbau der Chlorophyll-Pigmente verursacht. Kleinwüchsige Arten (z.B. *C. contraria*) wiesen geringere Unterschiede in Reflexion (< 2 % absolut) und Form der Spektren auf.

Des Weiteren wurden Unterschiede zwischen den beiden untersuchten Seen festgestellt. Dies ist zu einem gewissen Teil auf die unterschiedliche Artenzusammensetzung, aber auch auf die unterschiedliche Dichte der Makrophytenpolster zurückzuführen. Die größten spektralen Unterschiede waren im grünen Wellenlängenbereich zu erkennen. *P. pectinatus* reflektierte

am Bodensee in diesem Teil des Wellenlängenspektrums im Durchschnitt doppelt so viel Licht (8 %) wie am Starnberger See (4 %). Dagegen war die Reflexion der kleinwüchsigen *Chara aspera* mit 6 % am Bodensee nur halb so stark wie am Starnberger See (12 %). Diese seenspezifischen Unterschiede hatten zur Folge, dass für jeden neuen Datensatz separate statistische Analysen erforderlich waren. Eine vollkommene Übertragbarkeit zwischen den beiden Seen war nicht gegeben. Tagesabhängige Veränderungen im Reflexionsverhalten sowohl bei hochwüchsigen (*P. pectinatus*) als auch bei niedrigwüchsigen Pflanzen (*C. contraria*) können dagegen im Vergleich zur natürlichen Variabilität innerhalb einer Art als gering ($< 2\%$) eingestuft werden .

Auf Basis der statistisch nachgewiesenen, prinzipiellen Unterscheidbarkeit der Arten bei *in situ* Messungen wurde eine automatische Klassifikationsmethode entwickelt, die auf hyperspektrale (spektral sehr hochauflösende), von einem Flugzeug aus gemessene Fernerkundungsdaten angewandt werden kann. Es konnte nachgewiesen werden, dass die zusätzliche Verwendung der ersten und zweiten Ableitung der Reflexionsspektren die Trennbarkeit in den sichtbaren Wellenlängen wesentlich verbessern konnte. So wurde z.B. die erreichte Genauigkeit der Artentrennung von 90 % auf 98 % gesteigert. Im sichtbaren Wellenlängenbereich werden die *in situ* Spektren vor allem durch die Oberflächenstruktur der Pflanzenpolster und durch die Absorption von photosynthetisch aktiver Pigmente geprägt.

Um die besten Wellenlängen für eine optimale Klassifizierung zu ermitteln, wurde ein genetischer Algorithmus (GA) verwendet. Mit dieser multivariaten Technik können Wellenlängenkombinationen, die zur optimalen Trennbarkeit der Arten beitragen, automatisch selektiert werden. Für den Bodensee und Starnberger See wurden im Bereich zwischen $445-665\,\mathrm{nm}$ verschiedene Kombinationen aus je vier Wellenlängen selektiert. Im Einzelnen lagen die Wellenlängen für den Bodensee bei $510\,\mathrm{nm}$ (Reflexion), $530\,\mathrm{nm}$ und $625\,\mathrm{nm}$ (1. Ableitung der Reflexion), und $535\,\mathrm{nm}$ (2. Ableitung der Reflexion). Für den Starnberger See lautete die Wellenlängenkombination 445, 520, 625 und $665\,\mathrm{nm}$ der 1. Ableitung der Reflexion. Die mit dem genetischen Algorithmus (GA) ausgewählten Wellenlängen waren dabei mit den visuell ausgewählten Wellenlängen der Ableitungen weitgehend konsistent und stimmten mit bedeutenden Reflexions- und Absorptionsbanden der photosynthetischen Pigmente der Makrophyten überein. Die meisten der selektierten Wellenlängen lagen damit unterhalb von $625\,\mathrm{nm}$, also in einem Bereich, in dem die darüberliegende Wassersäule nur minimal absorbiert. Demzufolge kann davon ausgegangen werden werden, dass eine exakte Artentrennung auch bis in Wassertiefen von $2-4\,\mathrm{m}$ möglich ist.

Statistische Tests mit einer Hauptkomponenten Analyse (Principal Component Analysis) und mit Distanz Indizes (Jeffries-Matusita) wurden dazu verwendet, die Trennbarkeit der

Arten zu überprüfen. Mit Hilfe einer Linearen Diskriminanz Analyse (LDA), wurden die Makrophyten zu Arten klassifiziert. Es konnte nachgewiesen werden, dass bis zu 98 % der Arten mit nur vier optimal ausgewählten Wellenlängen richtig eingeordnet werden können. Dabei lag die Klassifikationsgenauigkeit der einzelnen Arten am Bodensee zwischen 68.2 % (*Chara tomentosa*) und 98.2 % (*Potamogeton perfoliatus*). Am Starnberger See konnten alle Arten zwischen 90.1 % (*Chara contraria*) und 99.6 % (*Potamogeton pectinatus*) genau klassifiziert werden. Die Ergebnisse dieser Studie demonstrieren, dass es möglich ist, submerse Makrophyten mit hyperspektralen Fernerkundungsmethoden zu erfassen, und dass mit geeigneten Datenanalyseverfahren verschiedene Makrophytenarten potenziell unterscheidbar sind.

Die Ergebnisse der beschriebenen Klassifikationsmethoden wurden auf hyperspektrale, aus einem Flugzeug aufgezeichnete Messungen (HyMap) übertragen. Diese Messungen wurden während der HyEurope Flugkampagne in den Jahren 2003 und 2004 aufgenommen. Mit dem physikalisch basierten Modular Inversion & Processing System (MIP) wurden die Einflüsse der Atmosphäre und der Wassersäule korrigiert. Die erreichbare Genauigkeit dieser Atmosphärenkorrektur liegt bei weniger als 0.3 % der absoluten Reflexion. Trotz der beträchtlichen Einflüsse der Wasserinhaltstoffe sind die Abweichungen des Inversionsverfahrens für Albedospektren vom Seegrund für Transmissionen > 50 % maximal 0.5 % im Vergleich zu *in situ* Messungen. Die Genauigkeit hängt dabei von der optischen Dicke des Wassers, vom Substrat und von der betrachteten Wellenlänge ab.

Nach Atmosphären- und Wassersäulenkorrektur wurden die Hyperspektraldaten durch linear spectral unmixing nach Bodenbedeckunsgraden klassifiziert. Als Ergebnis ergaben sich Bedeckungsgrade (in %) für niedrigwüchsige Pflanzen (z.B. Characeae), für hochwüchsige Pflanzen (z.B. *P. pectinatus*, *P. perfoliatus*) und für unbedecktes Sediment. Anschließend wurden diejenigen Pixel, deren Bedeckungsgrad größer als 70 % war, weiter nach sieben Arten klassifiziert und eine detaillierte Verbreitungskarte (in 4×4 m^2 Pixelauflösung) bis zu einer Wassertiefe von 4.5 m erstellt.

Dieser auf rein physikalische Grundlagen gestützte Ansatz bietet die Möglichkeit zur Automatisierung und forciert die Objektivität der Klassifikationsprozesse. Die prozessierten Daten können auf andere Gebiete und auf verschiedene Jahreszeiten übertragen werden. Der HyMap Sensor erwies sich als gut geeignet, um litorale aquatische Vegetation zu kartieren. Jedoch stellte sich die maximal erreichbare räumliche Auflösung des Sensors von 4×4 m^2 bei der Artenunterscheidung als Einschränkung heraus. Dies könnte insbesondere bei kleineren Seen ein Problem darstellen, in denen kleinere Polstergrößen und die Inhomogenität innerhalb der Vegetationsstrukturen räumliche Auflösungen des Sensors erfordern.

Die Qualität der Artentrennung aquatischer Makrophyten durch digitale Bilddatenanalyse hängt stark von der Artenvielfalt, von der Zusammensetzung der Arten und der Bewuchsdichte innerhalb eines Polsters, sowie von der allgemeinen Größe eines Polsters ab. Das Klassifikationsergebnis der HyMap Daten hat gezeigt, dass einige Arten mit Fernerkundungsmethoden nur schlecht getrennt werden können, hauptsächlich bedingt durch spektrale Überlappung (z.B. *Chara contraria* und *C. aspera*) oder aufgrund fehlender Messdaten (z.B. *Chara intermedia*, *Nitellopsis obtusa*). Obwohl zu erwarten war, dass die morphologisch ähnlichen *Chara* Spezies nur schwer nach Arten zu trennen sind, war es doch möglich drei von vier Chara Arten spektral zu unterscheiden. Diese Ergebnisse sprechen für weitere Untersuchungen zur Kartierung von litoraler Unterwasservegetation mit hyperspektralen Fernerkundungsdaten.

Angesichts der Tatsache, dass sich die Reflexionsspektren vieler Makrophytenarten als statistisch trennbar erwiesen, ist abzusehen, dass in zukünftigen Studien mit weiter verbesserter radiometrischer Kalibrierung der hyperspektralen Bildauswertung noch weitere Makrophytenarten präzise identifiziert werden können. Jedoch werden dazu weitere Untersuchungen nötig sein, um die sehr hochauflösenden spektralen Reflexionseigenschaften der aquatischen Makrophyten bis ins Detail zu erfassen. Der ständigen Erweiterung sogenannter 'spektraler Datenbanken' sollte Priorität eingeräumt werden.

Die erfolgreichen Ergebnisse eines halbautomatischen Ansatzes für die flächenhafte Bestandsaufnahme von submersen Makrophyten mit Fernerkundungsmethoden zeigen vielversprechende Möglichkeiten für die Kartierung von Flachwasserzonen in Binnen- und Küstengewässern. Die in dieser Arbeit vorgestellten Methoden legen den Grundstein für die zukünftige Entwicklung von präzisen, automatisierbaren Auswertungen. Folglich könnte sich die hyperspektrale Fernerkundung zu einer kostengünstigen und exakten Technologie ausbauen lassen, mit der die Wasserqualität von Inlandsgewässern beurteilt werden kann. Unsere Gewässerökosysteme werden durch die regelmäßige Kontrolle von Instandsetzungs-, Wiederherstellungs- und Schutzmaßnahmen davon profitieren.

Table of Contents

List of Tables

List of Figures

List of Abbreviations

AOP   Apperent Optical Properties

ARES   Airborne Reflective and Emissive Spectrometer

ATM   Airborne Thematic Mapper

AVIRIS Airborne Visible/Infrared Imaging Spectrometer

BH   Bhattacharyya

BP   Before Present

BRDF   Bidirectional Reflectance Distribution Function

BRF   Bidirectional Reflectance Factor

CASI   Compact Airborne Spectrographic Imager

Cdom   Coloured Dissolved Organic Matter

CPC   Cyanophycocyanin

CPE   Cyanophycoerythrin

DEM   Digital Elevation Model

DFG   Deutsche Forschungsgesellschaft

DGPS   Differential Global Positioning System

DLR   Deutsches Zentrum fr Luft- und Raumfahrt e.V.

EC   European Community

ENVI   Environment for Visualizing Images

EOMAP Earth Observation and Mapping tec.

ETM+   Enhanced Thematic Mapper Plus

EU   European Union

FEM   Finite Element Method

FOV   Field Of View

FWHM   Full Width of Half Maximum

GA   Genetic Algorithm

GALGO	Genetic Algorithm Decision Support Tool
GIS	Geographic Information System
GPS	Global Positioning System
HRV	Haute Résolution Visible
HyMAP	Hyperspectral Mapper
Hyperion	Hyperspectral Satellite sensor on board of EO−1
IGKB	Internationale Gewässerschutzkomission fr den Bodensee
IKONOS	Commercial earth observation satellite (*greek:'Image'*)
IOCCG	International Ocean Colour Coordinating Group
IOP	Inherent Optical Properties
IR	Infrared
ISF	Institut fr Seenforschung, Institute of Lake Research
JM	Jeffries Matusita
LAWA	Länderarbeitsgemeinschaft Wasser
LDA	Linear Discriminant Analysis
MERIS	Medium Resolution Imaging Spectrometer
MI	Macrophyte Index
MIP	Modular Inversion & Processing System
MIR	Mid-Infrared
MLHD	Maximum Likelihood Discriminant Function
MODIS	Moderate Resolution Imaging Spectroradiometer
MSS	Multi Spectral Scanner
NA	Not Available
NIR	Near-Infrared
PAR	Photosynthetically Active Radiation
PC	Principal Component
PCA	Principal Component Analysis
PDA	Penalised Discriminant Analysis
PVC	Polyvinyl Chloride
RAMSES	Radiation Measurement Sensor with Enhanced Spectral Resolution
RAS	Russian Academy of Sciences
ROSIS	Reflective Optics System Imaging Spectrometer
RTE	Radiative Transfer of Energy

SAM	Spectral Angle Mapping
SCUBA	Self Contained Underwater Breathing Apparatus
SFB	Sonderforschungsbereich
SNR	Signal-To-Noise Ratio
SPOT	Système Probatoire d'Observation de La Terre
TM	Thematic Mapper
TSM	Total Suspended Matter
TUM	Technische Universität München
UV	Ultraviolet Light
VIS	Visible Light
WASI	Water Colour Simulator
WFD	Water Framework Directive

Chapter 1

Introduction

1.1 Mapping aquatic macrophytes in lakes

Water is the most important substance for life on earth. Many interrelated physiochemical factors, such as depth, light, temperature, density, salinity, et cetera, play a role in the function of water-based ecosystems, which in turn are more or less dependent on each other for existence. Ecosystem water quality, defined here as the composition and concentration of dissolved and suspended constituents, is important not only in determining the biota in the water-based ecosystem itself (Logan and Furse, 2002), but also for influencing its surrounding environment, (e.g. Fariña et al. (2003); Mathewson et al. (2003)) and human life. Currently, inland surface waters are used for drinking water, irrigation, waste disposal, industrial processes and cooling, transportation, and hydroelectric power generation, as well as for various recreational pursuits (Lindell et al., 1999). Surface freshwater is thus an increasingly valuable natural resource with major impacts and benefits for surrounding populations and environments.

In Europe there are more than $500,000$ natural lakes larger than 0.01 km^2, covering a total surface area of more than $10,000$ km^2 (LAWA, 1985). The majority are of glacial origin, reflecting their concentration in alpine and northern regions. Simply because of their considerable number, these aquatic ecosystems make a significant contribution to the total biodiversity on the European landscape. In the past century, inland water quality has deteriorated significantly as a result of nutrients introduced by the discharge of wastewater and from agriculture, reducing this biodiversity.

Lake eutrophication was an important factor in the decision to introduce water protection legislation throughout Europe. The terms 'eutrophication' or 'trophic state' describe the concentration of (inorganic) nutrients leading to increased primary production, often a result of increased pollution (Melzer, 1988). Changes in nutrient concentrations can alter physical

characteristics and composition of benthic ecosystems, resulting in species diversity changes (Dennison et al., 1993). The increasing demand for cleaner rivers and lakes, groundwater and coastal beaches has been evident for considerable time, and was one of the main reasons why the European Commission has made water protection one of its priorities. A European-wide Water Framework Directive (WFD) (EG-Europäische Gemeinschaft, 2000) was adopted in 2000 as the operational tool, setting the objectives for water protection in the future.

The WFD is the most significant legislative instrument in the field of water management that has ever been established on an international basis. The EU WFD requires the ecological assessment and monitoring of all water bodies in Europe, with the principal goal to achieve or maintain a 'good ecological state' of all surface and ground water bodies by 2015. This requires an examination and assessment of all still water bodies in area from 0.50 km^2 upwards. As an unique innovation, ecological assessment is achieved by measuring various biological quality elements instead of relying primarily on chemical measurements (Melzer, 1988). One of the quality components used to evaluate ecological status are aquatic macrophytes (Melzer, 1999). Assessment is achieved by comparing a lake's current macrophyte species composition and abundance with those of type-specific reference conditions. A reference condition is the status that would exist if the water body was unaffected from any kind of pollution or nutrient influx (Schneider, 2000). The larger the differences in macrophyte species composition and abundance between current state and reference conditions, the worse the status of the respective site.

Germany has 13,076 standing water bodies with a surface area exceeding 0.01 km^2. The larger lakes (877 lakes $>$ 0.50 km^2 (Ostendorp, 2004)) are included in quality assessment and management programmes in accordance with the EU WFD. A rough estimation of their total shoreline length, the habitat for aquatic macrophytes, is in the order magnitude of 10,000 to 100,000 km, covering some 1000 km^2 of lakeshore (Ostendorp, 2004). These very considerable stretches of shore are currently not registered, mapped, or evaluated anywhere (Schmieder, 2004). As periodic assessment of the abundance and health of the submerged macrophyte communities is required to improve the management of these sensitive littoral ecosystems (Dennison et al., 1993), highly reliable data on the quality of surface waters is urgently needed. Consequently, there is a pressing need to develop and establish an adequate monitoring scheme for European lakes.

1.2 Problem Statement

1.2.1 Limnological background

Lakes, including their catchment areas, are complex ecosystems, as shown in a schematic view (Figure 1.1, adapted from Wetzel (2001)). Differences in water depth, flow, chemistry, available light, and temperature, key descriptors of aquatic ecosystems, produce physically distinct zones that can vary by day and season. Three major habitats, or zones, are identified: the littoral, the pelagial, and the profundal. The littoral zone extends from the shore just above the influence of waves to the depth where light penetration is 1% of the incident surface light. Littoral zones have especially high biodiversity of vertebrates, invertebrates, submersed and emergent macrophytes, epiphytes, and phytoplankton, with interactions often occurring between species.

The pelagial or limnetic zone is found farther from shore but near the water surface. The transition between the littoral and profundal zones is sometimes called the sublittoral subzone, which is the deepest area of plant growth. The profundal zone, if present, is the deepest zone, found below the light penetration level. The profundal and benthic (the bottom surface of lakes) zones contains mostly heterotrophic organisms, including organisms that feed off decaying organic matter called detritus. The benthic zone usually has higher biodiversity than the profundal zone.

The part of the lake that receives $< 1\%$ incident light is also called the aphotic zone, and extends from the lake bottom to the photic zone. Above the aphotic zone is the photic or trophogenic zone, where there is sufficient light for photosynthesis (primary productivity). Boundaries between these zones vary daily and seasonally with changing solar intensity and water transparency. There is a decrease in water transparency with algal blooms, sediment inflows from rivers or shore erosion, and surface waves.

Bioindication of lake trophic status Lakes are often differentiated by their photosynthetic production of organic matter, or trophic state. Five general states are recognised: ultra-oligotrophic, oligotrophic, mesotrophic, eutrophic, and hypereutrophic. Oligotrophic lakes are generally deeper lakes with clear blue water and have sparse nutrients, i.e. < 10 $\mu g^* L^{-1}$ dissolved phosphorus, with photosynthesis limited to a few diatom taxa. Mesotrophic lakes have dissolved phosphorus values between 10 and 30 $\mu g^* L^{-1}$. Eutrophic lakes tend to be shallow and have a rich nutrient supply with phosphorous > 30 $\mu g^* L^{-1}$. Hypereutrophic
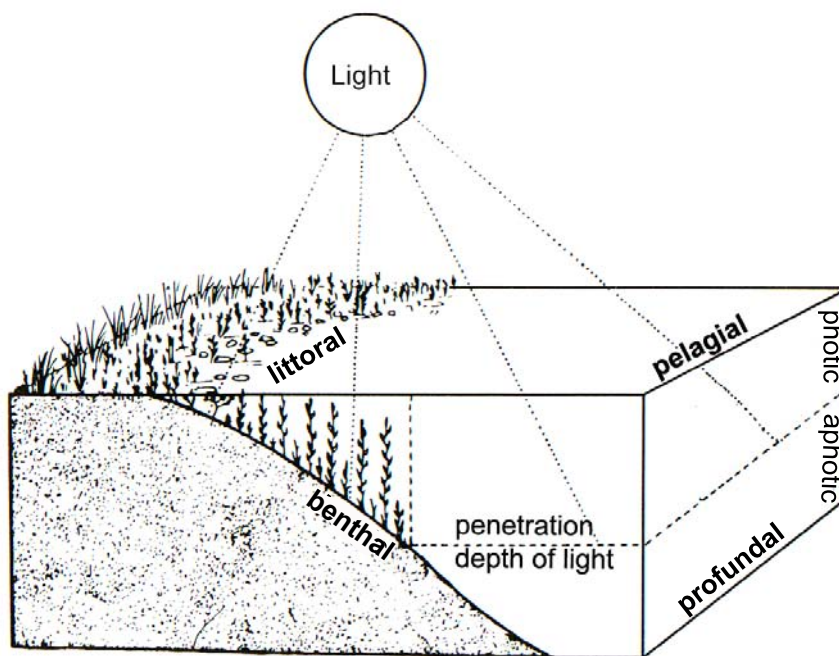
Figure 1.1: Scheme of the littoral ecosystem.(Adapted from Wetzel (2001))

lakes can have dissolved phosphorus values well in excess of 100 $\mu g^* L^{-1}$. Mesotrophic and eu-trophic lakes can have abundant photosynthetic communities, with many diatom and macro-phyte taxa. At very high nutrient levels, such as those in hypereutrophic lakes, light pene-tration is so reduced that few plants can grow,(e.g. Vestergaard and Sand-Jensen (2000)). Aquatic macrophytes are large (visible to the naked eye), multi-cellular aquatic plants with representatives from the spermatophyta (vascular flowering plants), bryophyta (mosses), and charophyta (larger macroalgae).

Submerged macrophytes are of particular importance in aquatic ecosystems, as they link the sediment with the overlying water (Schneider and Melzer, 2004). They are beneficial to lakes because they provide habitat for fish and substrate for aquatic invertebrates, offering protection against both currents and predators. Macrophytes also produce oxygen via photo-synthesis, which assists with overall lake functioning, and are an important food resource for some fish and other wildlife. Lakes with water plants thus have high ecological value. Because of specific growth requirements, macrophyte species tend to reflect the physical and chemical (nutrient) conditions of the lake in which they occur. Thus the composition of macrophyte species in a water body makes it possible to draw conclusions about local chemical and phys-ical conditions. Aquatic macrophytes have several advantages which make them attractive as limnological indicators, as opposed to other algae (diatoms) or macroinvertebrates.

They are especially sensitive to changes (increases) in nutrient concentrations (notably phosphorus and ammonium) and to organic pollutants and can be used as long-term indicators, as they change slowly and progressively (Melzer, 1999). Secondly, submerged macrophytes are rooted, therefore they reflect the nutrient status of their immediate habitat by their presence/absence and abundance. Thus they can indicate patterns of nutrient concentration, e.g. caused by natural or artificial inflows (Melzer, 1999). An additional advantage which makes them attractive to remote sensing applications is that they can generally be seen and identified to the species level at the sampling site (Schneider, 2004).

Three growth forms of macrophytes are generally recognised: floating, submersed, and emergent. Some macrophytes grow up to the water surface with many of their leaves floating just below the water surface, and are denoted in this thesis as 'tall growing species'. Other species remain close to the bottom, forming dense mats and are dependent upon the light that reaches the bottom after passing through the depth of water, and in this thesis grouped as 'short growing species'. Techniques for mapping macrophytes in littoral zones to provide a rapid and accurate estimation of water quality have recently been developed (Melzer, 1999; Schneider and Melzer, 2003; Stelzer, 2003; Meilinger et al., 2005; Stelzer et al., 2005). With these methods, the composition and relative and absolute abundance of macrophyte species are recorded. Based on these data, an assessment of water quality can then be made. In larger lakes or rivers, these methods face the problem of simultaneous mapping large areas. A compromise can be reached by SCUBA diving transects, which may or may not be entirely representative for the whole lake. Wide-scale SCUBA diving, particularly in the larger lakes, can be very complex, cost-ineffective, and time consuming.

Aerial photographic techniques have been commonly used as an alternative for large-scale macrophyte mapping (Malthus et al., 1990). Despite offering fine resolution (0.1 - 1.0 m) and relative ease of measurement and data handling, photographic techniques suffer from a number of drawbacks. Photo-interpretation is largely a subjective process and can be expensive over the long term due to time consuming analysis (Jensen et al., 1986). Although multi-band photography, such as the use of false colour infrared, has been shown to be useful for mapping of emergent plants, it is less useful in discriminating between species. Image analysis can be applied for more accurate vegetation mapping from photography but the results may not be transportable over space and time (Malthus and George, 1997).

The application of digital remote sensing has been shown to be a useful tool in supporting the mapping of submerged macrophytes in spatial and temporal scales (Heege and Fischer, 2004). It provides important additional information about the spatial distribution, density, and species composition over large spatial scales, allowing transfer of the transect results

to the whole lake and offers a supplementary and time-saving means of achieving a better spatial picture.

1.2.2   Principles of optical remote sensing

Remote sensing can complement traditional macrophyte mapping and monitoring methods as it has the advantages of allowing a quasi - instantaneous view of vast regions and repetitive investigation of isolated locations.

The use of water colour remote sensing for determination of an optical water quality variable was initially developed for the oceans. The optical properties of ocean waters are in general only affected by phytoplankton and its breakdown products. These optically relatively simple waters are known as Case1 waters. All other types of waters, i.e. those whose optical properties are influenced by dissolved organic matter from terrestrial origin, dead particulate matter, and particulate inorganic matter in addition to phytoplankton were determined to be Case2 waters. If the bottom reflectance influences the water leaving radiance signal, a water is also considered to be Case2 (Dekker et al., 2001)

Remote sensing techniques have been successfully applied for operational mapping of the biophysical properties of Case1 waters (Sathyendranath, 2000). However, Case2 waters continue to represent a challenge to remote sensing techniques. There are also various limnological parameters that can potentially be determined by remote sensing techniques, such as lake water constituents (e.g. chlorophyll a, gelbstoff, particulate matter), transparency (Secchi depth), biological primary production, bathymetry, and surface temperature (Keller, 2001). If the water column is sufficiently transparent and the substrate is within the depth where a sufficient amount of light reaches the bottom and is reflected back out of the water body, maps may be made of macrophytes, seagrasses, macro-algae, sand and sandbanks, coral reefs, and other bottom features (Dekker et al., 2001).

Imaging spectroscopy   Remote sensing methods are often differentiated or classified by their energy source. Active systems provide their own electromagnetic source (e.g. laser fluorescence sensor, radar), and have the ability to obtain measurements regardless of the time of day or season. They can also be used for examining wavelengths that are not sufficiently provided by the sun. Passive systems use the solar radiation that is reflected or absorbed and then re-emitted from the substrate(s) of interest. However, both active and passive systems create 'images' by measuring the strength of returned signal over a spectrum of wavelengths. *Imaging spectrometry* is the simultaneous acquisition of images in many narrow, continuous
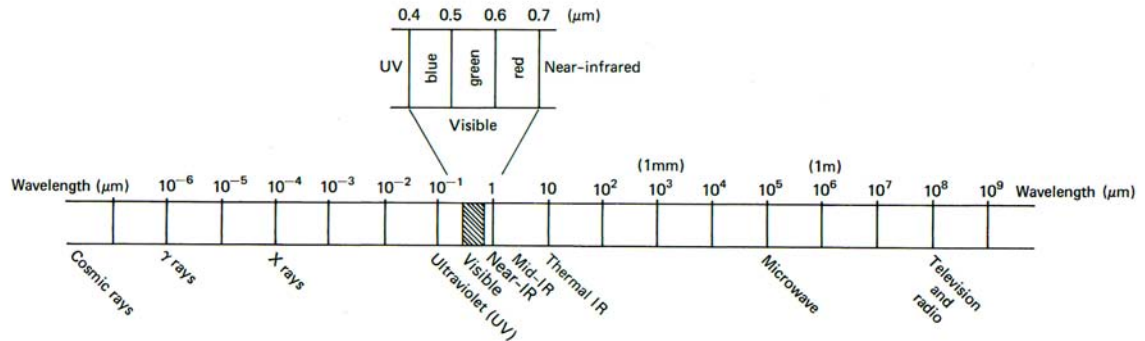
Figure 1.2: The electromagnetic spectrum, which encompasses the visible region of light, extends from gamma rays with wave lengths of one hundredth of a nanometer to radio waves with wave lengths of one meter or greater. (Adapted from Lillesand and Kiefer (2000))

spectral bands. These optical instruments have been developed as a new generation of airborne remote sensing systems specifically designed to acquire this hyperspectral information. The difference between hyperspectral imagery and conventional multispectral imagery, such as that of Landsat Thematic Mapper (TM), is the high spectral resolution of individual channels. It is less than 10 nm wide over a continuous spectrum throughout the visible, near-IR, mid-IR, and thermal IR portions of the electromagnetic spectrum. As the channel widths are relatively narrow, small spectral anomalies can be detected that might otherwise be masked using the broader bands of multispectral scanner systems.

Light and other forms of electromagnetic radiation are commonly described in terms of their wavelength. For example, visible light has wavelengths between 400 and 700 nm, as shown in Figure 1.2. A reflectance spectrum shows the reflectance of a material measured across a range of wavelengths. Most natural earth surface materials have diagnostic absorption features in the $0.4 - 2.5\,\mu m$ range of the reflected spectrum. The sensor measures reflected surface radiation, which then needs to be calibrated and corrected for atmospheric effects to derive reflectance. Reflectance is subsequently used for spectral signature analysis and comparison to spectral libraries of known substrates (e.g. an individual macrophyte species). An estimate of substrate is then calculated from the strength of the returned signal (Figure 1.3).

Most remote sensing research on limnological systems is based on airborne systems because of their flexible uses, large number of bands (i.e. hyperspectral), as well as high spatial and spectral resolution compared to spaceborne sensors. The latest generation of airborne imaging spectrometers offer new possibilities for the investigation of shallow water substrates.
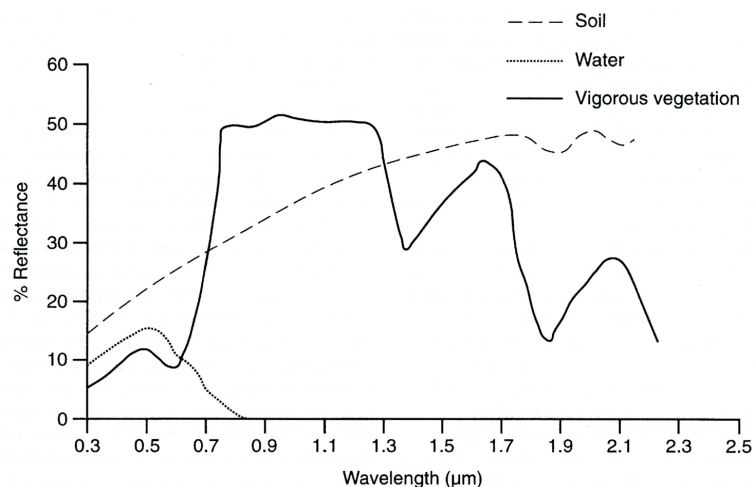
Figure 1.3: Generalised reflectance spectra for vegetation, soil, and water.(Adapted from Mather (1999))

The application of physics-based methods (e.g. MIP[1]) has made the determination of substrate types possible (Heege, 2000; Bogner, 2003). Examples of some important sensors are AVIRIS[2], CASI[3], ROSIS[4], HyMap[5], as well as new ARES[6] sensor (expected to be operational by 2007. Regardless of which sensor is used for macrophyte mapping or limnological research in general, there is an inherent concern with the attenuation of returned signal through the water column.

The natural colour of water is a complex optical feature created by the processes of scattering and absorption of incoming solar radiation, as well as radiation emitted by the water column and reflected by the substrate (Chapter 3.1, Figure 3.1). In shallow clear water, a significant portion of the light from the sun reaches the bottom and is reflected from it. Substrate reflectance (from macrophytes, macro-algae, sediment etc.) is a function of absorption and scattering (Dekker et al., 2001). In order to determine the substrate distribution in a lake, three main problems must be solved. First, signal correction for atmosphere effects must be performed. The atmospheric path between object and sensor modifies the characteristics of the returned radiation signal received at the sensor. Correction can be performed with a physics-based approach, analysing numerous spectral bands within

---

[1]   Modular Inversion & Processing System, EOMAP, c/o Anwendungszentrum, Gewerbegebiet Oberpfaffenhofen, 82205 Gilching, Germany
[2]   Airborne Visible/Infrared Imaging Spectrometer, http://aviris.jpl.nasa.gov/
[3]   Compact Airborne Spectrographic Imager, http://www.itres.com
[4]   Reflective Optics System Imaging Spectrometer, http.//www.dlr.de
[5]   Hyperspectral Mapper, http://www.hyvista.com
[6]   Airborne Reflective/Emissive Spectrometer, http://www.dlr.de

to model atmospheric conditions (Miksa et al., 2004). Second, signal correction for the air-water surface interface effect must also be applied. The air-water interface complicates matters since the amount of energy transmitted into the sea versus that reflected off the surface depends on sea surface state, wind speed and sun angle. Finally, correction for water column effects, that is to say, to separate the water column signal from that of the substrate reflectance at the bottom, must be possible.

Aquatic macrophyte mapping remote sensing approach   Since sustainable management of an aquatic ecosystem requires a thorough understanding of the vegetation composition and distribution (Landres et al., 1999), the remote identification and mapping of submerged vegetation must be possible to the species level, comparable to field mapping. In remote sensing techniques, the basic underlying premise is that the species are indeed spectrally separable, with the variance of the reflectance greater between species than within species. The separation between optically similar signals remains the last major obstacle to be overcome in the remote identification of subsurface features (Holden and LeDrew, 1998). Macrophytes, as close relatives to higher plants, have similar pigment composition and therefore have an optically green signal (Russell and Waters, 2002).

Discrimination of submerged aquatic vegetation, however, is more challenging since the water column attenuates most of the signal coming from the substrate at wavelengths beyond 680 nm due to significant absorption by pure water (Kirk, 1994). As a result of the physical properties of pure water and its optically active constituents, the remotely sensed optical signal is limited to the visible or optical part of the spectrum where light penetrates the water column and can be reflected back to a sensor. Strong light attenuation gradients may further be caused by a combination of water depth and factors that effect water colour and clarity, such as dissolved organic matter, suspended matter, and phytoplankton content (Dekker et al., 2006). It is therefore necessary to study, in detail, the spectral separability of the various bottom components, i.e. vegetation, in shallow lake environments.

Through the application of hyperspectral sensors, it might be possible to improve the ability to distinguish between macrophyte species. Differentiating spectral differences between *in situ* emergent and submerged aquatic vegetation species (Malthus et al., 1997), as well as aquatic vegetation communities in the laboratory, by contrasting the shape of vegetation spectra visually and through statistical analysis (Fyfe, 2004) has already been achieved. Using hyperspectral techniques, the need is to determine if and where the differences between vegetation spectra occur and which biophysical or biochemical characteristic contributes to these differences, when these are indeed the characteristics of interest. In the field and at

the canopy level, spectral discrimination between some seagrass species (Anstee et al., 2000), coral species (Kutser et al., 2003; Joyce and Phinn, 2003; Hochberg and Atkinson, 2000), mangroves species (Held et al., 1997; Schmidt and Skidmore, 2003), and major physiognomic categories (Stephens et al., 2003; Louchard et al., 2003) has been successful.

While remote sensing and substrate mapping of ocean coastal shallow waters is well established (Anstee et al., 2001; Holden and LeDrew, 1998; Mumby et al., 1997; Hochberg and Atkinson, 2003), freshwater environments are facing the problem of higher concentration and variation of water constituents. However, the experience gained there can serve as a basis for remote sensing of submerged aquatic vegetation in lakes, as shown in Alberotanza et al. (1999) and Malthus and Karpouzli (2003).

The main difficulty in discriminating macrophyte species is that they share basically the same physiology, biochemistry, and photosynthetic pigments, such that the wavelength of returning radiation to the remote sensor does not differ significantly between species (Schagerl and Pichler, 2000). However, the relative concentrations of photosynthetic pigments and the composition of accessory pigments do vary among taxa (Hilton et al., 1989), providing a means of spectral separability. The spectral reflectance in visible wavelengths can also vary in macrophytes species over space and time. Thus when applying remote sensing on the canopy scale, several factors influencing the spectral signatures recorded from macrophytes canopies must be taken into account, e.g. density and geometry of the canopy, shadowing by leaves, background reflectance in sparse patches (such as sediment), stage of growth, chromatic adaption to seasonal cycle, health and environmental condition, changing water depth or clarity, and epithetic growth on the surface of aquatic plants. Within-species variability may also increase the chance of spectral overlap with other species and make spectral discrimination using remotely sensed image data difficult or impossible (Fyfe, 2004). These influences can only be studied in the field to draw conclusions about natural variation within a species and their potential to be discriminated by remote sensing. Part of the problem with mapping aquatic plants using digital techniques is that little is known of the detailed, high-spectral resolution reflectance properties of *in situ* macrophytes. Similarly, limited investigations have been performed to determine the information content in spectral bands from airborne sensors, identifying the most appropriate bands for recognition and determination of biophysical parameters of rooted aquatic plant species.

1.3 Aim and Objectives

Remote sensing has recently been noted for its potential contribution to monitoring and management practices of submerged vegetation in inland as well as in coastal environments. However, useful applications of these data are currently limited by an incomplete understanding of the interactions of light with submerged vegetation features and the controlling factors of light reflection and absorption (Joyce and Phinn, 2003). To apply hyperspectral remote sensing techniques to submerged aquatic vegetation, the small scale bio-optical properties of submerged vegetation must be linked to the larger scale of a remotely sensed pixel. The high spectral resolution data in hundreds of bands should provide a wealth of information for macrophyte species discrimination, a conclusion supported by initial results which successfully discriminated statistically three seagrass species (Fyfe, 2003).

Thus the fundamental requirements for remote sensing of lake status become (1) that the bottom-types (i.e. different macrophyte species) each have characteristic spectral features and (2) that those spectral features are detectable by the remote sensor. The field-based component of this study is intended to be a cost-effective test of the first requirement. Instead of using laboratory data that omit the complexities of field conditions (Schmidt and Skidmore, 2003), *in situ* measurements will be used where the influence of real-life factors, e.g. fluctuation of light source energy, change of daily atmospheric state, the effects of canopy formation, the effect of seasonal changes, the effect of background soil and waters, the coarse spatial and spectral resolution of on-board hyperspectral sensors, and the cost of accessibility are taken into account. Thus conclusions can be made whether hyperspectral sensors (e.g. HyMap, ROSIS, CASI, etc.) can be effectively used for discriminating macrophyte species based on valid experimentation. The following questions are addressed in this study, with special focus put on the feasibility of using airborne hyperspectral remote sensors to detect macrophyte coverage and species distribution to meet the requirements for limnological applications.

First, the spectral reflectance of eight macrophyte species, *Chara aspera* DETH. ex WILLD., *C. contraria* A. BRAUN. ex KÜTZ., *C. intermedia* A. BRAUN. *C. tomentosa* L., *Nitellopsis obtusa* (DESV.) J. GROVES, *Najas marina* L. (in this study called *Najas marina*), *P. pectinatus* L., *P. perfoliatus* L. will be recorded under water using a submersible spectro-radiometer (RAMSES) to ascertain the differences in reflectance in visible (VIS) and near-infrared (NIR) radiation wavelengths. *In situ* underwater bottom reflectance measurements just above the macrophytes will be used for the spectral separability analysis to determine

whether they adequately contain useful spectral information for discriminating macrophytes at species level.

From this data, a comprehensive spectral library of these macrophyte species will be produced in order to

- characterise the spectral signatures of each species by defining the levels of spectral variability associated with these macrophytes over a range of natural conditions in which they grow in the field.

- explore how they differ in their reflectance characteristics in certain wavelength areas.

The second goal of this study will be to investigate methods for the automated classification of stands of macropyhte species to use on hyperspectral airborne data: It will be necessary to determine the location and width of wavebands that can be practically applied in the remote sensing of benthic aquatic plants.

The field based study will be validated on a HyMap hyperspectral remote sensor, flown in 2003 and 2004 at two different lakes with different water quality and macrophyte substrates in southern Germany. The results will be used to assess the suitability of hyperspectral remote sensing combined as a monitoring method for mapping aquatic macrophytes vegetation. Consequently, this study is intended to move one step closer to the conclusion whether hyperspectral technology could be used for macrophyte species discrimination in lakes.

1.4   Hypothesis

The hypothesis of this thesis is that (1) some macrophyte species will have distinct spectral reflectance properties based on presence or absence of pigments and (2) hyperspectral remote sensing can successfully be used to map macrophyte species in lakes. This study is intended to show that macrophyte substrates in lakes differ from each other optically and that various remote sensing sensors are able to detect these differences.

1.5 Thesis Outline

This thesis is organised as follows. **Chapter 2** is a comprehensive literature review of remote sensing of submerged aquatic vegetation. Previous works on remote sensing in shallow water mapping are presented, including aerial photography satellite remote sensing and airborne hyperspectral remote sensing. **Chapter 3** introduces background information of water optics, emphasising the radiative transfer processes in shallow water. **Chapter 4** describes the study area in which this work was completed, as well as the process of data collection and pre-processing steps. Statistical methods used and information of classification approach is described under the Methodology section in **Chapter 5**. The results of the *in situ* spectral analysis and remote sensing classification are presented in **Chapter 6**. In **Chapter 7**, the results are discussed in the context of macrophyte classification and mapping for the purpose of water quality assessment and contains some concluding remarks of the existing limitations and future challenges with the application of remote sensing.

Chapter 2

Literature Review

The following section provides a review of scientific literature of substrate mapping and will discuss in detail the current status of remote sensing techniques for mapping submerged vegetation in shallow water environments. Dekker and Jordan (ress) and Fyfe (2004) provide thorough reviews of the history and status of submerged aquatic remote sensing with special emphasis on seagrass mapping and coastal waters, and additional references are found in reviews by Malthus and Karpouzli (2003) and Dekker et al. (2001). A special issue of Limnology & Oceanography: Light in shallow water (2003) highlights several examples of remote sensing techniques applied to various types of shallow water environments.

2.1 Optical remote sensing and shallow water

The knowledge of distribution of submerged aquatic vegetation is essential in studying aquatic environments and is an important facet of water quality and resource management. Therefore, recent years have seen increasing interest and research in remote sensing of water quality of inland and coastal waters to map vegetation distributions, algal blooms, and substrate types, among other variables (Dekker et al., 1995; Doerffer, 1992; Kondratyev et al., 1998; Lindell et al., 1999). The first assumption in mapping benthic vegetation using remote sensing is that of optically shallow water. If there is a measurable reflectance contribution from the plants or substrate in the water column then the water is optically shallow. Optically shallow waters are a special case in remote sensing of aquatic systems, without measurable bottom influence on the remotely sensed reflectance, the water is effectively optically deep (Dekker et al., 2001). As the spectrum of light emanating from the ocean surface in shallow waters contains information on the optical properties of the water constituents and the benthic substrate, the challenges for extracting substrate composition from surface reflectance lie in the removal of the water column signal and in the interpretation of the substrate into

constituent aerial coverage. The degree of the difficulty in these challenges depends, in part, on the instrumental spectral resolution, but more importantly on the spectral uniqueness and relative strengths of the signals arising from the water and the substrate (Werdell and Roesler, 2003). The determination of a substrate cover, i.e. macrophytes, depends on the water column's spectral optical depth, the brightness, and the spectral substrate contrast, and the signal-to-noise performance of the remote sensing device. The water column optical properties and bathymetry are thus important in remote sensing of aquatic environments, especially with benthic vegetation and macroalgae mapping (Dekker et al., 2001).

2.2   Monitoring and mapping requirements

The water column signal is of major concern when mapping submerged vegetation with remote sensing techniques. In contrast to the remote sensing of terrestrial vegetation, there is practically no signal returning from the water or the substrate at wavelengths beyond 680 nm, due to absorption by pure water (Kirk, 1994). As a result of the physical properties of pure water and its optically active constituents, the remotely sensed optical signal is thus limited to the visible or optical part of the spectrum. Figure 2.1 show underwater reflectance measurements above a macrophyte patch at 3.7 m water depth. The increasing water column between the sensor and the substrate illustrates the influence of the water column to the signal reflected from the substrate plant material. With increasing depth of the water, the signal is rapidly attenuated and diminished as it is filtered through the water column. All remotely sensed measurements of reflected radiance over submersed species will be similarly influenced by water column effects, ultimately affecting the accuracy with which spectral classification of individual species can be performed (Mumby et al., 1998). Strong light attenuation gradients may be caused by a combination of water depth and factors that effect water colour and clarity, such as dissolved organic matter, suspended matter and phytoplankton content (Dekker et al., 2006). The spectral differences between the benthic substrates and attenuation of light by a water column above the substrate are the main factors limiting the ability of remote sensing techniques for monitoring macrophyte species. Submerged vegetation generally has low absolute reflectance, and increasing wavelengths normally results in decreased reflectance. Little evidence of red-edge increases in reflectance is seen, except in the shallowest of waters (Dierssen et al., 2003).

In turbid waters, where bottom albedo is not as high as that of carbonate sand and the diffuse attenuation in the water column is very large, the benthic albedo can contribute less than 10% of the total measured surface reflectance signature. This problem is compounded
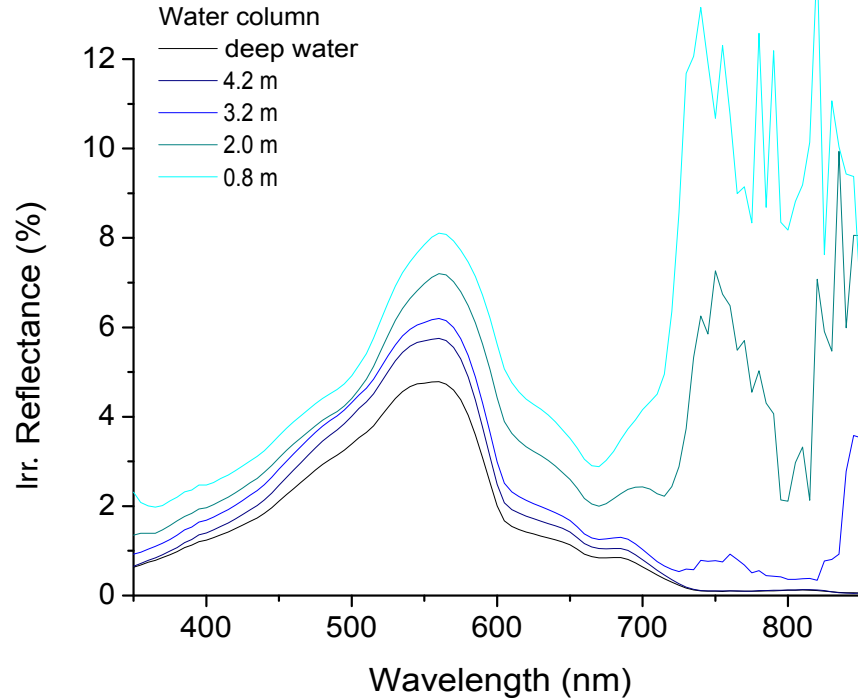
Figure 2.1: Underwater reflectances measured directly above a macrophyte patch (*Nitellopsis obtusa*) with a RAMSES spectroradiometer at Lake Starnberg. The water column increases from 0.8 m with the sensor at the bottom just above the plants to 3.7 m at the subsurface of the water column and shows the water column attenuation with increasing water depth. An additional deep water spectrum from a different location is also added for comparison.

by a green water column over a plant-dominated substrate (Mumby et al., 1998). Increasing water depth is responsible for rapidly attenuating the signal reflected from submerged plant material (Wittlinger and Zimmermann, 2000), ultimately affecting the spectral classification accuracy for individual species. The small-scale patchiness of macrophytes, growing either sparsely or spectrally confused by other habitats, i.e. areas of macroalgae, detritus or epibionts (Mumby et al., 1997), presents another problem in remote sensing. The changes in brightness and spectral shape associated with water column do not differ from those induced by variations in benthic substrate, presenting challenges during model inversion. However, removing the effects of the water column and water depth yields spectral signatures associated with benthic substrate. Within the spectral signature lies the potential for interpretation of complex substrate composition from albedo. The goal of reflectance inversion approaches

to habitat assessment is to unambiguously interpret changes in brightness and colour with respect to water depth and substrate composition. High radiometric resolution sensors, with greater signal-to-noise ratio than those used for terrestrial environments, are required for investigating aquatic environments (i.e. macrophytes, seagrass, sand, macroalgae, mud, coral reefs). To allow a range of brightness levels over which a classification can be performed and to be sensitive enough to detect the lower depth of macrophytes, the number of sensor quantisation levels, known as the sensor radiometric resolution, must be sufficiently large (Dekker et al., 2001).

2.3   Spectral reflectance of plant canopy

In addition to the substances present in the water column e.g. phytoplankton, suspended matter and gelbstoff, light reflected from the bottom of a water body can also influence the colour of the water, provided the water is sufficiently shallow and clear. The influence of the bottom on the colour of the water can also vary with water body depth, clarity of the water, substances present in the water, and bottom type. The bottom maybe rocky or sandy, or be partially or fully covered by a variety of benthic organisms or aquatic plants (e.g. macrophytes). Previous research into spectral reflectance properties suggests that differences exist between various benthic substrates (Andrefouet et al., 2001; Green et al., 2000; Mumby et al., 1997; Holden and Ledrew, 1999; Maritorena et al., 1994; Lubin et al., 2001; Myers et al., 1999; Holden and LeDrew, 1997; Hochberg and Atkinson, 2003; Holden and LeDrew, 1998; Kutser et al., 2003; Joyce and Phinn, 2003). However these studies have focused primarily on reflectance spectra of coral reefs and other coastal benthic types. In contrast, detailed, high spectral-resolution reflectance properties of in situ aquatic vegetation has received little attention, and only few studies, e.g. Penuelas et al. (1993); Malthus and George (1997); Fyfe (2003) describe spectra for a variety of species and differing growth habits.

Light availability plays an important role in determining the structure and distribution of macrophyte ecosystems (Duarte, 1991). Fyfe (2003) investigated the spectral signatures of three seagrass species to determine whether species could be discriminated by remote sensing. It was found that seagrass species were spectrally distinct regardless of whether or not the leaves were fouled by epibionts and despite spatial and temporal variability in the reflectance of each species. To identify different benthic species, sufficient spectral bands are required and the range of wavelengths detected by the sensor must also penetrate the water column to interact with the vegetation. Figure 2.2 presents reflectance spectra measured above eight types of freshwater macrophytes in Lake Starnberg, Germany. These spectra can

be used to draw conclusions about the nature of reflectance of different growths habitats for freshwater macrophyte species. Absolute reflectances of submersed species (e.g. *Potamotegon pectinatus*) are generally low, often lower than reflectance from deeper or background open water areas.
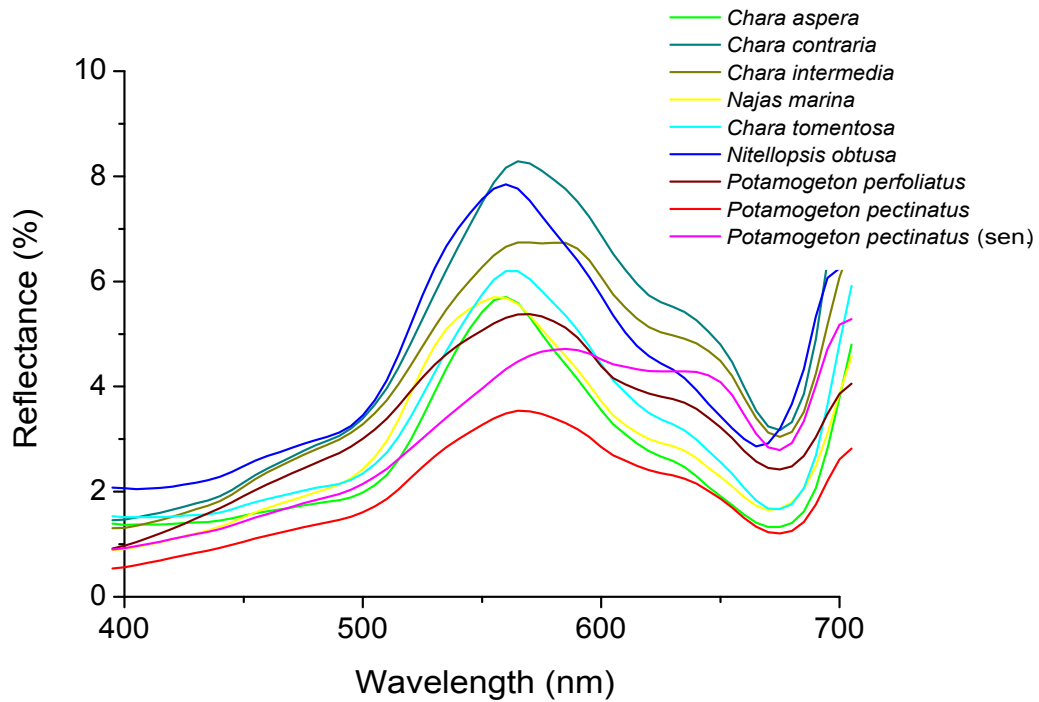
Figure 2.2: Bottom albedo measured over different macrophyte species in Lake Constance and Lake Starnberg. Measurements were made in the water approx. 15 cm above the substrates using a submersible RAMSES spectroradiometer.

2.3.1 Green plants species

The reflectance curve for healthy green vegetation is characterised by the absorption of blue $(400-500\,\text{nm})$ and red $(600-700\,\text{nm})$ wavelengths and by the reflectance of green radiation $(500-600\,\text{nm})$, and very strong reflectance of near-infrared (NIR $700-1300\,\text{nm}$) and mid-infrared (MIR $1300-2600\,\text{nm}$) radiation (Carter and Knapp, 2001). The steep rise usually observed in a vegetation curve at about $700\,\text{nm}$, the 'red edge' (Carter and Knapp, 2001) is

unique to the spectral signatures of green vegetation and indicates the limit of chlorophyll absorption by plant tissue. While the visible reflectance of green light gives plants their characteristic green colouration, plants absorb blue and red light as the energy source for photosynthesis. The chemical structure [1] and the absorption properties of phaeophytin, an accessory photosynthetic pigment and decomposition product of chlorophyll, are almost identical to chlorophyll. Chlorophyll-a absorbs around 70-90% of the radiation entering a plant at wavelengths centred at at 430 nm and 660 nm (Rowan, 1989). Chlorophyll-b absorbs slightly longer blue wavelengths (460 nm) and slightly shorter red wavelengths (640 nm) than chlorophyll-a, while a variety of carotenoid pigments absorb maximally at various points across the blue wavelengths (centred around 450 nm)(Blackburn, 1998; Hilton et al., 1989). The effects of individual carotenoids on blue light absorption may be small but the combined effect of the chlorophylls and carotenoids together results in the characteristic broad blue absorption trough observed in the spectral signatures of plants (Gitelson et al., 2002).

2.3.2   Pigment composition of aquatic plant species

Absorption of light by plants are controlled by leaf biochemical properties (e.g. water, photosynthetic pigments) (Curran, 1989; Asner, 1998), whereas the magnitude of reflectance of light from plant leaves depends primarily on leaf morphology (e.g. cell wall thickness, air space) (Gausman and Allen, 1973), leaf surface quality and leaf internal structure (Asner, 1998), where the internal structure of leaves controls the magnitude of reflectance and transmittance across the whole spectrum (Fyfe, 2004).

The relative concentrations of photosynthetic and accessory pigments will vary within a macrophyte species because of chromatic adaptation to seasonal cycles or genetic variation (van Dijk and van Vierssen, 1991; Schagerl and Pichler, 2000; Venanzi et al., 1988), stage of growth (Nielsen and Sand-Jensen, 1991) and health or environmental conditions (Wiegleb and Brux, 1991; Vestergaard and Sand-Jensen, 2000). Chromatic acclimation of pigments can occur in an individual aquatic plant grown under changing conditions of water depth or clarity (Fennessy et al., 1994; Dennison et al., 1993). Spatial and temporal variations in light (Schagerl and Pichler, 2000), nutrient availability (Lichtenthaler and Babani, 2000; Venanzi et al., 1988), water temperature, and water movement act in concert to influence growth and photosynthetic rate, and therefore also influence the spectral reflectance of macrophytes. Spectral changes in aging or diseased plants have been related to changes in the intercellular air spaces (Carter et al., 1989; Gausman, 1977), chlorophyll breakdown (Blackburn, 1998;

---

[1]   Chlorophylls are conjugated circular macromolecules. A magnesium atom is responsible for the coordination of the circle. Phaeophytin has the same structure, except that the magnesium atom is missing.

Merzlyak et al., 2003; Gitelson et al., 2002) and the subsequent unmasking of carotenoids and other leaf pigments. In addition, epibionts that grow on the surface of aquatic plants may mask their reflectance to some extent while contributing their own absorption and reflectance features to the spectral reflectance (Drake et al., 2003; Fyfe, 2003).

The most prominent macrophyte epibionts found in lakes which have the greatest impact on remote sensing are diatoms and chlorophyceae (Goos, 2003), as their major light harvesting pigments are chlorophyll-a, lutein and fucoxanthin (Goos, 2003; Förster, 2006). Chlorophyll-*a* can be found in all photosynthetic active organisms and is therefore a good indicator for biological activity in lakes. The carotenoids, such as carotenes and xanthophylls (Kirk, 1994), absorb light energy in the $400-500$ nm range, but at an efficiency of only $30-40\%$. Lutein, a xanthophylls pigment, absorbs light around 445 nm (Rowan, 1989) and occurs mainly in chlorophyceae whereas fucoxanthin absorbs maximally between $444-449$ nm (Rowan, 1989) and is a common pigment found in diatoms. The biomass and species composition of epiphytes on a single macropyhte species varies with location and time.

The absorption maxima of a specific pigment can vary *in vivo* up to 5 nm, the absorption strength less than 50% (Gege, 1994). This is caused by the fact that chlorophylls have different tasks in a cell and consequently are active in different environments. Additionally the absorption signature becomes flatter if the pigments are spatially concentrated. This packaging effect is caused by the complete absorption of light if the pigment concentration exceeds a certain level, whereas the pigment is still transparent at other wavelength. The increase in pigment concentration barely affects the spectra at the absorption maxima, but changes the spectra in other part more distinctly which flattens the signature (Keller, 2001).

Table 2.1: The chlorophylls and major carotenoids that characterise angiosperm plants and some selected classes of algae often found growing as epiphytes on macrophytes leaves ++: important pigment, +:pigment occurs, -:pigment is infrequent or occurs only in low concentrations (adapted from Gege (2000) and Fyfe (2004))

	Angiosperms (e.g. Potamogetonaceae)	Clorophyta (e.g. green algae)	Bacilliariophyta (e.g. diatoms)	Dinophyta (e.g. dinoflagellates)	Cyanophyta (e.g.blue green algae)
Chlorophyll					
a	++	++	++	++	++
b	++	++	-	-	-
c_1	-	-	++	+	-
c_2	-	-	++	++	-
Phycocyanin	-	-	-	-	++
Phycoerythrin	-	-	-	-	++
Carotenoide					
α - Carotene	+	+	-	-	-
β - Carotene	++	++	++	++	++
Echinenone	-	+	-	-	++
Lutein	++	++	-	-	-
Zeaxanthin	++	+	-	-	++
Neoxanthin	++	++	+	-	-
Violaxanthin	++	+	++	+	-
Fucoxanthin	-	-	++	+	-
Diatoxanthin	-	-	+	+	-
Diadinoxanthin	-	-	++	+	-
Peridinin	-	+	-	++	-
Myxoxanthophyll	-	-	-	-	++

Table 2.2: Location of absorption and flourescence *(italic)* maxima of selected chlorophyll, carotene and xanthophyll dependent on their solvent (adapted from Rowan (1989) in Gege (1994))

	Acetone	Diethyl- Ether
Chlorophyll		
a	$430,660 - 663, \mathit{668}$	$428 - 430,660 - 662, \mathit{668}$
b	$455,645 - 647, \mathit{652}$	$453 - 455,642 - 644, \mathit{648}$
c_1	$442 - 444,630 - 631, \mathit{633}$	$438,625, \mathit{632}$
c_2	$444 - 445,630 - 631, \mathit{635}$	$445 - 449,628 - 629, \mathit{632}$
Phycocyanin	$430, 660 - 663, \mathit{668}$	$428 - 430, 660 - 662, \mathit{668}$
Phycoerythrin	$430, 660 - 663, \mathit{668}$	$428 - 430, 660 - 662, \mathit{668}$
Carotenoid		
α - Carotene	$422 - 425$	$443 - 445$
β - Carotene	$420 - 432$	$447 - 450$
Echinenone	$459 - 460$	455
Lutein	445	$443 - 448$
Zeaxanthin	$449 - 452$	$447 - 450$
Neoxanthin	$436 - 445$	$437 - 444$
Violaxanthin	$440 - 442$	441
Fucoxanthin	$444 - 449$	$444 - 446$
Diatoxanthin	442	$439 - 443$
Diadinoxanthin	$448 - 449$	448
Peridinin	$461 - 471$	$453 - 454$
Myxoxanthophyll	$475 - 478$	

2.4 Remote sensing mapping approaches

A number of techniques exist for mapping and monitoring the benthos of shallow waters. The mapping of macrophyte distribution has traditionally involved the use of diver survey (Melzer, 1999) or relied on quadrat and transect based methods similar to those typically used for ground-based survey of plant matter in terrestrial ecosystems (Chipchase and Leach, 2000; Norris et al., 1997; Jäger and Dumfarth, 2004). SCUBA-based surveys provide great accuracy and high resolution yet are limited by the time and manpower necessary to monitor large bodies of water. Video (Norris et al., 1997; Lamb and O'Donnell, 1996; Everitt et al., 1999) and echo-sounding techniques (Jäger and Dumfarth, 2004; Vis et al., 2003; Valley et al., 2005) have also been applied to map distribution of emergent and submersed macrophytes. Echo-sounding collects data in profiles, the spacing being typically at intervals from 10 to 20 m in the littoral zone (Jäger and Dumfarth, 2004). However, no data are available between theses profiles. It provides good results in terms of distribution, but different species can not be differentiated. Acoustic methods, including side-scan sonar, have the ability to cover

areas within a wide swath but are generally restricted to zones greater than approximately 5 m in depth and their extrapolation to larger areas can give rise to significant errors in the estimation of the habitat types, area and quantity.

Remote sensing has become a standard tool for large scale coastal and inland water management, mainly because remote sensing technology allows information to be gathered from areas that would otherwise, logistically and practically, very difficult to survey. Since the early use of aerial photography for exploring the macrophyte, seagrass and coral reefs coverage in the 1920s, there has been mounting evidence, that remote sensing can be successfully applied to several aspects of water management (Vaiphasa et al., 2005), such as resource inventory and change detection. Remote sensing techniques have been successfully applied in operational mapping the biophysical properties of oceanic (Case1) waters for inventory purposes (Sathyendranath, 2000). Operational mapping and monitoring programs for assessing changes in oceanic productivity, based on the measurement of ocean colour through mapping concentration of organic constituents in the water column, have also been implemented (Gordon and Clark, 1995; Carder et al., 1989). Coastal and lacustrine waters (Case2) continue to represent a challenge for remote sensing techniques, though technological development in these environs has occurred in the past 30 years to allow mapping of various characteristics of aquatic environments, including water surface and column constituents and substrate cover types (Mumby et al., 1997; Green et al., 2000; Hochberg and Atkinson, 2003; Malthus and Karpouzli, 2003). Mapping of substrate cover types and their biophysical properties has been carried out successfully in optically clear, shallow (< 20 m), coastal and reef waters, with limited exceptions (Lee et al., 1998a, 1999). Mapping the concentration of organic and inorganic materials has been implemented extensively in lakes and rivers (Lindell et al., 1999; Dekker et al., 2001). These applications are based on a number of remote sensing instruments on both airplane and satellite platforms, including visible and infrared photographic cameras (Valta-Hulkkonen et al., 2003), video recorders (Norris et al., 1997), multispectral (Dekker et al., 2005) and hyperspectral sensors (Alberotanza et al., 1999). Accurately mapping submerged macrophytes requires repeated measurements, using high resolution radiometric sensors with sufficient spectral bands, as shown above. In previous studies, accurate maps of submerged aquatic vegetation coverage have been produced using some of the methods shortly outlined below.

2.4.1   Mapping by aerial photography

Given Europe's extensive lacustrine environments, techniques are required which facilitate the broad-scale mapping of macrophyte habitat and meet the requirements for routine monitoring. Application of aerial photography has been successful in marine (Meulstee et al., 1986; Ferguson et al., 1993; Chipchase and Leach, 2000) and littoral environments (Malthus et al., 1990; Marshall and Lee, 1994; Lehmann et al., 1997; Rutchey and Vilchek, 1999; Valta-Hulkkonen et al., 2003). The advantages of conventional film-based methods are the very fine resolution (0.1 to 1.0 m, dependent on scale) (Jensen et al., 1986) and cost-effective data acquisition compared to airborne multispectral scanner data (Green et al., 1996). However the results have been shown to be somewhat inaccurate (Lennon and Luck, 1990), as aerial photographs require careful geo-correction to overcome geometric distortions introduced by aircraft instability and the camera lens (Chauvaud et al., 1998). If manually undertaken, photo-interpretation of such media is more often than not a subjective process and, applied as an operational tool, can be time consuming and limited in temporal coverage (Valta-Hulkkonen et al., 2003). Digital images are an improvement over manual ones in that they provide better geographical positioning and can be superimposed upon and compared with other geographical data in order to study the interactions between parameters and temporal changes. As much of the interpretation of aerial photographs is based upon brightness, shallow submerged aquatic vegetation appears dark and is often indistinguishable from deep water. Variable water clarity, bottom sediments, macroalgae, and epiphytes add to the uncertainty in photographic identification of benthic vegetation habitats (Werdell and Roesler, 2003). Despite high spatial resolution, the poor spectral resolution of aerial photography is insensitive to subtle spectral variations and is certainly a limiting factor for successfully discriminating submerged features (Holden and LeDrew, 1998; Pasqualini et al., 1997; Picchiotti et al., 1997). However, the relatively high spatial resolution of aerial photographs can be suitable for terrestrial vegetation and emergent aquatic vegetation (Pasqualini et al., 1997; Picchiotti et al., 1997) where the signal is not influenced by an overlying water column.

2.4.2   Satellite remote sensing

The use of ocean colour remote sensing technology to estimate benthic constituents has been under development for over a decade. The 30 m resolution Landsat Thematic Mapper (TM) data have been used successfully to estimate submerged vegetation features in shallow waters (Lyzenga, 1978; Armstrong, 1993; Mumby et al., 1997; Zhang, 1998). For example, Zhang

(1998) used Landsat TM in Honghu Lake, China to establish a relationship between the submerged vegetation biomass and a principle component (PC) transformation. In this study it was assumed that submerged vegetation, water depth and lake sediment were included in each pixel on the image, which could be considered as three independent and uncorrelated variables. A linear relationship between submerged vegetation biomass and the first two principle components was found and used to determine the total biomass of submerged vegetation. Multispectral satellite sensors have been moderately successful in mapping benthic subtrata since the mid-1980s (Lyzenga, 1978; Jupp et al., 1985; Raitala and Lampinen, 1985; Armstrong, 1993; Luczkovich et al., 1993; Jensen et al., 1993). The spectral reflectance data obtained from digital remote sensing imagery include considerable advancements over conventional aerial photography and allow for physically-based analyses using spectral signatures inherent to specific benthic substrata. Broadband multispectral sensors on satellite platforms, including Multispectral Scanner (MSS) Landsat TM, SPOT, are most popularly used because of their cost-effective advantages, but they are mainly limited to the regional scale, owing to their relatively coarse spatial and spectral resolutions (Jensen et al., 1995; Maritorena, 1996; Ferguson and Korfmacher, 1997; Pasqualini et al., 1997; Picchiotti et al., 1997; Holden and LeDrew, 1998; Liceaga-Correa and Euan-Avila, 2002; Call et al., 2003; Dekker et al., 2005).

Improvements are needed in both these areas in order to enable mapping of aquatic vegetation at higher resolution. Satellite sensors also have the ability to perform repeated analyses, useful for living systems that change throughout the year, as demonstrated by Jensen et al. (1993, 1995). They were able to observe seasonal and yearly cattail and waterlily changes using panchromatic satellite data from SPOT. A retrospective seagrass change detection was also undertaken by Dekker et al. (2005) in Wallis Lake, Australia. They analysed Landsat5 TM and Landsat7 ETM satellite imagery spanning 14 years to reconstruct changes in seagrass and macroalgal communities in a shallow coastal lake. However application of conventional satellite data, i.e. found on Landsat MSS, TM and SPOT satellites, is restricted to large features, inland waters, or regional surveys of coastal areas (e.g. Jensen et al. (1986); Ackleson and Klemas (1987), primarily because of their coarse spatial resolution, poor radiometric resolution (256 measured radiance levels) and is limited in its spectral resolution. Improved spatial resolution, obtainable on IKONOS and Quickbird satellites, provide data at high spatial and radiometric resolution and offer considerable promise for monitoring spatial changes in marine habitats at scales acceptable to conservation agencies. However they may still be restricted because of limited spectral resolution. Several studies are currently investigating the accuracy and usefulness of IKONOS (Mumby et al., 2001; Maeder et al., 2002; Malthus

and Karpouzli, 2003; Wettle et al., 2004) satellite data for mapping submerged aquatic vegetation in marine environments. For example, in Honduras, submerged aquatic vegetation was classified using IKONOS multispectral (4 m resolution) satellite imagery (Maeder et al., 2002), extracting more detailed bottom class information than previously collected data. Similarly, Malthus and Karpouzli (2003) used IKONOS data imagery over the Eriskay region of Scotland to map subtidal and intertidal habitats. They found IKONOS sensor data to be of high quality and showed great potential for routine monitoring of habitats and change over targeted shallow waters, however the utility of the imagery for classification of bottom habitat on the basis of spectral differences was less evident because of limited spectral resolution. Wolter et al. (2005) used high resolution Quickbird satellite imagery (2.44 m resolution) to map submerged aquatic vegetation in the Great Lake Basin, where water clarity is lower and submerged aquatic vegetation richness higher than in most of the studies published on marine seagrass mapping. They found Quickbird imagery a useful tool for near-shore vegetation classification, but in terms of regional mapping efforts, were sceptical about its operational and economic feasibility. In contrast, the report of Galvão et al. (2005) demonstrate how more sensitive instruments such as the satellite mounted Hyperion[2] sensor that processes 220 bands between 400 and 2500 nm with a spatial resolution of 30 m, handle the task of discriminating coral communities in Australia Wettle et al. (2004), a task considered difficult for any multispectral sensor. Despite this success, Hyperion sensor have shown limited potential in vegetation classification because of low spatial resolution (Brando and Dekker, 2003).

2.4.3 Hyperspectral remote sensing

In order to overcome conventional satellite sensor limitations and to accurately monitor small-scale macrophyte dynamics (<10m), airborne remote sensing has been employed. The recent advances in computer and detector technology has generated this new field of imaging spectroscopy (Goetz et al., 1985; Green et al., 1991; Vane et al., 1993; Merton and Cochrane, 1995), as airborne sensors usually have higher spatial and spectral resolution than satellite sensors. This provides more spectral information on more pure targets, and thus greater spectral accuracy in detailed benthic habitat mapping (Mumby et al., 1997). Instrumentation and technique development in the 1990's was somewhat limited, with macrophyte species discrimination by absorption spectrum largely dependant on water column depth. Improved classification was achieved via increasing data storage capacity, developing broader

---

[2]   USGS EROS Data Center (EDC),USA

expert knowledge, and designing instruments capable of increased spectral resolution. Airborne hyperspectral sensors have three main advantages over broadband sensors. First, they are capable of detecting narrow spectral features which theoretically increases the number of substrates that can be separated, as their large number of spectral bands increases the potential to uniix substrate spectral signatures. Second, the high spatial resolution of the newly emerging remote sensing technology reveals fine scale variability in the benthos that is useful for mapping macrophyte populations that at first glance might appear homogeneous. Such fine-scale data can be necessary for evaluating small scale changes in habitat boundaries or standing crops. The last advantage is that hyperspectral sensors can also distinguish between substrates in deeper water (Kutser et al., 2003). Optimal selection of feature parameters for a concrete application goal is very important for making full use of the information in hyperspectral data (Louchard et al., 2003). Cochrane (2000) and Schmidt and Skidmore (2003) confirm that hyperspectral data have potential in discriminating terrestrial plants to the species level and recent reports show promising results for spectral discrimination of submerged aquatic vegetation (Fyfe, 2003). Several studies successfully used airborne digital sensors to examine benthic vegetation, e.g. Malthus and George (1997); Mumby et al. (1997); Jernakoff and Hick (1994); Bajjouk et al. (1998); Dunk and Lewis (1999); Alberotanza et al. (1999). Recent mapping applications of hyperspectral technology include an analysis of coastal seagrass (Anstee et al., 2001), the detection of bleached vs. unbleached coral reefs (Joyce and Phinn, 2003), mapping macrophyte distribution in lakes (Williams et al., 2003), and discrimination between mangroves and wetlands (Vaiphasa et al., 2005; Artigas and Yang, 2005). To date, only a few studies have reported spectra from a variety of macrophyte species and growth habits, e.g. Penuelas et al. (1993); Malthus and George (1997); Alberotanza et al. (1999).

Hyperspectral sensors with contiguous spectra allow for more sophisticated multiband algorithms, and will also allow the use of methods similar to those used in spectroscopy, such derivative analysis (Andrefouet et al., 2003a; Louchard et al., 2002; Hochberg and Atkinson, 2003), spectral modelling (Kutser et al., 2003; Voss et al., 2003) and matrix inversion (Lee et al., 1999; Maritorena et al., 1994) in the identification of macrophyte spectra and interpretation of remotely sensed data. Traditionally, interpretation of remote sensing data has been image based. The main disadvantage of image-based methods is that the algorithms are either sensor specific, site specific, or time specific such that the relationships cannot be applied to different sensors, in different places, or at different times with any confidence. With hyperspectral remote sensing, the ultimate goal is to establish a library of species spectra such that interpretation can be automated to provide accurate and rapid maps of substrata

across sensors, locations, and times. In order to do this, steps to correct the attenuation of the reflectance signal must be made. The radiative transfer model approach to signal correction is necessary to make hyperspectral remote sensing data comparable. This is feasible as most natural atmospheric and water-column influences are estimates. After correction, the modelled reflectances can be compared to *in situ* measurements and can be directly linked to remote sensing data, making remote sensing analysis of multi-temporal data sets operational within a modelled spectral library. Radiative transfer theory is used to evaluate water column effects on remotely sensed spectra to propagate bottom-reflected light through different water column depths for a given set of water optical properties. Radiative transfer models allow the modelling of radiation as it travels through the atmosphere and the water column. Physics based methods such as Hydrolight have the advantages of repeatability and reduced time consuming *in situ* measurements compared to traditional image-based methods (Kutser et al., 2003). Included in the modelling process is the overlying water column, thus allowing reflectance of underwater substrates to be predicted over a range of water depths (Kutser et al., 2003; Holden and LeDrew, 2000).

A number of models have been developed that describe irradiance reflectance as function of bottom albedo and water depth (Mumby et al., 1997; Philpot, 1987; Mobley et al., 1993; Lee et al., 1999, 1998a; Maritorena et al., 1994; Leathers and McCormick, 1999). For example, Werdell and Roesler (2003) investigated the utility of quantifying percent cover of benthic substrates constituents from surface multispectral reflectance measurements. They considered six substrates, each of them with a unique albedo spectrum that contributed differently to the upward light field in an optically shallow environment. Simplifications of the radiative transfer equation yielded an analytic solution for surface reflectance on optically shallow environments. The objective was to test the inverse model to predict bottom albedo from measurements of surface reflectance. A linear mixing model was used to deconvolve the derived albedo spectra into contributions by the six constituents and was able to differentiate the six homogeneous habitats. Spectral libraries as the basis for developing routine methods of applying remote sensing to aquatic vegetation surveys (Jupp et al., 1985) and are a fundamental part of many hyperspectral image classification and radiative transfer modelling procedures, including atmospheric and water column correction, spectral unmixing and endmember mapping, e.g. Jupp et al. (1996); Anstee et al. (1997); Held et al. (1997); Kruse et al. (1997). Kutser et al. (2003) studied the separability of eight substrate types (live coral, dead coral, soft coral, sand, brown algae, green algae, red algae, and cyanobacteria) and the influence of the overlying water. They collected a spectral library of coal reef benthic communities and simulated remote sensing reflectance using Hydrolight. Spectral libraries will

ultimately have the potential to serve as valuable tools for identifying characteristic wavelengths that can be incorporated into bottom classification and bathymetry algorithms. The success of these image processing techniques depends on the comprehensiveness and quality of the spectral library applied. Spectral libraries also provide information needed to make an informed choice about the spectral resolution required of a sensor and the wavebands that will be most useful for a particular application. After spectral libraries are obtained, analysis of the data to identify significant components of the signal must be made. Another technique commonly used to extract qualitative maps of submerged aquatic vegetation is to measure reflectance spectra of different substrate *in situ* or in the laboratory to create spectral libraries of substrates (Louchard et al., 2000).

Principle component analysis (PCA) is a commonly used analytical tool in multispectral detection as data reduction technique, and has been successfully applied in several studies to determine the most representative spectra (Pasqualini et al., 1997; Bajjouk et al., 1996; Holden and LeDrew, 1998). Other researchers have developed specific algorithms to discriminate between substrate. For example Bajjouk et al. (1996) used CASI airborne imaging spectrometers with ground based spectroradiometry for mapping benthic plant species the principal seaweed and seagrass beds along the coast of Brittany (France). The algorithm was developed to discriminate between the dominant species. Visible wavelengths allowed good discrimination between green, red and brown algae and infrared wavelengths allowed separation of brown species, seagrasses and floating seaweed. A different study undertaken by Dunk and Lewis (1999) used HyMap imagery for the mapping of seagrass distribution in a coastal environment in the upper Spencer Gulf, Australia. The data were atmospherically and track illumination corrected. Three feature extraction techniques were evaluated: band ratios, principle component analysis (PCA), and spectral angle mapping (SAM). SAM was assessed to reliably discriminate features from selected endmembers (Alberotanza et al., 1999). The spectral reflectance characteristics of features within a submerged coastal environment are optically similar, so confusion can arise in identification. High spectral resolution sensors are required to perceive the subtle difference, which is demonstrated through analysis of in situ measurements in a study by Holden and LeDrew (1998). There, the proportion of correctly identified spectra using first derivatives was 75% with the main source of error resulting from the inability to identify algae-covered surfaces. Similarly, Malthus and George (1997) evaluated the ability of Daedalus ATM imagery for mapping the distribution of freshwater aquatic macrophyte species in the Cefni Reservoir on the Isle of Anglesey, UK. Discriminant analysis indicated that good identification of macrophytes could be achieved by a combination of green, red and near infrared wavebands. A minimum distance supervised classifier using

three bands showed separation of the species surveyed. The results indicated that airborne remotely sensed data have good potential for monitoring freshwater macrophyte species. In a similar study Bogner (2003) tested the Daedalus AADS1268 multispectral airborne scanner at Lake Constance, Germany, in a multi-temporal analysis. Bottom reflectances were classified to three endmembers of specific reflectance spectra by linear unmixing using the Modular Inversion & Processing System (MIP). Specific reflectance spectra of bottom sediments, short growing macrophytes (e.g. Characeae), and tall macrophytes (e.g. *Potamogeton pectinatus*, *P.perfoliatus*) were successfully identified.

In comparison to conventional spaceborne sensors such as Landsat TM and SPOT, airborne hyperspectral sensor data is more accurate and precise (Jakubauskas et al., 2000). AVIRIS, ATM, HyMap, and CASI airborne hyperspectral sensors show highly accurate results in mapping aquatic vegetation. Hyperspectral sensors increase the spectral resolution of mixed pixels and together with spectral libraries, improve the ability to uniix the signal and resolve the make up of each mixed pixel scene. Until recently, airborne sensors were the only way to acquire hyperspectral images of submerged aquatic vegetation. The high spectral and spatial resolution of these instruments makes them very suitable for investigating the highly complex substrates found in shallow lake systems. Other spaceborne sensors with a similarly high spatial resolution (e.g. IKONOS) do not yet have comparable spectral reflectance spectra, whereas the hyperspectral instrument Hyperion, with a spatial resolution of 30 m, has also shown limited potential in vegetation classification (Dekker et al., 2001). Water column depth, turbidity, surface effect (sunglint, waves), and issues associated with spatial, spectral and radiometric resolutions are all challenges of above surface approaches to benthic vegetation surveys of littoral and marine environments. Detecting the change in habitats over time remains a key objective for remote sensing studies (Green et al., 2000). In multitemporal data analysis, the interactions between radiation and the optically-active water column constituents, vegetation and sediment must be both qualified and quantified; only then can image differences be attributed to actual measurement differences.

Chapter 3

Optical Remote Sensing and Water

This chapter provides an overview of the physical parameters of optical properties of water (referred to here as 'the physics'), as a comprehensive introduction to remote sensing and physical properties of water by Dekker et al. (2001) exists. They review the historical and background information describing how light is influenced in the water column and from bottom substrates for the purposes of remote sensing. Much of the mathematics and definitions in this chapter are based on those found in Kirk (1994); Mobley (1994); Maritorena et al. (1994).

3.1 Introduction to the physics

When direct and diffuse sunlight penetrates a lake surface, it may be absorbed or scattered by water molecules or by various suspended and dissolved materials present (see Figure 3.1). Only a fraction of the scattered and reflected photons find their way back to a remote sensor. Following the pathway of light (known as the radiative transfer process) is paramount in understanding the various facets to remote sensing. Four so-called pathways are commonly identified (Eq. 3.1): first, incoming light can be scattered by atmosphere back to a sensor (L_{sky}). Second, light can reach the water surface and be reflected back to the sensor. If this portion of light is reflected from diffuse sky radiance it is called skyglint (L_{skygl}) and if it is reflected from direct sunlight it is called sunglint (L_{sungl}). Third, light can pass through the air-water interface, but be scattered back to the sensor by constituents within the water column (L_w). This radiance value is related to the inherent optical properties (IOP) of the water. A portion of this upwelling light is reflected down into the water body at the air water interface. Last, light can pass through the air-water interface, reaching a submerse substrate (macrophytes, bottom). Reflection occurs and light returns upwards through the water column exiting the air-water interface and reaching a sensor (L_b). This radiance value

33
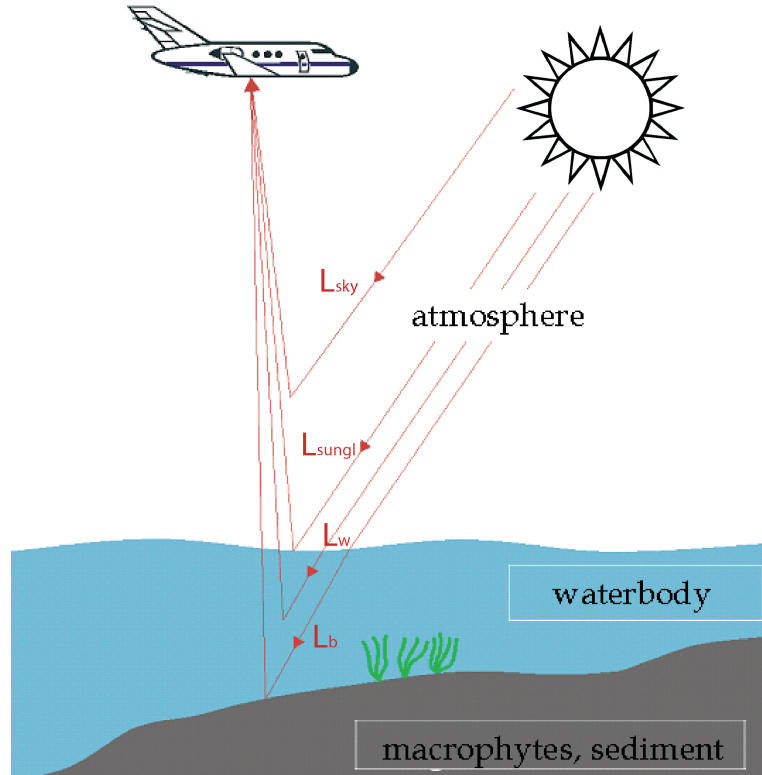
Figure 3.1: Schematic diagram of radiative transfer influenced by surface, phytoplankton, gelbstoff, suspended matter, and water molecules as well as different bottom types that contribute to the signal as measured by a remote sensor in shallow water.

is containing information on both water quality and substrate type (e.g. macrophytes, macro-algae, sediment).

$$L = L_{sky} + (L_{skygl} + L_{sungl}) + L_w + L_b \qquad \text{(Heege, 2000)} \qquad (3.1)$$

Each image pixel of remotely sensed surface water contains signals, or radiances, from these four pathways. The atmospheric contribution, the air-water interface contribution, and the water column component must be corrected for in order to gain information on the bottom substrate. The physics based approach to remote sensing is a means to isolate the portion of signal that pertains to the substrate.

3.1.1   The remote sensing approach

There are different methods of estimating macrophytes using optical remote sensing. One approach, where a statistical relationship is established between the parameter and the image data (Bostater et al., 1997; Durand et al., 2000), correlates signal strength to abundance. A

second, and likely better approach, is in developing an analytical model of radiative transfer and making estimates from physical principles (Jupp et al., 1985). This second approach is broken down into its various steps below.

First, inherent (IOP) and apparent optical properties (AOP) are needed to describe the water light field. *Inherent* optical properties (IOPs) depend only on the medium and are independent of the light field. For example absorption and scattering coefficients are inherent optical properties. *Apparent* optical properties are dependent on both the medium and the ambient light fields geometric directional structure. Apparent and inherent properties are connected via radiative transfer theory, which forms the basis for water quality and substrate determination.

This determination is called *forward modelling* if all concentrations of the lake constituents and other model parameters are known and the radiation is unknown. In practice, the radiation is known and the water constituents are to be determined, thus the process is called *inversion* or *backward modelling*.

Different approaches for solving the inversion problem exist (Gordon and Morel, 1983; Prieur and Sathyendranath, 1981), e.g band ratios (Gordon and Morel, 1983; Dekker, 1993), factor analysis (Krawczyk and Hetscher, 1997; Fischer et al., 1986), curve fitting (Doerffer and Schiller, 1994; Gege, 1994), matrix inversion (Hoge and Lyon, 1996; Hoogenboom et al., 1998), non-linear optimisation (Lee et al., 1999; Albert, 2004), look-up tables or the neural network-method (Schiller and Doerffer, 1999), but in most cases a distinction is made between empirical and analytical methods.

Empirical methods use only statistical dependencies, whereas *analytical* methods use physical knowledge of the light-water system. Empirical (i.e. statistical) methods are not suitable for inland waters, as not all constituents (e.g. Chlorophyll, gelbstoff, suspended matter etc.) are statistically correlated. Analytical models are less restricted, as the influence of various parameters can be included, but their optical properties must be known. Intermediate stages between empirical and analytical models also occur. *Semi-empirical* methods use physical knowledge for the determination of a model equation, but determine the model parameters statistically, based on measurements. Many (semi-) empirical algorithms make simplifications regarding water composition, such as the optical domination of one constituent over all the others.

The processing of remote sensing data into macrophyte distribution maps requires a careful and precise simulation, of light pathway in the water, at/through the air-water interface, and in the atmosphere, e.g. using statistical *Monte Carlo* photon propagation tracking methods or radiative transfer numerical models. Development and adaptation of algorithms is done

by performing simulations of radiative transfer and comparing the output against measured (*in situ*) conditions. Organised field campaigns and laboratory analyses to determine in-water optical properties, constituent concentrations, and macrophyte distributions are carried out for this purpose (Dekker et al., 2001).

3.1.2   Radiative transfer in water

The theory of light in water, or radiative transfer process is incorporated within Radiative Transfer of Energy theory (RTE). RTE links apparent and inherent optical properties. Mobley (1994) explains RTE in terms of radiance and irradiance values and the effects of the water column due to various constituent's optical properties. He suggests radiance can be seen as a beam of photons, where six basic interactions with water and its constituents occur:

- loss of photons by conversion of radiant energy to non-radiant energy (absorption)

- loss of photons by scattering to other directions without change in wavelength (elastic scattering)

- loss of photons by scattering with change in wavelength (inelastic scattering)

- gain of photons by conversion of non-radiant energy into radiant energy (emission)

- gain of photons by scattering from other directions without change in wavelength (elastic scattering)

- gain of photons by scattering with change in wavelength (inelastic scattering)

Furthermore variations in the suspended sediment, phytoplankton, and coloured dissolved organic matter concentrations in inland waters result in many different light climates. Optical modelling approaches utilise radiative transfer models or analytical solutions which describe the physical behaviour of the light field based on the inherent optical properties of the media. They are used to quantify the effects, water constituents have on optical variables obtained from either *in situ* or remote sensing measurements.

There is a wide range of optical models available, from generic radiative transfer models, e.g. Hydrolight (Mobley and Sundman, 2000) and FEM (Kisselev et al., 1995; Bulgarelli et al., 1999) to those based on specific water bodies or conditions, e.g. WASI (Gege, 2001; Albert, 2004), see also section 3.3.2. Analytical models are advantageous that, due to their relative simplicity, they can be solved and inverted with relative ease. This is important in a remote sensing application where a model must be evaluated at every image pixel.

3.2 Optical properties of water

The optical properties as described by Mobley (1994) are summarised as follows:

- the inherent optical properties (IOP) are those pertaining to the medium itself (i.e. water plus constituents). Regardless of the ambient light field, IOPs are usually measured by active (i.e. having their own light source) optical instruments;

- the apparent optical properties (AOP) are combinations of radiometric variables that can be used as indicators for the colour or transparency of the water, for example the reflectance or vertical attenuation coefficient. Note that radiometric variables are properties of the light field that are usually measured by passive optical instruments (using the sun as the light source)(Dekker et al., 2001);

- the diffuse inherent optical properties are a combination of IOPs and AOPs and play an intermediate role in the derivation of the analytical model.

A variety of substances influence the optical properties of lake water, and can be differentiated based on their optical behaviour. If the inherent optical properties of these substances are sufficiently known, then it becomes possible to determine their contribution to water column colour, leading to an estimate of their concentration.

3.2.1 Composition of naturally occurring lake waters

Whereas the optics of open ocean water is influenced by phytoplankton and pure water itself, the optics of littoral water with bottom visibility is much more complex (Lindell et al., 1999). Naturally occurring lakes contain a continuous distribution of particles sizes ranging from water molecules $\sim$ 0.1 nm to fishes $\sim$ 10 cm long. Each of these components contributes in some manner to the optical properties of a water body. Traditionally, matter in waters is subdivided into 'dissolved' and 'particulate' forms of inorganic and organic origin, both living and non-living (Mobley, 1994). The border between dissolved and particulate matter is usually set at 0.4μm. In water optics, only particulate and dissolved constituents are distinguished, though limnologists often distinguish between particulate ($> 0.4\mu$m), colloidal, and dissolved substances.

In lake waters, three main components influence the total absorption and scattering co-efficients of pure water: phytoplankton, dissolved substances, and particulate matter. Because they significantly influence turbidity and transparency, the concentrations of these constituents are often used as water quality parameters. The partitioning of these constituents

into particulate and dissolved components are adopted for convenience from an optical point of view. It is important to note here that particulate matter includes phytoplankton, also know as *seston*, whereas the particulate matter without the phytoplankton component is called *tripton*. The final optical breakdown of water and its components are: pure water (W), gelbstoff (Y), phytoplankton (P), particulate matter (X) and are discussed in detail below.

3.2.2   Optically active constituents

Current interest in remote sensing is directed towards measuring the absorption and scattering due to the various particulate and dissolved substances in a given water sample. To quantify the role of individual components from each of the constituents *in situ* measurements and/or collection of water samples for subsequent laboratory analyses are required.

Pure water

Light absorption by pure water has been well documented by Pope and Fry (1997), Smith and Baker (1981), and most recently by Buiteveld et al. (1994) and Hakvoort (1994). Scattering is inversely proportional to wavelength, and therefore pure water has a blue colour (Figure 3.2). At 680 nm, a one metre thick layer of pure water will absorb about 35% of the incident light. There are absorption shoulders at $610-620$ nm and $660-670$ nm. Absorption of pure water ($a_W(\lambda)$) and scattering of pure water ($b_W(\lambda)$) can be considered constant to environmental conditions, except for a slight temperature dependent absorption peak in the near infrared (NIR).

Phytoplankton pigments

One of the most optically interesting organic matter are algae, also called phytoplankton (P). They occur in different shapes and sizes and form the basis of trophic interaction in lakes (Wetzel, 2001). Chlorophyll-a concentrations are often used as a proxy for phytoplankton concentration, as chlorophyll occurs in all photosynthetic organisms. Chlorophyll concentration (in milligram of chlorophyll per cubic metre of water) usually refers to the sum of chlorophyll-a and the related pigment phaeophytin-a, often simply called pigment concentration. The specific coefficients of absorption and scattering of algae are estimated relative to chlorophyll concentration. Phytoplankton pigments are strong absorbers of visible light and therefore play a major role in determining the absorption properties of natural waters. Algal pigments strongly absorb light in the blue and red wavelengths (peaking at $\lambda \sim 438$ nm and
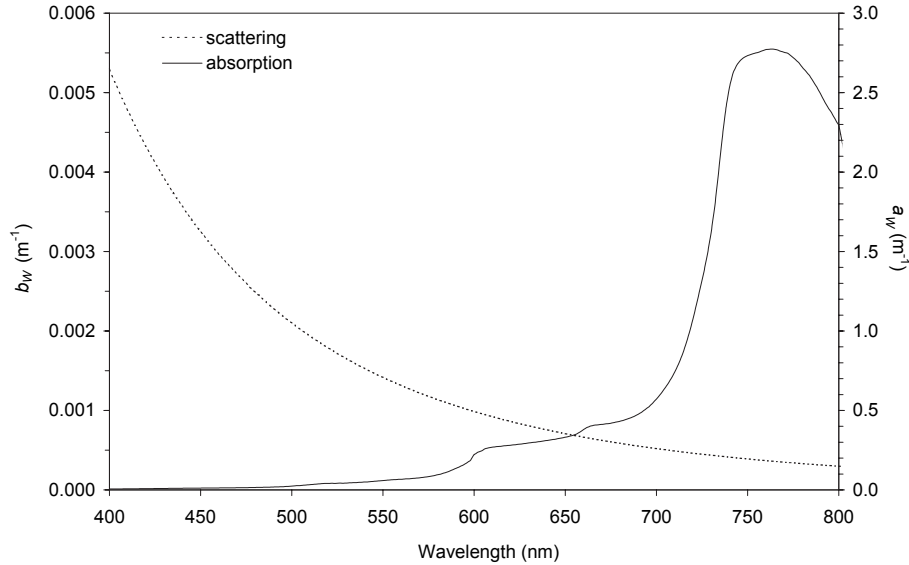
Figure 3.2: Absorption $a_W(\lambda)$ and scattering coefficient $b_W(\lambda)$ of pure water at a temperature of $T = 20$°C after Buiteveld et al. (1994).

$\lambda \sim 676$ nm for chlorophyll-a, 480 nm for β-carotene, 624 nm for cyanophycocyanin (CPC), 565 nm for cyanophycoerythrin (CPE)). Absorption by algae is negligible beyond 720 nm (Dekker, 1993). The specific absorption coefficient of phytoplankton, denoted $a_{ph}^*(\lambda)$, is the absorption coefficient of a phytoplankton suspension corresponding to a concentration of 1 mg Chl-a m^{-3} or (μg Chl-a/l). It is expressed in m^2 mg^{-1} Chl-a(m^{-1}/mg Chl-a m^{-3}). The specific absorption coefficient depends on the algal species that make up the phytoplankton population and their physiological state, and can therefore vary with time and space. Specific cyanobacteria are nuisance organisms, potentially forming toxic substances and can be eutrophication indicators. A general trend has been found that phytoplankton populations that are found in oligotrophic waters have higher specific absorption coefficients than phytoplankton in eutrophic waters (Package effect)(Kirk, 1994).

Gelbstoff

Gelbstoff (Y) is the optical constituent of water that passes through a 0.2 μm filter. Backscattering of gelbstoff is assumed to be zero. Dissolved organic compounds are produced during the decay of organic decay products and consist mostly of humic and fulvic acids. The compounds are generally brown in colour and for this reason are referred to as yellow substance (Bricaud et al., 1981), coloured dissolved organic matter (Cdom), or gilvin (Kirk, 1976). Gelbstoff may have a local origin or come from a distant source (Sathyendranath, 2000).
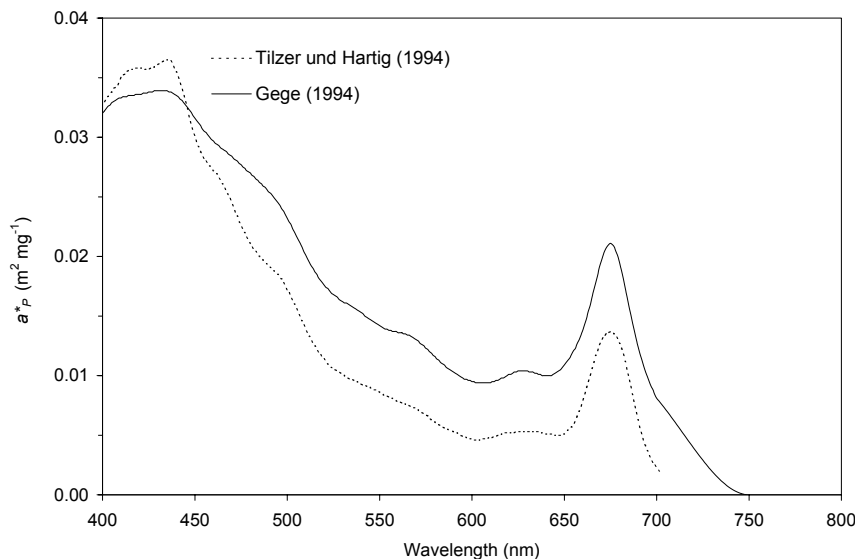
Figure 3.3: Specific absorption coefficient of phytoplankton after Heege (2000).

It absorbs very little in the red wavelengths, but its absorption increases rapidly with decreasing wavelength and can be significant at blue and ultraviolet wavelengths. Gelbstoff can efficiently remove blue light in the top few cm's of the water column, imparting a yellow colour to the water. It can influence the UV inhibition of primary production due to its strong absorption in this region of the spectrum (Figure 3.4). From the remote sensing perspective, this parameter is interesting as it can influence the determinability of other water quality parameters. The absorption coefficient of dissolved organic matter follows approximately an exponentially decreasing function, often expressed as:

$$a_Y\left(\lambda\right) = a_Y\left(\lambda_0\right) \cdot e^{-S_Y(\lambda-\lambda_0)} \qquad \left(\mathrm{m}^{-1}\right) \tag{3.2}$$

where $a_Y\left(\lambda_0\right)$ is the absorption due to gelbstoff at a reference wavelength λ_0, usually at 440 nm, and S is the slope of the function usually varying between 0.01 and 0.02 (Dekker, 1993)($S = 0.0142 \pm 0.0012$ nm^{-1} for Lake Constance (Gege, 2000)).

Suspended particles

Particulate matter (X) can be divided into living organic material (mainly phytoplankton), non-living organic particles (*detritus*) and inorganic material. The sum of dead organic and inorganic components is referred to as *tripton*, thus, it includes particulate material that is not phytoplankton. It can serve as a vehicle for toxic anthropogenic substances, and is one main source of aggradation of lakes as it determines the sedimentation rate. It

makes an impact on primary production because it can lower the eutrophic depth[1] due to its scattering and absorption properties. Additionally, it can have consequences on both the fish and macrophyte distributions in lakes. Inorganic particles are due to suspended minerals coming from inflows and are mainly consisting of quartz, clay and calcite. Inland water bodies are regions where particulate matter often plays an important role in determining the optical properties of the water (Sathyendranath, 2000). In general, the absorption of the total suspended matter absorption is very low and mainly due to the organic fraction of the particles (detritus). The spectra often resemble gelbstoff spectra (Dekker, 1993) (Figure 3.4). This suggests that the absorption is high at short wavelengths and decreases exponentially to be close to zero at longer wavelengths. If the mineral particles are strongly coloured however, the suspended matter absorption is also a function of the mineral particles. The discrimination between phytoplankton, detritus and inorganic particle is generally not trivial (Bricaud and Stramski, 1990). Due to close correlation to phytoplankton, in this study the absorption of organic particulate matter is treated as part of specific absorption of phytoplankton (Gege, 1994; Heege, 2000).

Total spectral absorption The influence of phytoplankton pigment absorption on the reflected radiance is often masked by absorption of gelbstoff and detrital material, especially in the blue wavelengths (Figure 3.4). The combined absorption of the gelbstoff, phytoplankton, suspended matter and the pure water spectrum suggest that at short wavelengths, gelbstoff, suspended matter, and the first chlorophyll-a absorption peak causes high absorption. For this reason, low reflectances are observed in this spectral area. Beyond 500 nm, the spectral information becomes less ambiguous and reflectance increases allowing better discrimination of spectral features. The lowest absorption values occur at 550 to 600 nm, at 650 nm, and at 705 nm coincident with maxima in reflectance. It is also evident from the specific absorption spectra that water absorption is the single most dominant absorbing factor beyond 720 nm.

Total spectral scattering Scattering of natural waters is considered to consist of two different contributions, pure water (b_W) and particulate matter (b_X). Scattering of gelbstoff is assumed to be zero. The particle scattering can be specified by a power law as defined by Maffione and Dana (1997). The shape of the scattering spectrum is mainly a function of size distribution of the particles. An increased scattering of a water body is closely correlated to an increase in particulate matter concentration.

---

[1] The depth where photosynthesis = respiration
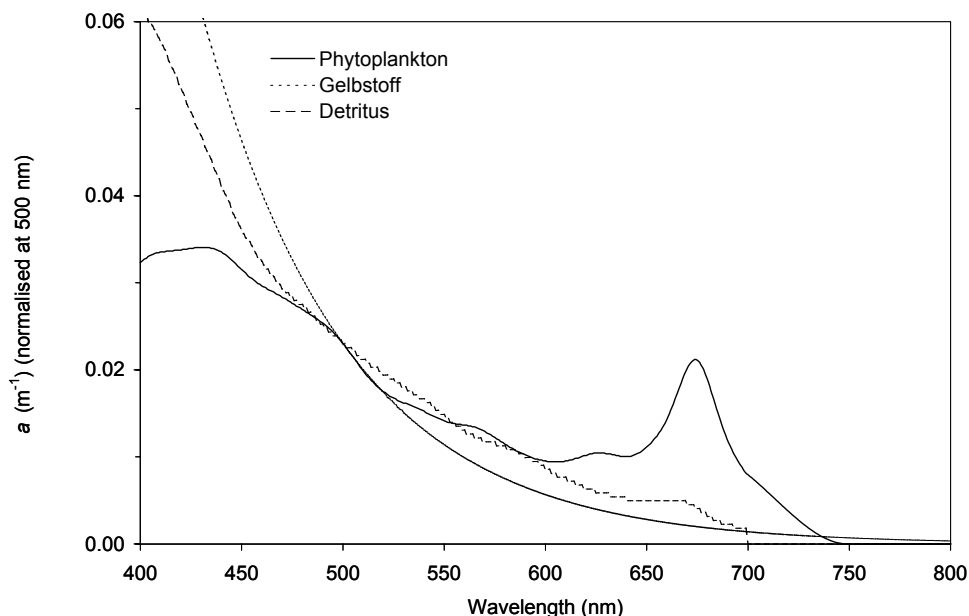
Figure 3.4: Absorption of phytoplankton, gelbstoff and detritus, spectra were normalised to specific phytoplankton absorption $(0.023\,\mathrm{m}^{-1})$ at 500 nm after Heege (2000).

3.2.3   The inherent optical properties

The relevant inherent optical properties (IOP) are the spectral absorption and scattering coefficients. The spectral absorption coefficient $a(\lambda)$ is the fraction of incident power at wavelength λ, that is absorbed per unit distance, in the medium. The spectral scattering coefficient $b(\lambda)$ is the fractional part of the incident power per unit distance that is scattered out of the beam. Together $a(\lambda)$ and $b(\lambda)$ form the spectral beam attenuation coefficient $c(\lambda)$:

$$c(\lambda) \equiv a(\lambda) + b(\lambda) \qquad (\mathrm{m}^{-1}) \qquad (\text{Mobley, 1994}) \tag{3.3}$$

The way in which scattering affects the penetration of light into the medium depends not only on the value of the scattering coefficient, but also of the angular distribution of the scattered flux resulting from the scattering process. Scattering influences the light budget of the medium by changing the direction of photon propagation. This angular distribution has a characteristic shape and is specified in terms of the volume scattering function, i.e. elastic scattering. Scattering can be partitioned into elastic and inelastic processes. Elastic scattering is the process where the wavelength and frequency of the scattered photons remain unaltered, whereas inelastic scattering implies a change in the wavelength and frequency (Dekker et al., 2001). Two types of inelastic scattering are Raman scattering and fluorescence.

3.2.4 Specific absorption and backscattering coefficients

Inherent optical properties are additive parameters, which means that the absorption and the scattering coefficients are proportional to the concentration. To quantify individual absorption components, the absorption coefficient $a(\lambda)$ can be expressed as the sum of contributions from each of the constituents (see Eq.3.4). The contribution of each of the four components (phytoplankton, suspended matter, gelbstoff and water itself) can be determined from the product of the concentration of that substance and a corresponding specific absorption coefficient (Sathyendranath, 2000). This equation can be written as:

$$a(\lambda, T) = a_W(\lambda, T) + pa^*{}_P(\lambda) + ya^*{}_Y(\lambda) + xa^*{}_X(\lambda) \tag{3.4}$$

where a_W, $a^*{}_P$, $a^*{}_Y$, $a^*{}_X$ are the specific absorption coefficient of water (W), phytoplankton (P), gelbstoff (Y) and suspended matter (X) respectively. In the notation used here, the asterisks indicate specific coefficients, T is the dependence on the temperature, and p, y, x stand for the corresponding concentrations.

To quantify individual backscattering components, the backscattering coefficient $b_b(\lambda)$ can be expressed as the sum of contributions from each of the constituents (see Eq.3.5).

$$b_b(\lambda, T) = b_{bW}(\lambda, T) + pb^*_{bP}(\lambda) + xb^*_{bX}(\lambda) \tag{3.5}$$

where b_{bW}, b^*_{bP}, b^*_{bX} are the specific scattering coefficients of water (W), phytoplankton (P) and suspended matter (X) respectively.

Equations 3.4 and 3.5 are clearly multivariate in nature, and if a and b_b are known in concert with p, y, and x, then the IOPs can be estimated. Similarly, if a and b_b are known in concert with the IOPs, then p, y, and x can be estimated. This is the reason for determining the concentrations of the different components in natural waters by measurements of the inherent optical properties and thus, for a mechanistic approach in remote sensing. These determinations comprise the directives of the so-called bio-optical algorithms and water quality parameter extraction methodologies (Dekker et al., 2001).

3.2.5 Radiometric variables and apparent optical properties

The optical variable measured by most passive optical remote sensing instruments is radiance L. From radiance, a number of other radiometric quantities can be derived, such as the downwelling and upwelling irradiances. Apparent optical properties are those that depend both on the medium and the geometric structure of the ambient light field, and display sufficient regular features and stability to be useful descriptors of a water body (Mobley, 1994).

Because AOPs are relatively stable, it is relatively easy to relate them to the water composition in comparison to (ir)radiance measurements. In particular, the reflectance just below the surface $R(0-)$, and the diffuse attenuation coefficient for downwelling light K_d, are very suitable, as they are sensitive to changing water compositions.

Radiometric variables

Spectral radiance is the fundamental radiometric quantity of interest in hydrologic optics providing the foundation from which all other radiometric quantities can be derived, and describes the spatial ($\vec{x}$), temporal (t), directional($\vec{\xi}$), and wavelength (λ) structures of the light field. Spectral radiance L is the radiant energy $\Delta\Phi$, within the unit solid angle that enters a sensor and is incident upon a detector element of area ΔA within time Δt and over a wavelength band $\Delta\lambda$; ∂ is the partial derivative (Eq.3.6). Descriptions and definitions of the spectral radiometric variables are, where Ξ is within the unit sphere, the set of all directions **s** with solid angle $d\Omega$ and the cosine μ of the zenith angle to the horizontal plane (Dekker et al., 2001).

$$L(\vec{x}, t, \vec{\xi}, \lambda) \equiv \frac{\partial^4 \Phi}{\partial t \partial \Omega \partial A \partial \lambda} \qquad (\text{Wm}^{-2}\text{sr}^{-1}\text{nm}^{-1}) \qquad (\text{Mobley, 1994}) \qquad (3.6)$$

Irradiance E is defined as the radiant flux per unit area of a surface (Kirk, 1994). The downwelling irradiance E_d is the irradiance of the upper hemisphere (Eq.3.7).

$$E_d = \int_{\Xi_d} \mu L(\mathbf{s}) d\Omega \qquad (\text{Wm}^{-2}\text{nm}^{-1}) \qquad (\text{Mobley, 1994}) \qquad (3.7)$$

The upwelling irradiance E_u is the irradiance of the lower hemisphere (Eq.3.8).

$$E_u = \int_{\Xi_u} |\mu| L(\mathbf{s}) d\Omega \qquad (\text{Wm}^{-2}\text{nm}^{-1}) \qquad (\text{Mobley, 1994}) \qquad (3.8)$$

The scalar irradiance E_0 is the integral of the radiance distribution at a point over all directions about the point. Scalar irradiance is thus a measure of the radiant intensity at a single point which treats radiation from all directions equally (Eq.3.27).

$$E_0 = \int_{\Xi} L(\mathbf{s}) d\Omega \qquad (\text{Wm}^{-2}\text{nm}^{-1}) \qquad (\text{Mobley, 1994}) \qquad (3.9)$$

In biological studies the relevant measure of the underwater light field is in terms of photosynthetically active radiation (PAR), the light within $400-700\,\text{nm}$ utilised by plants for photosynthesis. Since photosynthesis is a quantum process, it is the number of available photons rather than their total energy that is relevant to the chemical transformation. The light requirement for the production of a given quantity of oxygen is a fixed number of photons[2],

---
[2]   nine einsteins per mole of oxygen formed

(Kirk, 1994; Mobley, 1994). PAR can be calculated using E_0 (Eq.3.27). To retrieve the number of photons, $E_0(\lambda)$ is divided by the energy of the light hc/λ, where h is Plancks constant, c is light velocity and Einst is the number of photons[3]

$$PAR = \int_{400nm}^{700nm} \frac{\lambda}{hc} E_0(\lambda) \, d\lambda \qquad (\mu\text{Einst m}^{-2}\text{s}^{-1}) \qquad (\text{Mobley, 1994}) \qquad (3.10)$$

Apparent optical properties

Irradiance reflectance R is the ratio of upwelling and downwelling irradiance at a given point and is defined as:

$$R(z) \equiv \frac{E_u(z)}{E_d(z)} \qquad (3.11)$$

Subsurface irradiance reflectance $R(0-)$ is the irradiance reflectance just below the water surface. Optical models for subsurface reflectance have been developed which can be related to remote sensing reflectance measured from (far) above the water surface. $R(0-)$ plays an important intermediate role in many remote sensing applications on water quality:

$$R(0-) \equiv \frac{E_u(z = 0)}{E_d(z = 0)} \qquad (3.12)$$

The radiance reflectance $R_L(\theta, \phi)$ is defined as:

$$R_L(\theta, \phi) = \frac{\pi L_u(\theta, \phi)}{E_d} \qquad (3.13)$$

The remote sensing reflectance $R_{rs}(\theta, \phi)$ makes use of upwelling radiance rather than irradiance and is defined as:

$$R_{rs}(\theta, \phi) = \frac{L_u(\theta, \phi)}{E_d} \qquad (\text{sr}^{-1}) \qquad (3.14)$$

A proportionality factor Q relates remote sensing reflectance R_{rs} to irradiance reflectance $R(z)$, and is defined as the ratio of upwelling irradiance to upwelling radiance:

$$Q(\theta, \phi) = \frac{E_u}{L_u(\theta, \phi)} \qquad (\text{sr}) \qquad (3.15)$$

The downwelling and upwelling average cosine $\bar{\mu}_d$ and $\bar{\mu}_u$ describe the angular distribution of the photons that have been scattered downwards and upwards at a depth z and are defined as:

$$\bar{\mu}_d \equiv \frac{E_d}{E_{0d}} \qquad (3.16)$$

---

[3]   1 Einst corresponds to one mole of photons. The number of photons in an einstein is Avogadro's number $(6.023 \ 10^{23}$ photons). It is named in honour of Albert Einstein, who explained the photoelectric effect and introduced the idea of light quanta, now called photons (Einstein, 1910).

$$\bar{\mu}_u \equiv \frac{E_u}{E_{0u}} \tag{3.17}$$

If the relevant optical lake water constituents were uniformly distributed in the water column, then the downwelling irradiance would decrease exponentially with depth. The vertical diffuse attenuation coefficient of downwelling irradiance K_d defines the rate of decrease of downwelling irradiance with depth z:

$$K_d = \frac{d \ln E_d}{dz} = -\frac{1}{E_d}\frac{dE_d}{dz} \qquad (\text{m}^{-1}) \tag{3.18}$$

The vertical diffuse attenuation coefficient for upwelling irradiance K_u defines the rate of exponential decrease in upwelling irradiance with decreasing depth z. K_u is approximately K_d for a infinitely deep water column (Kirk, 1989).

$$K_u = \frac{d \ln E_u}{dz} = -\frac{1}{E_u}\frac{dE_u}{dz} \qquad (\text{m}^{-1}) \tag{3.19}$$

In shallow water systems κ is the vertical diffuse attenuation coefficient for $E_u(z)$, where the flux scattered upwards from a thin layer of water with depth z and is combined with bottom albedo (Kirk, 1994). $\kappa(z)$ is always $> K_d$ and to a reasonable approximation is $\kappa \sim 2.5 \cdot K_d$ in the middle of the photic zone.

Another parameter related to K_d is optical depth ξ, which can be used to define the depth at which photosynthesis occurs. The optical depth ξ is defined by:

$$\xi = K_d \cdot z \tag{3.20}$$

Optical depths of particular interest to limnologists concern primary productivity, and correspond to the attenuation of downward irradiance to 10% and 1% of the surface values. These are $\xi = 2.3$ and $\xi = 4.6$, respectively. These optical depth correspond to the midpoint and the lower limit of the photic zone, within which significant photosynthesis occurs (Wetzel, 2001).

3.2.6   The diffuse apparent optical properties

An intermediate set of optical properties, called diffuse apparent optical properties, describe absorption and scattering of downwelling and upwelling irradiance. These properties are used primarily for mathematical convenience in analytical model derivations (Dekker et al., 2001).

3.3   Relationships between IOPs and AOPs

3.3.1   Optically deep waters

Inherent optical properties are physically related to the subsurface irradiance reflectance $R(0-)$ which is a key parameter of the remotely sensed irradiance data. $R(0-)$ is relatively

stable under varying solar angles, atmospheric conditions and water surface states. A number of approximate relations among various IOPs and AOPs have been developed over the years, based on radiative transfer theory combined with analysis of actual data or numerical simulations. In order to arrive at an analytical solution of the radiative transfer equations, three important assumptions were made (Mobley, 1994). First, that the water is optically deep, such that bottom effects are negligible. Second, inelastic scattering, especially fluorescence, is not taken into account. Last, that the absorption and scattering coefficients (inherent optical properties) are homogenously distributed, i.e. constant with depth. In such cases, the use of simple formulas (Eq.3.21) are justified. However, if a and b_b do not covary with depth, the prediction of $R(0-)$ requires detailed calculations based on the RTE (Mobley, 1994).

The relationships between subsurface irradiance reflectance R(0-) and the inherent optical properties for ocean (Gordon et al., 1975; Aas, 1987), coastal (Kirk, 1991; Walker, 1994), and inland water systems (Dekker et al., 1997) have been investigated. Dekker et al. (2001) recommend using the following reflectance model by Walker (1994), as it has the least assumptions and is easiest to use in simulations. Even though this model contains approximations, it may be expected to yield quite accurate results for turbid waters. In terms of the backscattering and absorption coefficients, the analytical model for irradiance reflectance can be written as:

$$R_\infty(0-) = f \frac{b_b}{a + b_b} \qquad \text{where} \qquad f = \frac{1}{1 + \frac{\mu_d}{\mu_u}} \tag{3.21}$$

f is a coefficient for the anisotropy of the light field and is likely to fall within a range of 0.33 to 0.38.For Lake Constance Albert and Gege (2006) derived a coefficient of 0.38 for a given concentration of suspended matter $C_X = 1mg/l$.

A parameterisation for remote sensing reflectance $R_{rs}(\theta, \phi)$ (Eq 3.14) can accordingly be calculated after Albert and Mobley (2003), which incorporates sun-angle effects, using following relationship:

$$R_{rs,\infty}(0-) = f_{rs} \cdot \frac{b_b}{a + b_b} \tag{3.22}$$

where

$$f_{rs} = 0.015 \cdot (1 + 4.6659 \cdot \omega_b - 7.8387 \cdot \omega_b^2 + 5.471 \cdot \omega_b^3) \cdot \left(1 + \frac{0.1098}{cos \cdot \theta'_{sun}}\right) \cdot \left(1 + \frac{0.04021}{cos \cdot \theta'_v}\right)$$

Parameters of f_{rs} are $\omega_b = b_b(\lambda)/(a(\lambda) + b_b(\lambda))$, the sun-zenith angle in water, θ'_{sun}, and the viewing angle in water θ'_v (Albert and Mobley, 2003).

3.3.2 Optically shallow water

In contrast to optically deep waters, optically shallow waters are those where the substrate (e.g. submerged macrophytes and sandy bottoms in lakes) signal is detectable through the

water column by a remote sensor. If remote sensing data are analysed including optically shallow waters, the bottom depth z_B and the bottom albedo A have to be taken into account.

In optically shallow waters the upwelling irradiance just below the water surface $E_u(0-)$ is the sum of the flux backscattered by the water column $E_u(0-)_W$ (as if the bottom were black) added to the flux reflected by the bottom $E_u(0-)_B$(when it is not black), so that (Lee et al., 1998a):

$$E_u(0-) = E_u(0-)_W + E_u(0-)_B \qquad (3.23)$$

The first term in Eq.3.23 corresponds to the photons that have not interacted with the bottom, whereas those that have interacted with the bottom at least once form the second term.

Different authors (Maritorena et al., 1994; Philpot, 1987) have formulated approximations of the irradiance reflectance for shallow water. Their equation result from a two-flow approximation including the bottom influence:

$$R = R_\infty(1 - \mathrm{e}^{-2Kz_B}) + A\mathrm{e}^{-2Kz_B} \qquad (3.24)$$

where R_∞ is the subsurface irradiance reflectance over a hypothetical optically deep water column, A is the bottom albedo, z_B is the bottom depth, and K is the diffuse attenuation coefficient of the water column and is equal for the downwelling and upward directions. According to Lee et al. (1998b), this equation can be transformed to the remote sensing reflectance R_{rs}:

$$R = R_{rs,\infty}(1 - \mathrm{e}^{-2Kz_B}) + \frac{A}{\pi}\mathrm{e}^{-2Kz_B} \qquad (3.25)$$

Equation 3.24 is an analytical formula expressing the reflectance of shallow waters as a function of observation depth, bottom depth, and albedo. This equation also involves two apparent optical properties of the water body: a mean diffuse attenuation coefficient and a hypothetical reflectance, which would be observed if the bottom was infinitely deep. This equation expresses the $E_u(0-)_C$ as a function of the reflectance of an infinitely deep water column, the vertical attenuation coefficients, and the irradiance reflectance of a substrate. It shows how different reflecting substrates contribute to the reflectance observed on a water surface. Assuming a substrate (e.g. sand) reflects more than the signal coming from the water column, R_∞, the signal from the substrate is added to the water column reflectance resulting in an increased reflectance on the water surface. If the bottom is darker (e.g. *Potamogeton pectinatus*), the reflectance on the water surface decreases. In case of a similarly reflecting bottom target, the reflectance from the water column and from the substrate are more or less at equilibrium and subsurface reflectance becomes nearly zero. Nevertheless,

some characteristic differences between water body and bottom types (e.g. macrophytes, corals, red algae, sediment) do exist (Fyfe, 2004).

However in reality the diffuse attenuation coefficient of the upwelling and downwelling light is not equal. A more accurate expression is derived by Lee et al. (1998b, 1999), where the effective attenuation coefficient is divided into a upwelling and a downwelling part. The upwelling part distinguishes between radiation from the water column (W) and from the bottom (B). This results in the following equation:

$$R = R_\infty \left(1 - e^{-(K_d + K_{u,W})z_B}\right) + Ae^{-(K_d + K_{u,B})z_B} \tag{3.26}$$

An new analytical parameterisations of irradiance reflectance and the remote sensing reflectance in deep and shallow waters were developed by (Albert and Mobley, 2003; Albert, 2004). The new model separates the dependencies on inherent optical properties, wind speed, viewing, and solar zenith angle to obtain an invertible equation for remote sensing data. Additionally, a new parameterisation for the upward diffuse attenuation coefficient was developed. The Parameterisation of irradiance reflectance was used in the following analysis.

$$R = R_\infty \cdot \left[1 - C_1 \cdot \exp\left\{-\left(\frac{\kappa_0}{cos\,\theta_s} + \left(1 + \frac{b_b}{a + b_b}\right)^{\kappa_{1,W}} \cdot \left(1 + \frac{\kappa_{2,W}}{cos\,\theta_s}\right)\right)(a + b_b)z_B\right\}\right]$$
$$+ C_2 \cdot A \cdot \exp\left\{-\left(\frac{\kappa_0}{cos\,\theta_s} + \left(1 + \frac{b_b}{a + b_b}\right)^{\kappa_{1,B}} \cdot \left(1 + \frac{\kappa_{2,B}}{cos\,\theta_s}\right)\right)(a + b_b)z_B\right\} \tag{3.27}$$

where C_1 and C_2 are additional coefficients introduced to adapt the equations to the simulated situations, A is the bottom albedo, z_B is the bottom depths, and four coefficients $\kappa_{1,W}$, $\kappa_{2,W}$, $\kappa_{1,B}$, $\kappa_{2,B}$ for upward and downward diffuse attenuation coefficient from the water column W and the bottom B were determined.

Chapter 4

Experimental Description

This chapter describes the study sites, the *in situ* methods of optical measurements by submersible instruments, and the water sample analysis protocols used in optical modelling and for validation of classification results. A description of remote sensing and field data is followed by presentation of analysis tools used, and pre-processing steps of the field and remote sensing data are demonstrated in the last section.

4.1 Description of study areas

Two sites in two different lakes were selected for investigating submerged macrophyte mapping potential using hyperspectral HyMap data (Figure 4.1): the Lower Lake (Constance) (Figure 4.2) and Karpfenwinkel at Lake Starnberg (Figure 4.3, Table 4.1). These test sites were chosen because of their size, water depth, and similar abundance of dominant macrophyte species. The Lower Lake (Constance) is ideal for testing remote sensing applications as it has very shallow littoral area and large patches of macrophytes in high diversity combined with clear water and high visibility ($6 - 7\,\text{m}$). In contrast, the shallow areas at Karpfenwinkel (Lake Starnberg) are turbid, contain high epithetic growth, and have sparse, patchy macrophytes and thus is sub-optimal for remote sensing. Choosing one 'optimal' and one 'sub-optimal' test site allows the investigation of the potentials and limits of hyperspectral mapping in shallow lake water habitats.
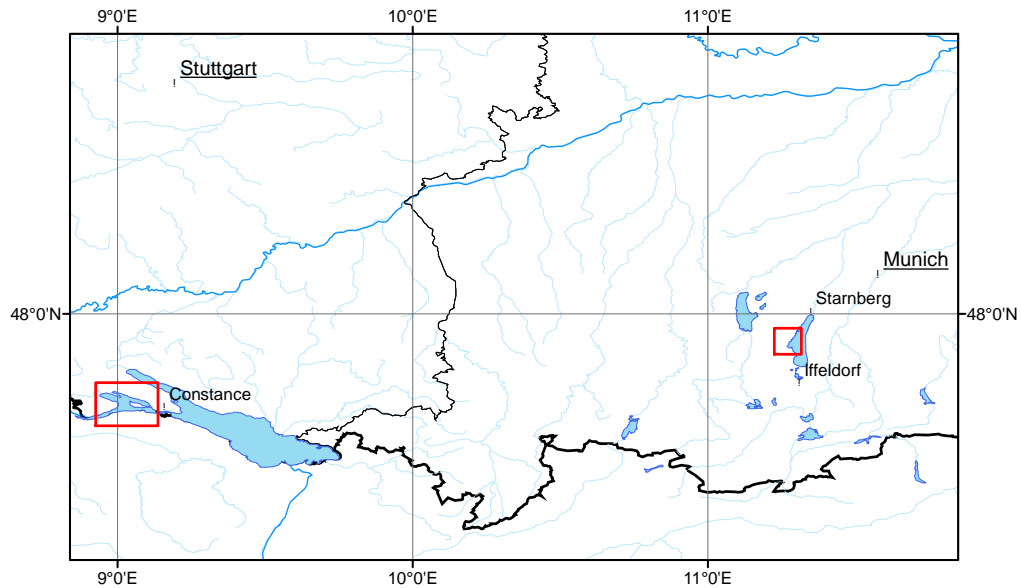
Figure 4.1: Geographical location of study sites Lake Constance and Lake Starnberg

Table 4.1: Limnological parameters of the investigated lakes (LAWA, 1985)

	Lake Constance Lower Lake	Lake Starnberg
Altitude above sea level	395 m	584 m
Area	63 km^2	56 km^2
Maximum depth	46 m	128 m
Average depth	13 m	53 m
Catchment area	11 454 km^2	315 km^2
Water exchange time	4 weeks	21 years
Secchi depth [m]	4.4	7.2
Mix type	di-holomictic	monomictic
Trophic state[1]	oligo-mesotrophic	mesotrophic
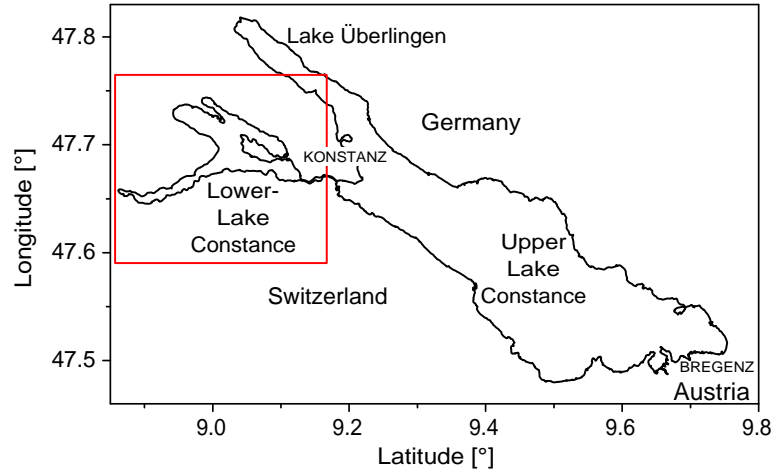
Figure 4.2: Map of location of Lower Lake Constance (Bodensee)

4.1.1 Lake Constance

Lake description and climate Lake Constance (german: *Bodensee*) lies at the southern border of Germany, adjacent to Switzerland and Austria (47° 35′ N, 9° 25′ E). This freshwater lake is 395 m above sea level and is the second largest pre-alpine European lake (after Lake Geneva) both by area and volume, covering approximately 539 km^2 (shoreline of around 273 km) and containing approximately 55 km^3 (IGKB, 2002).

The lake is warm-monomictic, with its holomixis in late February or March, at a temperature of 4 ℃The Rhine river is importing significant amounts of mineral particles. There are several communities surrounding the lake, including Lindau, Friedrichshafen, Bregenz and the city of Constance, with approximately 2.2 million residents. Due its important role of drinking water source for about 4.5 million people, public interest and water quality monitoring is a high priority.

The lake is sub-divided into three parts: the south-east main basin *Upper Lake* (*Obersee*) is the largest (472 km^2) and deepest basin (252 m). The fjord-like appendix to the north-west is the *Überlinger See* (61 km^2). The shallow Lower Lake *Untersee* (63 km^2) located to the south-west, is the test site examined here. The climate around Lake Constance is moderate-warm because of moderating influence of the lake. Monthly mean temperatures for the city

---

[1] **Oligotrophic**: natural lake with low concentration on chlorophyll and nutrients($<$ 10 $\mu g[P]$); **Mesotrophic**: higher concentration on chlorophyll and nutrients, (10–30 $\mu g[P]$); **Eutrophic**: very high concentration of chlorophyll and nutrients $>$ 30 $\mu g[P]$

of Constance between 1982-2004 vary from 19.9 ℃ (July) to 0.9 ℃ (January). The mean annual precipitation is approximately 833 mm (1982-2004).

Hydrographic characters   The lake basin was occupied by the Rhine glacier about 30 000 years BP and at the end of this glaciation, ca. 15 000 years ago, its area was more than twice its present size, including large parts of the Rhine Valley and both Lakes Walen and Zurich. Today surrounding catchment drains an area of approximately 11 500 km^2 resulting in an annual water budget of about 12 km^3 and a water residence time of 4 to 5 years. The Rhine river is the main tributary contributing 75 % of the total inflow from the southeast (near Bregenz) through the Upper Lake (Obersee), past the city of Constance, and drains westward through the Lower Lake (Untersee) near Stein am Rhein. Due to its alpine origin, the river carries abundant inorganic suspended particles into the eastern part of Lake Constance. Other inflows, such as these from the northern part of the catchment, influence the lake chemistry because of agricultural landuse. The Schussen River, for example, stands out with its high loads of organic yellow substances, nitrates, and phosphates likely derived from fertilisers.

Physical/chemical/biological properties   In its natural state, Lake Constance was a typical oligotrophic pre-alpine lake with low concentrations of nutrients, low densities of phytoplankton, high water transparency, and high hypolimnic oxygen concentrations (von Grafenstein et al., 1992). With an increase in human population and fundamental changes in the economy and human social behaviour, the trophic state of the lake deteriorated over the past decades. By the end of the 1970s water quality had decreased to a eutrophic state, however due to sewage diversion and waste water treatment in the catchment area the lake is recovering. The chlorophyll concentration at the end of the 1970s was approximately 80 μgl^{-1}, whereas at present their concentrations range from 0.5 μgl^{-1} in winter to 30 μgl^{-1} in spring (Bäuerle and Gaedke, 1998; Häse et al., 1998). In summer between June and October concentrations can vary typically between 5 and 15 μgl^{-1}. The average current annual primary production rate is around $200 - 300g\,Cm^{-2}y^{-1}$ (Häse et al., 1998). The concentration of suspended particles lies between 0.3 and 10 mgl^{-1}, but can also be higher next to the Rhine delta. Variations in dissolved organic carbon (Cdom) are comparatively low, ranging between $1 - 1.8$ mgl^{-1}. Information regarding spatial variabilities in the concentrations of water optical properties suggest large differences, varying by a factor of $2 - 5$ times for phytoplankton and suspended matter (Heege et al., 1998). The lakes flora is comprised of emergent macrophytes such as *Phragmites communis*, and submerged macrophytes, such as *Najas marina*, *Chara aspera*, *C. contraria* and *C. tomentosa*. In deeper areas $(1.5 - 4\,\text{m})$ fairly dense patches of *P. pusillus*, *P. perfoliatus*, *P. pectinatus* are found. Since 1959, the
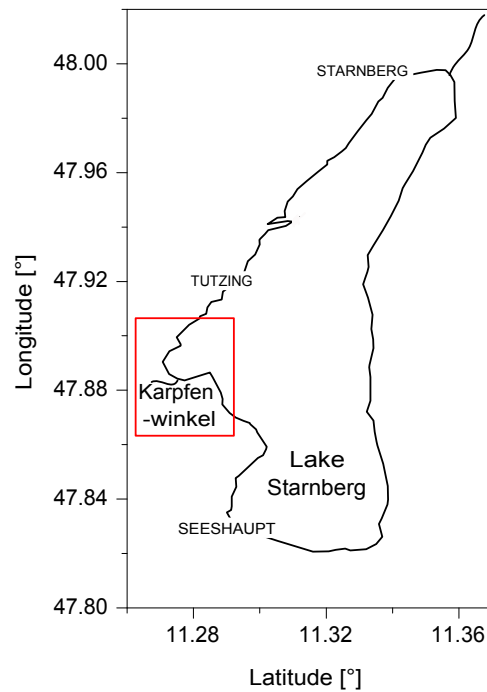
Figure 4.3: Map of location of the study site Karpfenwinkel in the west at Lake Starnberg

IGKB[2] has been responsible for the protection and observation of the lake. The Wollmatinger Ried nature reserve next to Reichenau Island in the Lower Lake, is a wetland area of reeds which is used by many birds for the stop-over during their annual migration.

4.1.2 Lake Starnberg

Lake description and climate Lake Starnberg (german: *Starnberger See*) is located 20 km north of the northern periphery of the Alps ($47°48'$ N, $11°20'$ E). The lake lies at 596 m above sea level and has a maximum depth of 127 m (average depth 54 m). Its volume is about 2.998 km^3 and covers approximately 56.36 km^2 with a shoreline length of around 49 km (approx. 21 km from north to south, average width is approx. 2.8 km).

Surrounding settlements are mostly rural with Starnberg (located at the lake outlet) being the largest city with 17 000 inhabitants. As Munich, the capital of Bavaria with a population of 1.2 million, is situated nearby (15 km), the area is frequented for recreation activities. Towns by the lake are Seeshaupt in the south and Tutzing in the west. The climate may be described as temperate, having a July mean temperature of 16.8℃ and -2.2℃ in January (measured in the period of 1931–1980 in Starnberg). The mean annual

---

precipitation is approximately 1101 mm (1931–1980).

Hydrographic characters   The $314.7 \, km^2$ catchment area is 5.6 times as large as the lake itself. The water residence time is about 21 years as only a few small rivers flow into the lake, the largest of which stems from the Osterseen, a chain of oligotrophic groundwater fed lakes on its southern end. The lake basin was occupied by the *Isar-Loisach-Glacier* glacier during the last glacial period some 15 000 - 20 000 years ago. It has a single, small island, the Roseninsel, and a single outlet at the northern end, the Würm River.

Physical/chemical/biological properties   The originally oligotrophic lake has been influenced by developments, more specifically by nutrient loading (Alefs, 1997). The installation of a circular sewer line system from 1964 to 1976 and a treatment plant at the lake outlet improved the water quality such that Lake Starnberg can now be called mesotrophic with a tendency to oligotrophic. Because of its limited inflow, there is a certain danger of eutrophication. The thermocline formation may be described as dimictic with complete turnover in spring and fall (Schaumburg, 1996). Present chlorophyll concentrations range from 2.4 to $4.8 \, \mu g \, l^{-1}$ in winter, and in summer (July to October) range typically between 6 and $12 \, \mu g \, l^{-1}$. The average annual primary production rate is around $889g \, C m^{-2} y^{-1}$. The concentration of suspended particles lies between 0.3 and $2 \, mg \, l^{-1}$, whereas variations of dissolved organic carbon (cdom) can range between 8 and $12 \, mg \, l^{-1}$. The lake flora is comprised of emergent macrophytes such as *Phragmites australis*, *Scirpus lacustris*, *Iris pseudacorus*, and submerged macrophytes such as *Chara contraria*, *Nitellopsis obtusa*, *Potamogeton perfoliatus* and *P. pectinatus* with a few patches of *C. intermedia*, *C. fragilis*, and *C. aspera*. The test site Karpfenwinkel lies in the south-west of the lake protected by a shallow, mesotrophic embayment where submerged macrophytes occur. Water depths are up to 4.5 m. Light coloured silt-mud and sand characterises the lake bottom material. The inflow from the south-east is the Rötlbach which greatly reduces water clarity within this meso-eutrophic bay.

4.2   Intruments and water samples

4.2.1   Biochemical *in situ* data

The mechanism of remote sensing is the measurement of absorption and scattering of light due to the various substrates, particulate and dissolved substances in a given water body. To quantify the role individual components have in determining a spectrum, water samples from different locations around the study sites for subsequent laboratory analysis were required. The major advantage to laboratory analyse of absorption is that it allows each component's

Figure 4.4: Filtration set up on the boat

absorption coefficient to be separated. The water samples were collected in shallow water (0.5 m water depth) with an opaque plastic bottle (1 l) and filtered immediately. Biochemical analyse for phytoplankton concentrations C_P, and total suspended matter C_X were performed by B. Beese and C. Gebauer[3]. Remote sensing and *in situ* measurements were undertaken during flight campaigns in 2003 and 2004.

Phytoplankton

Photometric determination of pigment concentrations were performed using the sum of chlorophyll-*a* and phaeophytin-*a*. Depending on (particulate matter) concentrations, a known water volume (0.5 to 2.0 l) was filtered after sampling using a glass fibre filter (Schleicher & Schuell No 6 VG[4]), retaining particles > ca. 1 μm. The samples were shaded from direct sunlight during filtration and were stored in dark, cool boxes. The filter samples were analysed immediately or were placed in a refrigerator at about -18 °Cfor later analyis. The pigments were extracted in the laboratory using hot ethanol (90 %) following a method described by Nusch (1980). Particulates were separated via centrifugation. Transmission through the pigment solution was measured in 10 cm cuvettes at 665 and 750 nm using a photometer. The

---

[3]   University of Konstanz, Limnological Institute, Mainauserstr. 252, 78464 Konstanz, Germany, mailto: baerbel.beese@uni-konstanz.de

[4]   Schleicher & Schuell, Hasthnestr. 3, 37582 Dassel, Germany, http://www.schleicher-schuell.de

750 nm value is used for turbidity correction of the 665 nm value. The correction of phaeo-phytin was accomplished by a second photometric measurement at the same wavelength, subsequent to a hydrochloric acid (2 mol/l HCL)[5] treatment. Transmission measurements at the same wavelengths were used to calculate the concentrations according to methods described by Tilzer (1983).

Suspended matter

Total suspended matter (TSM), or seston, is the sum of organic and inorganic particles and was measured by weighing the dry residuum from the filter. As described for the phytoplank-ton determination, a known volume of water (0.5 to 2.0 l) was filtered through a pre-weighed glass fibre filter (Schleicher & Schuell No 6 VG[6](not preheated)), retaining particles $\geq 1\,\mu$m. The filters were transported to the laboratory in a cooler and stored at about -18℃ prior to analysis. The filters were dried in an oven for about two hours at 105℃ and the TSM was determined as the difference between dry weight of the filters before and after filtration. Normalisation with the water volume yielded TSM concentration. Standard Loss-on-Ignition procedure (Heege, 2000) was used to estimate the inorganic particles concentration.

Gelbstoff

Concentration (Y) and spectral shape (S) of gelbstoff were measured from samples obtained from about 0.5 m depth. To remove particulate matter water samples were filtered using glass fibre filters retaining particles $> 1\,\mu$m (Schleicher & Schuell No 6 VG) and re-filtered using a pre-rinsed membrane filter of 0.2 μm pore size (Sartorius Type 11307[6]) (Gege, 2004). The filtered water was transferred to small bottles of PVC or glass and stored cool prior analysis. Spectral measurements were performed in the laboratory within 24 hours of sam-pling using a Varian CARY-1[7] ultraviolet-visible double beam spectrophotometer and quartz cuvettes with 5 and 10 cm pathlengths. In both cuvettes, the transmission of each sample was measured from 190 to 900 nm at 1 nm intervals. The ratio between transmission spectra was converted into water absorption and gelbstoff using the Lambert-Beer law. The gelbstoff absorption spectrum $a_Y(\lambda)$ was calculated by subtracting the pure water absorption spec-trum. Absorption at 440 nm is a measure of concentration (Y), and spectral slope (S) is an indicator of wavelength-dependency. Both Y and S were calculated by a linear regression of $\ln a_Y(\lambda)$ from 420 to 460 nm as the use of a logarithm compensates for the (near) exponential

---

[5]   Hydrochlorid acid (2 mol/l HCL) converts chlorophyll-a into phaeophytin-a (Albert, 2004)
[6]   Sartorius AG, Weender Landstr. 94-108, 37075 Goettingen, Germany, http://www.sartorius.com
[7]   Varian Inc., 3120 Hansen Way, Palo Alto, CA 94304-1030, USA, http://www.varianinc.com

wavelength dependency of $a_Y(\lambda)$ (Gege, 2000).

4.2.2 In water optical data

Besides measuring inherent optical properties (IOP) and the constituents concentrations on which these properties depend, it is also desirable to measure the apparent optical properties (AOP) to directly verify the remote sensed measurements and verify models using the IOPs. Unlike the IOPs, AOPs are not measured by analysing water samples, because they depend on ambient radiance distribution.

RAMSES

The commercially available Radiation Measurement Sensor with Enhanced Spectral Resolution (RAMSES)[8] is a combination of submersible radiance and irradiance sensors for optical measurements in water (Figure 4.5). The system employed simultaneously in this study consisted of one sensor measuring L_u, the upwelling radiance (RAMSES-ARC-VIS 010–03–810E), one sensor measuring E_u, the upwelling irradiance (RAMSES-ACC-VIS 010–03–8109), and one sensor measuring E_d, the downwelling irradiance (RAMSES-ACC-VIS 010–03–8110). The detected signal, collected every 10 seconds, was transmitted from each sensor unit to the built-in MMS[9] spectrometer consisting of a 256-channel silicon photodiode array. The spectrometer optics allows for the use of 190 independent channels from 320 to 950 nm with a spectral sampling interval of 3.3 nm. The wavelength position accuracy is 0.3 nm at a resolution of 10 nm (FWHM). In air, the radiance detector has a field of view of 7° and the noise equivalent radiance is about $0.3 \cdot 10^{-6}\,\mathrm{Wm^{-2}nm^{-1}sr^{-1}}$ at 500 nm with an integration time of 8 s. The three sensors were mounted such that their optical axes were aligned parallel to each other and their entrance optics are on the same level (Figure 4.6). Spectral averaging of between 10 and 20 spectra was performed to ensure an optimal signal-to-noise ratio. The upwelling irradiance sensor also contains a 2-axes tilt ($\pm 45°$) and pressure sensor (50 bar). A PSA-916[10] sonar altimeter was attached to the frame estimate water depth. All sensors were connected to a RS232 interface to ensures that all measurements were made simultaneously. The data were transferred from the sensors to an on-board computer by a 25 m long cable. Irradiance reflectance (R), remote sensing reflectance (R_{rs}), and Q-factor were subsequently derived from the signals recorded (Albert, 2004).

---

[8] TriOS Optical Sensors, Werfweg 15, 26135 Oldenburg, Germany, http://www.trios.de

[9] Carl Zeiss Jena GmbH, Carl-Zeiss-Promenade 10, 07745 Jena, Germany, http://www.zeiss.de

[10] Benthos Inc., Undersea Systems Including Datasonics Inc., 49 Edgerton Drive, North Falmouth, MA 02556, USA, http://www.benthos.com

Figure 4.5: RAMSES spectroradiometer, radiance sensor (left), and irradiance sensor (right)

4.2.3   Airborne data

HyMap

The HyMap sensor, built by Integrated Spectronics Ltd.[11], and operated by HyVista Corp.[12], is an airborne imaging system that was originally used for mineral exploration and environmental monitoring, and records images in a large number of wavelengths. The system functions as a 'whisk-broom' scanner, recording an image by using a rotating scan mirror, allowing the image to be built line by line as the aircraft flies forward. The reflected sunlight collected by the scan mirror is then dispersed into different wavelengths by four individual spectrometer units. The wavelengths range between 400 and 2500 nm (visible to infrared) is covered in 125 spectral bands, each with a bandwidth of approx. 16 nm (Table 4.2). The instrument offers a high signal-to-noise ratio (SNR) of more than 500:1 which is essential for mapping low reflecting targets such as submerged vegetation. The HyMap uses real time altitude and differential global positioning system (DGPS) measurements to provide geocoded imagery. The spectral and image information from the spectrometer is digitised and recorded on tape. To minimise distortion in the image by aircraft pitch, roll, and yaw motions, HyMap is mounted on a gyro-stabilised platform. While the platform minimises the effect of aircraft motion, small image distortions remain which are monitored using a three axis accelerometer system (IMU[13] C-MIGITS II). The field of view (FOV) of the recorded image is 61.3° or about 2.3 km when operating 2000 m above ground level. Typically, the spatial resolution achieved with the HyMap sensor is in range of 3 to 10 m, flying at an operational altitude of 1500 to 4500 m.

---

[11]   Integrated Spectronics Pty Ltd, Baulkham Hills, NSW 1755, Australia, http://www.intspec.com
[12]   Hyvista Corporation, Baulkham Hills, NSW 1755, Australia, http://www.hyvista.com
[13]   Inertial Monitoring Unit

Table 4.2: HyMap spectral bands from $400 - 900$ nm calibrated in 2003 and 2004, their band number and full width half maximum (FWHM)

Band Nr	HyMap2003 [nm]	FWHM [nm]	HyMap2004 [nm]	FWHM [nm]
1	438.000	11.000	445.000	8.100
2	450.000	11.400	454.700	13.600
3	462.400	16.000	469.300	16.500
4	478.100	15.500	485.200	15.600
5	493.400	16.500	500.100	15.600
6	508.500	15.700	515.000	15.400
7	524.100	15.600	530.700	16.400
8	539.400	16.300	546.300	15.900
9	554.900	16.000	561.400	15.200
10	570.200	15.400	576.300	15.300
11	585.200	15.000	591.500	15.500
12	600.200	15.800	607.000	16.100
13	616.300	16.100	622.500	15.300
14	631.700	15.400	637.600	15.400
15	646.500	15.300	652.600	15.100
16	661.600	15.800	667.600	15.300
17	677.100	16.000	682.800	15.500
18	692.400	15.700	698.200	15.900
19	707.500	15.900	713.500	15.300
20	722.900	16.400	728.500	15.200
21	738.100	16.000	743.500	15.400
22	753.000	15.900	758.700	15.600
23	768.000	16.100	773.800	15.100
24	783.100	16.600	788.600	15.300
25	798.300	16.600	803.700	15.600
26	813.400	16.500	818.900	15.700
27	828.500	16.900	834.100	15.600
28	843.900	17.200	849.200	15.900
29	859.200	16.900	864.500	16.200
30	874.300	17.400	879.600	16.200
31	878.200	16.300	880.500	16.900
32	895.400	16.000	897.100	16.100
33	911.100	15.700	913.300	16.700

4.3   Data set

4.3.1   Ground campaigns

Field samples were collected in summer 2003 and 2004 under sunny conditions. To assess the range of spectral variability and to characterise spectral features found in various macrophyte species, a sampling strategy was adopted to measure the spectral reflectance of as many homogenous macrophyte species as possible. The field sampling was carried out at the two test sites in the main growing season (from June to August) between 10 am and 4 pm local time to measure seasonal and local variations. The selection of macrophytes species was made according to their abundance and distribution, size and homogeneity of the patches and the presence of species types in both lakes.

Figure 4.6: RAMSES spectroradiometer, measurement setup on the boat

RAMSES submersible radiometers were used for optical measurements in the water, as described in section 4.2.2. The instruments were placed at a distance of 2 to 3 m from the boat, beyond its shading influence. Sampling of macrophytes was carried out following systematic measurements of hyperspectral reflectance within a small area 15 cm above the benthic habitat. Bottom albedo spectra A were measured above either homogeneous patches of macrophytes or sediment. Since the instrument was kept at a nadir angle approximately 15 cm above the target, the water column between the sensor and the target is assumed to be negligible, such that no correction for attenuation is required. The equivalent reflectance measured 50 cm below the water surface, the so called subsurface reflectance $R(0-)$, was also determined for validation of remote sensing data. Averaging of 10–15 individual spectra per sample was performed to ensure optimal signal-to-noise ratio and that the random measurements covered the range of variance within the homogeneous substrate type. A hand held

Table 4.3: The macrophyte types sampled with one type determining species, their codes used, the number of sample plots contributing to each type, and the total number of spectra collected. (Lake 1 = Lake Constance, Lake 2 = Lake Starnberg)

Species	Lake	Type Code	Nr.of Plots	Nr. of Spectra
Chara aspera	1	1.1Ca	4	38
Chara aspera	2	1.2Ca	4	35
Chara aspera	2	1.3Ca	7	52
Chara contraria	1	2.1Cc	15	132
Chara contraria	2	2.2Cc	9	50
Chara contraria	2	2.3Cc	20	111
Chara intermedia	2	3.2Ci	2	18
Chara tomentosa	1	4.1Ct	4	37
Najas marina	1	5.1Nm	7	13
Najas marina	2	5.2Nm	6	32
Nitellopsis obtusa	1	6.1No	4	15
Potamogeton pectinatus	1	7.1Pp	12	58
Potamogeton pectinatus	2	7.2Pp	24	171
Potamogeton pectinatus	2	7.3Pp	27	173
Potamogeton perfoliatus	1	8.1Pf	7	32
Potamogeton perfoliatus	2	8.2Pf	8	46
Sediment	2	9.2Ss	4	35
			158	976

echo-sounding device recorded water depths for each spectral measurement, which ranged from 0.5 to 4.5 m. A Trimble differential global positioning system[14] (DGPS) provided geographic coordinates of each sample location. A photograph was taken to accompany each suite of measurements for a given target. A full species composition description, with their percentage cover estimates, water depth, growth height, and status of epithetic growths was made at each location (Table 4.3 and Table 4.4).

---

[14]   Trimble GmbH, Am Prime Parc 11, 85479 Raunheim, Germany, www.trimble.com

Table 4.4: Overview of frequency and location of sampled species. Ca=*C. aspera*, Cc=*C. contraria*, Ci=*C. intermedia*, Ct=*C. tomentosa*, Nm=*N. marina*, No=*N. obtusa*, Pp=*P. pectinatus*, Pf=*P. perfoliatus*, Ss=*Sediment* and Wd=*Water deep*, +: indicates data collected, –: indicates no data collected.

Lake	Date sampled	HyMap	Water samples	Ca R(b)	Cc R(b)	Ci R(b)	Ct R(b)	Nm R(b)	No R(b)	Pp R(b)	Pf R(b)	Ss R(b)	Wd R(0-)
Starnberg	2003/06/26	-	+	-	+	-	-	-	+	+	+	+	-
	2003/07/07	+	+	-	-	-	-	-	+	+	+	+	+
	2003/07/08	-	+	-	+	-	-	-	-	+	+	-	-
	2003/07/14	-	+	-	+	-	-	-	-	+	+	-	-
	2003/07/24	-	+	-	+	-	-	-	+	-	+	+	+
	2004/06/26	+	+	-	-	-	-	-	-	-	-	-	-
	2004/06/29	-	+	-	+	-	-	-	-	+	-	-	+
	2004/07/08	-	+	+	+	+	-	-	-	+	-	+	-
	2004/07/18	-	+	+	+	+	-	-	-	+	-	+	-
	2004/07/20	-	+	+	-	-	-	+	-	+	-	+	-
	2004/08/04	-	+	-	-	-	-	+	-	-	-	-	-
	2004/08/12	-	+	-	-	-	-	-	-	+	-	-	-
	2004/08/16	-	+	-	+	-	-	-	-	+	-	-	-
Constance	2003/07/19	+	-	-	-	-	-	-	-	+	-	-	-
	2003/07/29	-	-	-	+	-	+	+	+	+	+	-	-
	2003/07/30	-	+	+	+	-	-	+	-	+	+	+	-
	2004/06/26	-	+	-	-	-	-	+	+	+	+	+	-
	2004/06/30	+	+	-	-	-	-	+	-	-	-	-	+
	2004/07/28	-	+	-	+	-	-	+	+	+	-	-	-
	2004/07/29	+	+	-	+	+	-	+	-	+	+	-	+
	2004/07/30	-	+	+	+	-	-	+	+	-	-	-	-

4.3.2 Flight campaigns

HyMap imaging spectrometer data were acquired by the HyVista Corp.[15] over the study sites in June/July 2003 and 2004 (see Table 4.5) coincident with the campaign. The data were collected onboard a DLR[16] research aircrafts (either a Cessna 208B or a Dornier DO 228) from an altitude of $\sim 1800\,\mathrm{m}$, providing an effective pixel resolution of roughly $4.2\,\mathrm{m}$ and a $2.1\,\mathrm{km}$ swath. The weather conditions during each overpass were clear and sunny with no clouds. In addition to the collected image data, aircraft altitude, such as inertial navigation information were collected for correction of aircraft altitude, pitch, roll and yaw. The aircraft geographic location was monitored using DGPS, which allows the image data to be fully geocoded. Flights to obtain airborne imagery were undertaken considering solar zenith angles of 30° to 60° and a flight path at 0° or 180° headings with respect to the solar azimuth to minimise imaging of sunglint effects. This means the aircraft flew either into or away from the sun. An overview of date, time, and location of the acquired HyMap flightlines is found in Table 4.5.

---

[15]   Hyvista Corporation, Baulkham Hills, NSW 1755, Australia, http://www.hyvista.com
[16]   German Aerospace Center (DLR Oberpfaffenhofen), Münchnerstr. 20, 82234 Wessling, http://www.dlr.de

Table 4.5: Parameter of HyMap flightlines, date, time, and location

Parameter	7 July 2003	26 June 2004	19 July 2003	30 June 2004	29 July 2004
Lake	Starnberg	Starnberg	Constance	Constance	Constance
Overflight time (UTC)	7:47	7:15	7:51	7:53	7:42
Ground level over sea level (m)	585	585	395	395	395
Altitude over ground level (m)	1977	1885	1837	1829	1811
Swath width (m)	2301	2194	2138	2129	2108
Pixel resolution (m)	4.49	4.28	4.18	4.16	4.12
Latitude (°N)	47.87°	47.88°	47.69°	47.69°	47.70°
Longitude (°E)	-11.27°	-11.30°	-9.05°	-9.06°	-9.05°
Flight heading[a]	131.75°	-40.83°	-41.48°	-49.2°	139.49°
Sun-zenith/azimuth (°)	48.9/101.6	53.4/94.8	51.2/101.7	48.8/100.6	54.2/101.6
P (μg/l)	1.0	0.5	0.9	0.6	1.0
SM (mg/l)	1.0	4.0	2.5	1.5	4.0
Y(m^{-1}) at 440 nm	0.2	0.2	0.1	0.2	0.3

[a] Azimuth from north

4.4 Data processing

4.4.1 Field spectroscopy

Analysis tools

RAMSES spectra were extracted from the computer using TriOS MSDA 1.99 -IPS104/4[17] software. Statistical analysis was carried out using the free statistic software package **R** Version 2.2.1[18](R Development Core Team, 2005). The principle component analyses were generated using the **R** function prcomp() from **stat** package (Venables and Ripley, 2002). The linear discriminant analysis uses the **R** function lda() in **MASS** package (Venables and Ripley, 2002). The Genetic algorithm GALGO for feature selection were all generated in **R** using the modules **galgo** (Trevino and Falciani, 2006). The derivatives were all calculated from reflectance spectra and Savitzky–Golay smoothed using ORIGIN 7.0[19].

Pre-processing

The RAMSES spectrometer automatically calculates from the measured radiance and irradiance spectra remote sensing reflectance and irradiance reflectance. Spectra used in the following analysis are the average of $10 - 15$ spectra of the same target and their mean and standard deviation was calculated. The locations selected for analysis had a standard deviation of less than 2.5 % in order to improve the quality of the measurements and to obtain spectra of homogenous substrates. Those measurements with standard deviation higher than 2.5 % were re-processed, calculating the median reflectance and its 95% percentile. The spectra beyond that percentile were discarded and mean reflectance was calculated again to increase number of useful spectra for statistical analysis. For all analyses, the following Pre-processing of data was performed. First, spectral curves were truncated below 400 nm and above 700 nm, since the measurements are extremely noisy outside of this range. This left 61 bands, each with a width of about 5 nm, corresponding to RAMSES spectral sampling interval. These spectra were simulated to HyMap spectral sampling interval 2003 and 2004 (Table 4.2), resulting in 33 resampled bands from 440 to 910 nm (Table 4.2).

---

[17] TriOS Optical Sensors, Werfweg 15, 26135 Oldenburg, Germany, http://www.trios.de
[18] The R Foundation for Statistical Computing, Vienna, Austria, Version 2.2.1 (2005-12-20 r36812) ISBN 3-900051-07-0, http://www.r-project.org
[19] http://www.OriginLab.com

4.4.2   Hyperspectral data analysis

Analysis tools

Atmospheric, and air-water interface, and water column correction was performed using the Modular Inversion & Processing System (MIP) developed by EOMAP[20], DLR[21], TUM[22] and RAS[23]. Image visualisation and spectral analysis was performed using ENVI Version 4.1[24] and image processing software XDIBIAS (Müller et al., 2002).

Pre-processing

Pre-processing which involves calibration, masking out of land features and geo-referencing was performed using XDIBIAS image analysis software. The raw image data were first processed to 'at-sensor' radiance ($\mu W cm^{-1} sr^{-1} nm^{-1}$). The HyMap data were radiometrically calibrated, corrected for the motion of the aircraft, and georeferenced using RECTIFY and XDIBIAS software, developed at the German Aerospace Centre (DLR).

The images were further corrected for atmospheric, air-water interface and water column effects using MIP (Miksa et al., 2004; Heege et al., 2003a). This physical-based correction method allows for direct comparison of image data once distortion effects are removed. Details about the program may be found in Heege and Fischer (2004); Miksa et al. (2005).

Bottom depth is one parameter of shallow waters that can be retrieved by means of inverse modelling. This inversion procedure is the basis for the retrieval of water parameters in MIP. Different modules in the software support algorithms to derive bio-physical parameters by inverting the measured radiance signal at the sensor. Inverted parameters include e.g. aerosol concentrations, the concentration of water constituents, and the reflectance characteristics of substrates in shallow waters (Heege, 2000; Heege and Fischer, 2004).

A previous application of MIP for mapping water constituents in Lake Constance demonstrated that the software was an efficient and reliable tool for the inversion of remote sensing data from natural waters (Heege and Fischer, 2004). Details about the processing with MIP for the retrieval of bottom depth are not yet published, though the overall processing methodology used by MIP is found in Figure 4.7. This scheme follows the same structure as the one

---

[20]   EOMAP, c/o Anwendungszentrum, Sonderflughafen Oberpfaffenhofen, 82205 Gilching, Germany ,http://www.eomap.de

[21]   German Aerospace Center (DLR Oberpfaffenhofen), Münchnerstr. 20, 82234 Wessling, Germany http://www.dlr.de

[22]   Technische Universität München, Limnologisches Institut, Hofmark 3, 82393 Iffeldorf, Germany http://www.limno.biologie.tu-muenchen.de

[23]   St.Petersburg Institute for Informatics and Automation of RAS, St. Petersburg, 14 line 39, 199178 Russia, http.//www.spiiras.nw.ru

[24]   CREASO GmbH, Talhofstrasse 32A,82205 Gilching, Germany http://www.CREASO.com

adapted from Van der Piepen et al. (1987) and Dekker et al. (1995)

An azimuthally resolved radiative transfer model for a multilayer atmosphere-ocean system with a flat water surface is used for aerosol retrieval, sun glitter, and atmospheric correction modules (Figure 4.7). The retrieval of water constituents is achieved by an iterative fitting algorithm to adjust modelled and measured underwater reflectances. The radiative transfer modules and database system in MIP was implemented by Kisselev et al. (1995); Kisselev and Bulgarelli (2004) and is based on the Finite Element Method (FEM) (Bulgarelli et al., 1999). Here, it is used for the atmospheric, water surface and Q-factor correction of the underwater light field in the same manner as explained in Heege and Fischer (2004).

Databases are generated by this radiative transfer model which calculates radiances in a vertically inhomogeneous (multilayer) atmosphere-ocean system (with respect to all angle dependencies of the sun and observer geometry). The first database contains a Lambert reflector of defined reflection $R_L(0-)$ (underwater radiance was assumed to be isotropic). The free parameters of the database are three types of aerosols: τ_1, τ_2, τ_3 (continental, maritime, urban), each with four optical depths between 0.01 and 0.5 (at 550 nm), seven reflection values for $R_L(0-)(\lambda)$ between 0.0 and 0.6, 17 observer altitudes (h), 17 azimuth differences ($\Delta\phi$) between sun and observer, eight sun-zenith angles (θ_{sun}) and eight observer zenith angles (θ).

The second database is needed to correct the artificial Lambert reflectance values $R_L(0-)$ for the bi-directionality of the underwater light field to $R(0-) = E_u/E_d$ by

$$R(0-) = R_L(0-)\pi/Q \tag{4.1}$$

Values of $Q = E_u(0-)/L_u(0-)(\theta\phi)$ were calculated with a standard atmosphere, but with a fixed medium aerosol concentration and an expanded water body. Q is calculated as function of λ, h, $\delta\phi$, θ, θ_{sun} and the water constituent concentrations (P, Y, X). The initial step of using MIP, irrespective of making forward calculations or inverse modelling, is to reduce the two databases to smaller, so called *mission databases*. This is accomplished by using the geometric and flight information given of the recorded scene. The main parameters which have to be taken into account are flight heading, pitch angle, and the position of the sun. This information is stored in a *mission file* which is used to document all program settings and specifications for the processing of the specific scene. The processing can be summarised in Figure 4.7.

1. Coupled retrieval of aerosol and water constituents The **Fitaerorefbased** module was used, to retrieve aerosol and water constituent (phytoplankton pigments, suspended matter, gelbstoff) concentrations in the deep water areas of the remotely sensed scene, as

described in Miksa et al. (2005). With the knowledge of the aerosol concentrations, subsurface irradiance reflectance $R(0-)$ can be retrieved after atmospheric- and air-water interface - correction. The water constituents (phytoplankton pigments, suspended matter, gelbstoff) concentrations are used in order to correct the bidirectional effect of the water body itself (Heege, 2000; Heege and Fischer, 2004).

2. Atmospheric- and water surface-correction   This part was done as described in Heege (2000); Heege and Fischer (2004). The MIP module **Atmossurfcorr** was used to correct for atmospheric influences using constant values of aerosol concentrations and water constituents, previously retrieved and registered in the mission file. They are the result of a retrieval performed only in certain points of the scene, as keeping the values fixed for the whole scene assumes that there is low heterogeneity in relation with those parameters, such that the conditions are constant. The output of this part of the processing are subsurface reflectances $R(0-)$.

3. Bottom albedo, bottom coverage and water depth retrieval   The MIP module **Watrecor** is used to estimate bottom albedo, bottom coverage and water depth. The procedure consists of the inversion of the shallow water areas. Inputs are constant values for water constituents and the underwater reflectance image (output of the previous step). The output is a set of 29 products which stores different information about the parameters retrieved. One of these products is an underwater digital elevation model (DEM) which comprises the water depth information (z) for the whole scene.

Bottom albedo spectra A are calculated from $R(0-)$ after Albert and Mobley (2003) (Section 3.3.2, Eq. 3.27) $R(0-)$ using one set of water constituent concentrations previously retrieved (Heege and Fischer, 2004; Kisselev and Bulgarelli, 2004; Kisselev et al., 2005) and the Gaussian expression for the spectral behaviour of yellow substance absorption (Gege, 2000). The water depth z_B is retrieved iteratively in combination with the bottom albedo A. During the inversion of shallow water, the bottom albedo and the subsurface albedo (comparison of model spectra with 'measured' spectra from HyMap) are fixed while depth and bottom coverages of three main bottom types are iterated (Heege et al., 2003b)
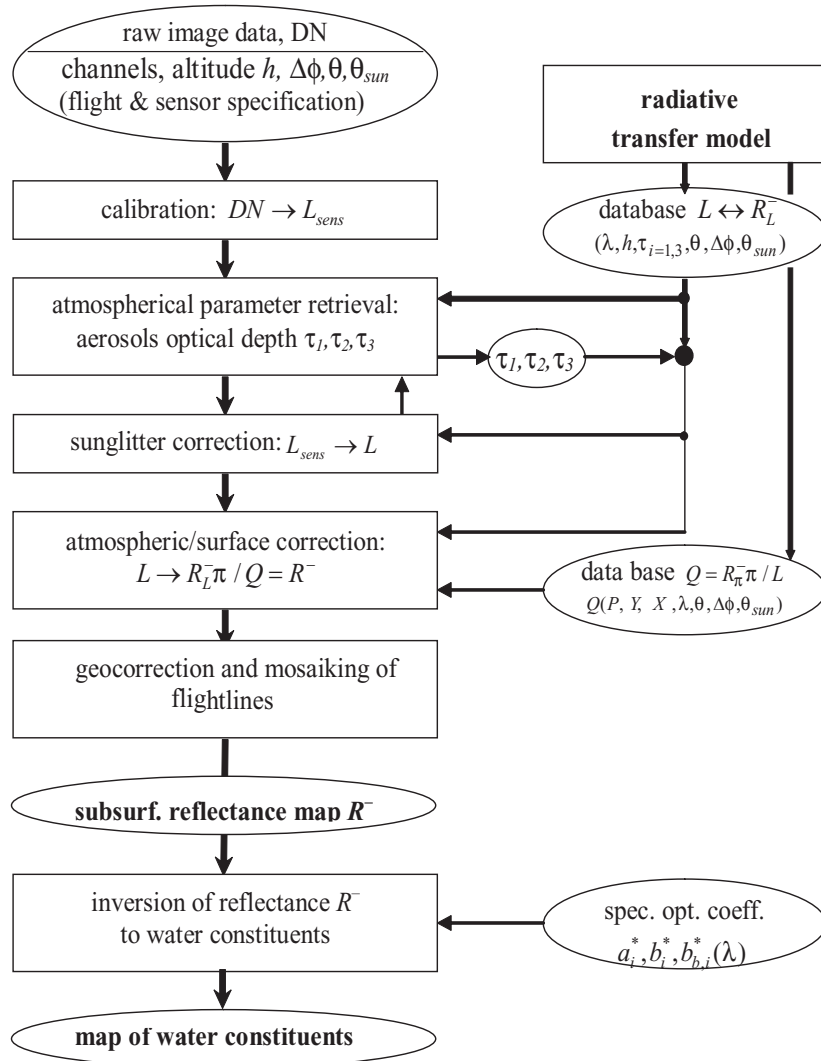
Figure 4.7: Process chart of the Modular Inversion Program (MIP) to calculate water constituents and substrate cover from remote sensing imaging spectrometry data.
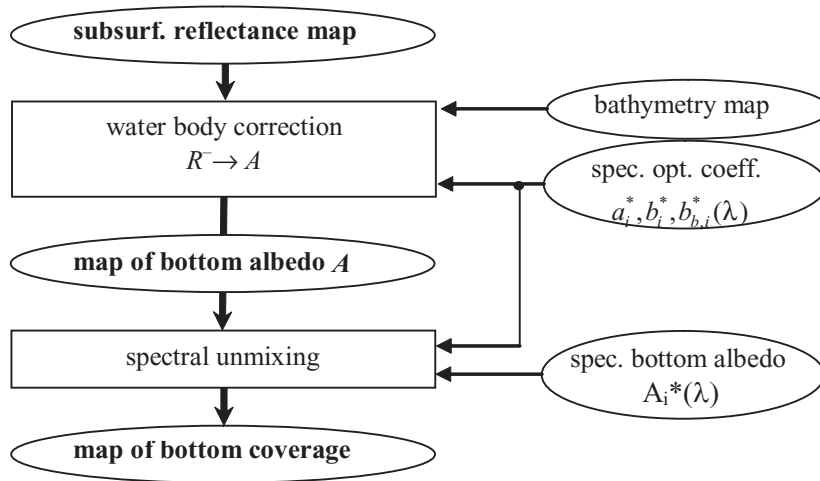
Figure 4.8: Additional modules for shallow water applications, applied after atmospheric and surface correction modules

Chapter 5

Research Approach

The spectral properties of eight common species of aquatic macrophytes were investigated to establish whether or not they revealed sufficient information for differentiation, such that water quality may eventually be inferred (Schneider, 2004). *In situ* measurements took place between June and August 2003 and June and August 2004 (Table 4.3). The algal species were chosen because of their widespread occurrence throughout central Europe. To assess the range of spectral variability that may be found in each species, reflectance spectra of homogeneous macrophyte patches were measured with a spectroradiometer according to the procedures described in section 4.3.1 during each growing season in Lake Constance and Lake Starnberg. The total number of patches measured for each species was not equal because not all species occurred at all sites. Hence, the total sample sizes were n = 70 for *Chara aspera*, n = 246 for *C. contraria*, n = 25 for *C. intermedia*, n = 26 for *C. tomentosa*, n = 37 for *Najas marina*, n = 4 for *Nitellopsis obtusa*, n = 249 for *Potamogeton pectinatus*, and n = 70 for *P. perfoliatus* (Table 4.3). Spectra were analysed using Principal Components Analysis (PCA) and derivative analysis to determine if differences exist, and were subsequently assessed for significance using a Jeffries-Matusita distance method.

5.1 Scientific value

This study is intended to move hyperspectral technology one step closer towards discriminating macrophyte species in lakes. Instead of using laboratory data (Schmidt and Skidmore (2003)) that omit the difficulties and variability imposed by field conditions (e.g. the fluctuation of light source energy, change of daily atmospheric state, the effects of canopy formation, the cost of accessibility, the coarser spatial and spectral resolution of on-board hyperspectral sensors, the effect of seasonal changes, the effect of background soil and waters), *in situ* underwater bottom albedo measurements A taken just above macrophyte patches were

analysed for spectral separability to establish whether real-life hyperspectral sensors (e.g. HyMap, ROSIS, CASI etc.) can be used to differentiate macrophyte species. The second goal of this study was to develop algorithms for macrophyte spectra classification. Therefore it was more appropriate to use *in situ* spectra which can be directly related to real field conditions. The classification procedure was tested on *in situ* measured reflectance spectra and then subsequently applied to HyMap hyperspectral data. Results show the potential of applying hyperspectral remote sensing to macrophyte mapping for the purposes of water quality monitoring.

5.2   Analysis of spectral *in situ* data

The composition and abundance of submerged macrophytes in any given littoral zone are influenced by the sum of physical and chemical conditions at that location. Unique combinations of canopy structure and substrate composition may be associated with individual species, and are features in remote sensing that ultimately determine a bottom albedo signal. *In situ* underwater bottom albedo measurements have negligible water column effects, as measurements are taken directly above the macrophyte patches, as described in section 4.2.2. In this study, a total of 158 mean reflectance spectra were measured (after averaging) from eight macrophyte species at Lake Constance and Lake Starnberg (Table 4.3). For some locations in each lake, a single species or uniform patch was measured multiple times. Before statistical analyses were performed, spectra were selected and processed as described in section 4.3.1.

5.2.1   Unsupervised feature extraction

An in-depth discussion of the theory behind the statistical analyses is presented following a description of how they were applied in this study. Principal component analysis, derivative analysis, and the Jeffries-Matusita distances were the three statistical techniques employed.

Methodology

The first stage of the analysis was to test for differences between the reflectance spectra of the eight macrophytes by determining the principal components contained within the data set. The second step in the analysis was to determine whether any statistical differences could be enhanced by using first and second order derivatives. The third step, after statistical differences were found, was to determine how significantly different, or distant in spectral space, the macrophytes were from each other by using the Jeffries-Matusita (JM) distance

index. The potential of correct classification of the macrophyte species using hyperspectral remote sensing is predicted by these distance measures.

Principal component analysis Principal component analysis (PCA) was used to view the data in a two-dimensional space and to identify possible separation between species. A two-dimensional graphic has the potential to reveal previously unsuspected groupings, or draw attention to misclassified samples. The PCA was performed on pre-selected spectra reflectance data between $400-700$ nm wavelengths, listed in Table 4.3. PCA was chosen to illustrate spectral differences, as spectral variations within an individual species (i.e. intra-specific spectral variation) in unprocessed data had overlaps that made it very difficult to resolve differences between species (i.e. inter-specific spectral variation). The PCA loadings were used to pre-select for relative contributions of particular wavelengths and to identify poor spectral locations (wavelengths within the spectra).

Jeffries–Matusita distance The spectral separation between each pair of macrophyte species was quantified using the Jeffries-Matusita (JM) distance index. Because the JM distance is a parametric method, it was necessary to use a reduced number of spectral features (bands) for calculation, therefore only the first and second principal components were included in the calculation (Mutanga et al., 2003). The JM distance is asymptotic to the value of two, thus an index value of two indicates separation, whereas an index less than 1.9 assumes the pair is unlikely to be separated in the following classification procedure.

Derivative analysis To optimise separation and enhance species discrimination, derivative analyses were performed. Differences in rates of change (slope) of the macrophyte spectra were calculated with first and second order derivatives and were subsequently used to identify spectral regions where the macrophyte species had distinct features. Derivatives are thought to be useful in detecting changes in relative pigment concentration pigment balances between macrophyte species and to enhance absorption features in reflectance signals associated with a change of vegetation type or physiological state. Higher derivatives are not useful for establishing spectral differences because their profiles are generally noisy (Joyce and Phinn, 2003). The Savitzky-Golay smoothing method, which generates a local polynomial regression around each point (Tsai and Philpot, 1998), was used in this study's derivative computation. The maximum derivative value was also selected as a potential variable for discriminant analysis (Section 5.2.2). Qualitative information regarding pigment composition was obtained by noting wavelength position of absorption features in the derivative spectra. Absorption features were compared against published values of pigment absorption peak wavelengths (see Table 2.1 and 2.2). Based on these statistical analyses, spectral bands were selected where

the macrophytes appeared spectrally unique.

Principles of statistical pre-processing

Principal component analysis   Principal components analysis (PCA) is a multivariate method of statistical analysis and has been used widely with large, multi-dimensional data sets. Multi- or hyperspectral images are often highly correlated, caused either by similar materials which make up the spectrum or through sensor band overlap. PCA is an ideal method for transforming correlated variables in a sample data set into a new, uncorrelated co-ordinate system or vector space. Each new variable is a linear combination of the original variables, such that the sequence of new factors successively represent the a maximal variance of the data. In general, a data matrix $\boldsymbol{X}$ has the form $\boldsymbol{X}^T = [\boldsymbol{x}_1, \ldots, \boldsymbol{x}_n]$, where $\boldsymbol{x}_i$ is the ith training sample.

To derive principal components, the covariance matrix $\boldsymbol{\Sigma_X}$ will be used, as defined by (Richards, 1993) as:

$$\boldsymbol{\Sigma_X} = \frac{1}{n-1} \sum_{i=1}^{n} (\boldsymbol{x}_i - \boldsymbol{\mu_x})(\boldsymbol{x}_i - \boldsymbol{\mu_x})^T \tag{5.1}$$

where $\boldsymbol{\mu_x}$ is the sample mean vector. A matrix $\boldsymbol{A}$ is sought, which linearly transforms the original variables into vectors, such that the covariance matrix $\boldsymbol{Y}$ of the new co-ordinate system is diagonal and thus without correlation between any of its components.

$$\boldsymbol{\Sigma_Y} = \frac{1}{n-1} \sum_{i=1}^{n} (\boldsymbol{y}_i - \boldsymbol{\mu_y})(\boldsymbol{y}_i - \boldsymbol{\mu_y})^T = \boldsymbol{A}^T \boldsymbol{\Sigma_X} \boldsymbol{A} \tag{5.2}$$

A new data matrix $\boldsymbol{Y}$ can be derived by a linear transformation from data matrix $\boldsymbol{X}$;

$$\boldsymbol{Y} = \boldsymbol{A}\boldsymbol{X} \qquad \text{with} \qquad \boldsymbol{A}^T\boldsymbol{A} = \boldsymbol{I}. \tag{5.3}$$

Each resulting eigenvalue is equal to the variance of the respective principal component along transformed coordinate axes, and the sum of all eigenvalues is equal to the sum of all band variances in the original data. Associated with each eigenvalue is a set of coordinates defining the direction of the associated principal axis (Krzanowski, 2000).

Eigenvalues and eigenvectors therefore describe the lengths and direction of principal axes. Eigenvectors can also be interpreted as correlations between the abstract principal components and individual bands in the original spectra (or image). These correlations or *loadings* are used in the interpretation of the principal components and describe how closely a particular spectrum resembles the principal component (Holden and LeDrew, 1998). Principal components are ordered by decreasing variances. The result is a removal of any

correlation present in the original data with a simultaneous compression of most of the total variance in fewer dimensions. For more details the reader is referred to Jolliffe (1986) and Krzanowski (2000).

Jeffries-Matusita Distance A main objective of this study is to establish whether or not the *in situ* spectra contain adequate spectral information to discriminate between macrophytes at the species level. Separation of species based on their spectra is possible if different species' spectra have high statistical distance in feature space and variation within a species' spectra is less than among species' spectra (Clark et al., 2005). For the purposes of this study, it was necessary to calculate the spectral separability index of every macrophyte pair to determine if significant differences exist.

The JeffriesMatusita (JM) distance between a pair of spectral classes is the measure of the average distance between the two class density functions. For normally distributed classes, this distance becomes the Bhattacharyya (BH) distance (Kailath, 1967). For the BH distance, a larger value indicates greater average distance, while the JM distance[1] is asymptotic to the value two for increasing class separability.

Whereas an increasing BH distance does not necessarily indicate how successful the two classes are discriminated, a JM distance of 2.0 between two spectral classes would imply classification of those two classes with 100 % accuracy (Richards, 1993), which means the within group difference is smaller than the between group difference.

A common practice in remote sensing is to use a squared JM distance threshold of $\geq$ 1.90 to indicate if any two macrophyte species are spectrally separable. Additional details regarding separability analysis can be found in (Richards, 1993). The JM distance calculation in this study was based on Eq. 5.4.

$$J_{ij} = \sqrt{2(1 - e^{-B})} \tag{5.4}$$

where

$$B = \frac{1}{8}(\boldsymbol{\mu}_i - \boldsymbol{\mu}_j)^T \left(\frac{\boldsymbol{\Sigma}_i + \boldsymbol{\Sigma}_j}{2} \right)^{-1} (\boldsymbol{\mu}_i - \boldsymbol{\mu}_j) + \frac{1}{2} \ln \left(\frac{(1/2)|\boldsymbol{\Sigma}_i + \boldsymbol{\Sigma}_j|}{\sqrt{|\boldsymbol{\Sigma}_i| \times |\boldsymbol{\Sigma}_j|}} \right)$$

Note i and j are two signatures (classes) of macrophyte species being compared, $\boldsymbol{\Sigma}_i$ is the covariance matrix of signature i, $\boldsymbol{\mu}_i$ is the mean vector of signature i, ln is the natural logarithm function, T denotes matrix transposition, and $|\boldsymbol{\Sigma}_i|$ is the determinant of $\boldsymbol{\Sigma}_i$.

Derivative analysis Derivative spectroscopy, a technique derived from analytical chemistry for resolving overlapping spectral features, was first applied primarily in hyperspectral

---

[1] The Jeffries-Matusita distance method delivers a value between 0 and $\sqrt{2}$ ($\sim$ 1.41), such that the squared distance gives a number between 0 and 2.

sensing of terrestrial environments (Demetriades-Shah et al., 1990). Increasing use of hyperspectral sensors in aquatic or marine settings, e.g Holden and LeDrew (1998); Clark et al. (2000) opened the possibility of using derivative techniques for studies of algae in littoral environments (Louchard et al., 2002; Richardson, 1996).

Derivative spectroscopy uses wavelength changes in spectral reflectance or radiance to sharpen spectral features, separating components in the derivative spectrum clearer than in the reflectance spectrum. Another advantage is that second and higher order derivatives are relatively insensitive to variations in illumination intensity, regardless whether caused by changes in sun angle, cloud cover, or topography. At the spectral sampling interval typical of hyperspectral systems, derivatives should also be relatively insensitive to the spectral variations of sunlight and skylight (Tsai and Philpot, 1998).

Several investigations using spectral derivatives in shallow water environments have used high-order derivatives, however first and second order derivatives have been most common (Butler and Hopkins, 1970; Demetriades-Shah et al., 1990; Holden and LeDrew, 1998; Fraser, 1998; Tsai and Philpot, 1998; Andrefouet et al., 2003b). The simplest numerical method for generating derivatives divides the differences between successive spectral values by the wavelength interval that separates them. The first order derivative provides information on the rate of change in reflectance, which is the slope with respect to wavelength; the second order derivative reveals the change in slope with respect to wavelength (Holden and LeDrew, 1998). Derivatives were computed as change over bandwidth $\Delta\lambda$, defined as $\Delta\lambda = \lambda_j - \lambda_i$ where $\lambda_j > \lambda_i$. The estimation for the first derivative is shown in Eq. 5.5. The 2nd derivative is given by Eq. 5.6

$$\frac{dR}{dy} \approx \frac{R(\lambda_j) - R(\lambda_i)}{\Delta\lambda} = R' \tag{5.5}$$

$$\frac{d^2R}{dy^2} = \frac{d}{d\lambda}\left(\frac{dR}{d\lambda}\right) = R'' \tag{5.6}$$

Derivatives are particularly sensitive to noise, thus smoothing or otherwise minimising random noise is a major concern. In this study, first and second derivatives of spectra were calculated by use of a least-squares third order polynomial smoothing filter of 15 nm width (Savitzky and Golay, 1964). The general equation of the least squares convolution can be given as follows:

$$I_j^* = \frac{\sum\limits_{j=-m}^{j=m} C_j I_i + j}{M} \tag{5.7}$$

where I_i $(i = 1, 2, \ldots, n)$ are the original brightness values, and I^* is the resultant value, C_j is the coefficient for the value of the filter (smoothing window) (Jonckheere et al., 2005),

and M is the number of convoluting integers and is equal to the window size $2m + 1$. Further details about the derivative technique are found in early analytical chemistry literature, e.g. Procter and Sherwood (1982); O'Haver and Green (1976).

5.2.2 Supervised feature extraction

An automated, transferable, and repeatable classification methodology is not only dependent on the accuracy of the physical model of corrected remote sensing images but also on the classification approach. The goal of the final classification step is to obtain biological meaningful classes of substrates using objective statistical methods.

Statistical modelling techniques can be described as either uni- or multivariate. *Univariate* approaches test one feature at a time for their ability to discriminate or identify a significant dependent variable. The top-most significant features are then used to develop a statistical model. *Multivariate* approaches take into consideration that many variables may be highly correlated. For example, hyperspectral data sets have hundreds of contiguous wavelengths (variables) that are obviously correlated.

Multivariate approaches are therefore better suited for hyperspectral data classification and were employed in the following methodology. There are two basic strategies which can be used to discriminate high dimensional spectral data. First, the dimensionality of the data can be reduced by some feature extraction pre-processing method, and then classified with an appropriate *low-dimensional* test, e.g. linear discriminant analysis (LDA) (Everitt, 2005). An alternative procedure is to use a classifying technique which is capable of handling a large number of variables (Mallet et al., 1996; Donald et al., 2006), referred to as a *high dimensional* classifier, e.g. penalised discriminant analysis (PDA) as discussed in detail by Yu et al. (1999) and Hastie et al. (1995). In this study, the feature extraction approach was used.

Methodology

Prior to feature extraction of the RAMSES measured *in situ* spectra, first and second derivatives were standardised, resulting in all column means equal to zero and all column standard deviations equal to one. First, feature selection was performed based on genetic algorithms using the GALGO component (R Development Core Team, 2005) in the **R** software package as described in later in this section. The *in situ* measured reflectance spectra were used to derive an 'optimal' band set to obtain maximum accuracy in classification. A maximum likelihood discriminant function (MLHD) (see below) was selected in the GALGO routine. For discriminant analysis, the underwater bottom albedo (A) were reduced to 61 wavebands
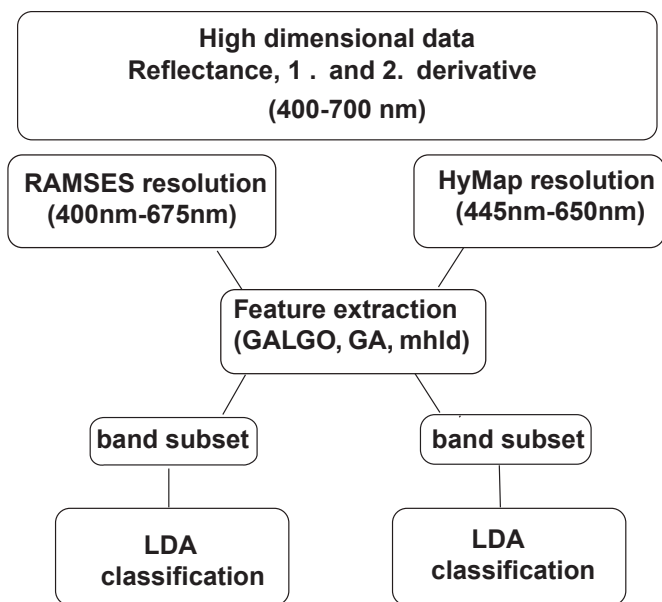
Figure 5.1: Schematic diagram of supervised classification approach and feature extraction

over the $400 - 700$ nm wavelength region and resampled to 5 nm intervals (RAMSES spectral resolution, see section 4.2.2).

Genetic algorithm was employed to select the best band combination out of the total 183 bands (61 bands of the reflectance spectra, 61 bands in the 1st order derivative, and 61 bands in 2nd order derivative). The search parameters in the genetic algorithm utilised included up to a maximum of 1000 iterations and an estimated classification accuracy with optimising criterion of 98%. The subset size (chromosome) was set to equal four (variables) and was estimated after a series of runs according to the optimal number of bands for classifying species in the backward selection process. The genetic algorithm was applied separately to 45 spectra measured at Lake Constance and 113 spectra from Lake Starnberg, as previous unsupervised classifications using PCA indicated a strong separation exists between these two lakes.

The same data set was further resampled to HyMap spectral resolution performance, as flown in 2003 and 2004, resulting in 54 spectral bands (18 bands of the reflectance spectra, 18 in the 1st order derivative, and 18 bands in the 2nd order derivative). During the calibration procedure, spectral bands from HyMap flown 2003 were significantly different from those of 2004 (see Table 4.2) and were therefore treated separately. The feature selection algorithm was performed, changing the genetic search parameters to 93% as an optimising criterion for classification accuracy and the subset size was set to four (variables).

The optimal band combination was calculated in GALGO for three different wavelength ranges:$400-700$ nm, $480-650$ nm and $480-600$ nm, corresponding to available wavelengths for different optical depths. Only the best performing wavelengths are presented in the results. This multivariate statistical technique was employed to identify wavelengths at which the macrophyte spectral separation was greatest. These wavelengths can be used to classify a remote sensing image or can provide the basis for the monitoring of macrophyte growth via remote sensing.

An error estimation, a so-called training and test validation strategy using single or multiple random splits, was performed after each run and applied to the data. The ability of the selected discriminant function to separate the macrophyte species was evaluated by classifying a separate set of pixels. The two-part accuracy assessment was comprised of a self-test with the original samples and a cross-validation test, and was conducted with the discriminant functions constructed from the LDA after feature selection. These accuracy assessments were used to analyse the performance of selected spectral bands in discriminating reclamation levels of macrophyte species. The datasets were randomly split into two groups, a model training set (1/3) and an independent test set (2/3). The models were built and optimised on the training set and then independently tested against the second set. A confusion matrix plot was generated for each classification (Gong et al., 1997) and compared for its performance.

All calculated band set combinations were compared to visually selected derivative bands and to pigment locations found in the literature (see Chapter 2.3.2). Emphasis was given to spectral ranges corresponding to PCA loadings. The separation between macrophyte species was determined for the selected bands to find the best separation ability (maximum JM distance index) in the two most similar species (Galvão et al., 2005).

Principles behind image classification

Linear discriminant analysis LDA is a supervised transformation method for dimensionality reduction in order to find the best way in which two or more populations can be distinguished. LDA is a linear coordinate transformation which maximises between-class variance and minimises within-class variance (Krzanowski, 2000). The discriminant function may then be used to describe and interpret the difference between populations, and is appropriate when the independent variables are metric (Everitt, 2005; Mallet et al., 1996). The most important assumption of LDA classification is that all classes share the same covariance matrix (i.e. homogeneity) (Clark et al., 2005). Application of LDA to hyperspectral remote

sensing images transforms the data onto a hyperplane such that the class separability function is maximised, which is the ratio of between-class variance $\boldsymbol{\Sigma}_b$ and within-class variance $\boldsymbol{\Sigma}_w$ (Eq. 5.11) (Krzanowski, 2000).

Discriminant analysis models comprise sets of equations that are linear combinations of the independent variables, resulting in the maximum possible separation between groups. The first step is to standardise the data by subtracting the mean and dividing by the standard deviation. Standardisation was performed, such that x_{ij} changes to:

$$(x_{ij} - \boldsymbol{\mu}_j)/\sigma_j \tag{5.8}$$

where $\boldsymbol{\mu}_j$ and $\boldsymbol{\sigma}_j$ are the mean and the standard deviation as calculated for the jth variable, respectively. After standardisation, all column means will equal zero and all column standard deviations will equal one. Factors which determine the separability of the macrophytes include the distances between species and the compactness of each species. In the next step, the ratio of the between-to-within variability of the transformed training data vectors (i.e. spectra) is maximised (Jarvis and Goodacre, 2005; Hernández et al., 2005). The within-class covariance matrix $\boldsymbol{\Sigma}_w$ is defined as:

$$\boldsymbol{\Sigma}_w = \sum_{i=1}^{g} \sum_{j=1}^{n_i} (x_{ij} - \boldsymbol{\mu}_i)(x_{ij} - \boldsymbol{\mu}_i)^T \tag{5.9}$$

The between-class covariance matrix $\boldsymbol{\Sigma}_b$ is defined as:

$$\boldsymbol{\Sigma}_b = \sum_{i=1}^{g} n_i(\boldsymbol{\mu}_i - \boldsymbol{\mu})(\boldsymbol{\mu}_i - \boldsymbol{\mu})^T \tag{5.10}$$

where g is the number of classes, n_i is the number of samples in class i, x_{ij} is the value for the jth observation in group i $(i = 1, \ldots, g_i; j = 1, \ldots, n_i)$, $\boldsymbol{\mu}_i$ is the sample mean vector in the ith group, and $\boldsymbol{\mu}$ is the overall sample mean vector. LDA maximises the function

$$\boldsymbol{F} = \frac{\boldsymbol{v} \cdot \boldsymbol{\Sigma}_b^x \cdot \boldsymbol{v}^T}{\boldsymbol{v} \cdot \boldsymbol{\Sigma}_w^x \cdot \boldsymbol{v}^T} \tag{5.11}$$

where $\boldsymbol{v} = (v_1, v_2, \ldots, v_d)^T$ is the vector of discriminant coefficients, and $\boldsymbol{\Sigma_b}$ and $\boldsymbol{\Sigma_w}$ are the between- and within-covariance matrices of the data matrix $\boldsymbol{X}$, respectively. One of the requirements for correct application of discriminant analysis is normality in the variables (Jarvis and Goodacre, 2005; Hernández et al., 2005). However, a problem inherent within LDA is that with many highly correlated variables, there is too much flexibility in the choice between discriminant functions. It leads to what statisticians call 'over-fitting', and it manifests itself by having perfect classification on the training set but very poor performance on the test set. A common solution to this dilemma is to reduce data dimensionality through spectral feature (i.e. band) selection.

Feature extraction Data sets from microarray experiments typically have values for each of a large number of features. Having numerous variables, such as in hyperspectral remote sensing, does not necessarily improve the performance of the classifier. In fact, an over supply of variables is likely to cause a substantial deterioration in the classification performance. When the ratio of training objects per class is comparable to or less than the dimensionality of the data, the parameter estimates of the discriminant model become highly variable (imprecise), and in some instances may not be obtained due to numerical instability.

Feature selection simply involves selecting a smaller set of variables from a larger set on the basis of some criteria. Discriminant analysis can determine the particular set of variables most relevant in describing differences among possible groups. In this context, it is appropriate to assess the adequacy of a subset of feature variables in terms of the separation they provide among the groups. In many situations, focusing only on one subset of available feature variables is inappropriate; the intention should be to find the 'best subset' in some sense (McLachlan, 1992).

Several techniques are available as a way of identifying key wavebands in high spectral resolution spectra for particular applications. Such techniques include multiple regression (Lefsky et al., 1999), derivative analysis (Demetriades-Shah et al., 1990), linear discriminant analysis (Mallet et al., 1996) and cluster analysis (Holden and LeDrew, 1998), random forest (Gentleman et al., 2005) or genetic algorithms (Yu et al., 1999).

Feature extraction is a linear or non-linear pre-processing data transformation method where the type of transformation is chosen with the aim of retaining as much discriminatory information as possible, whilst simultaneously eliminating redundant features that do not contribute to, or have an adverse effect upon, the classification procedure. Besides improving the performance of classifiers, having fewer variables often means results can be obtained with reduced computational and monetary expense. Performing feature extraction may also simply result in obtaining more meaningful information than the raw data (McLachlan, 1992).

Genetic algorithm (GA) Stochastic search strategies have been developed and tested on functional genome datasets in order to address the problem of feature extraction. *Genetic algorithms* (GA) use a randomised approach based on the processes of mutation and crossover procedures and have become popular in recent years as a robust search procedure. The same general approach to variable reduction used in bioinformatics studies (Trevino and Falciani, 2006) can be taken here with the common challenge to find a smaller subset of features which may improve discrimination. The GALGO [2] component of the software package **R** is based

---

[2]   http://www.bip.bham.ac.uk/bioinf/galgo.html

on a GA multivariate variable selection strategy, primarily to develop statistical models from large-scale datasets (Trevino and Falciani, 2006).

The GA is an evolutionary computing technique that can be used to solve problems efficiently for which there are many possible solutions (Jarvis and Goodacre, 2005). The basic concept in both exercises, typical of many GA applications, is the optimisation of a problem where a range of solutions falls within a large search space (Mallet et al., 1996). The problem is defined within a fitness function against which each individual is evaluated in order to provide a measure of its accuracy (Jarvis and Goodacre, 2005). The advantage GAs have, is the selection of combinations of variables. For example, two features chosen separately may produce less favourable results than two features chosen in combination.

The starting point of any GA is a random population, where only a small portion of the total search space is explored. Different searches therefore are likely to provide different solutions. In order to extensively cover the space of models that can be explored, it is necessary to collect a large number of variable combinations (chromosomes). The classifications are then determined by a count (majority vote) of the classifications from each subset within the selection space. This strategy of randomly selecting observations and subsets of variables for constructing new combinations can play a significant role in the analysis of hyperspectral data (Donald et al., 2006), as the variable selection approach avoids the problems associated with high wavelength correlation such that localised regions within the spectrum can be identified rather than just a single wavelength. Additionally, it helps to mitigate the effects of over fitting that can occur in a single classification. The optimal number of features is determined by repeating the cross-validation procedure for each feature combination, then choosing the number that gives the greatest predictive accuracy (Maindonald and Burden, 2005).

The GA methodology is applicable, in principle, to use in any discriminant analysis to obtain a low dimensional graphical representation. A detailed description of the procedure is available in Trevino and Falciani (2006).

5.3   Transfer to remote sensing data

5.3.1   Remote sensing data classification approach

In previous section the analysis of *in situ* derived spectra is presented. In the following section the methods applied to airborne remote sensing data are described.

The algorithms for macrophyte species discrimination were tested on the hyperspectral imagery taken with the airborne sensor HyMap using the Modular Inversion & Programming system (MIP) (Heege, 2000; Heege and Fischer, 2004). The first 33 bands of HyMap (in

the VIS from 465 to 900 nm) were used. After atmospheric, air-water interface, and water column correction (see chapter 4.4), the hyperspectral data for each year and from each lake were classified in two separate steps:

1. initial classification, giving an overview of distribution and an estimate of percent cover of tall growing vegetation (up to the water surface), short growing vegetation, and exposed sediment (see Figure 5.2.)

2. subsequent classification of pixels with greater than 70 % vegetation cover to species level, based on derivatives and distinct spectral features derived from the genetic algorithm approach. For each pixel, a probability for each species was calculated. The species with highest probability was used as a final class label.

The initial determination of percent cover of vegetation classes (tall growing (t), short growing (s), and uncovered sediment (u)) was performed using a linear spectral unmixing model, and is described in detail by Mather (1999). The underlying premise of spectral mixture analysis is that the spectral variation in an image is caused by mixtures of a limited number of bottom materials. The result is an approximation of the proportions of the ground area per pixel that are occupied by each of the reference classes. The pure reference spectral signatures are referred to as *endmembers*, as they represent the cases where 100% of the sensor's field of view is occupied by a single cover type. The reflected photons from a given pixel area on the ground and subsequently intercepted by a sensor can be described in terms of a simple linear model (Eq. 5.12):

$$r_i = \sum_{j=1}^{n} a_{ij} f_j + e_i \qquad (5.12)$$

in which r_i is the reflectance of a given pixel in the ith of m spectral bands. The number of mixture components is n, f_j is the jth fractional component (proportion of endmember j) in the make-up of r_i, and a_{ij} is the reflectance of endmember j in spectra band i.

The term e_i expresses the difference between the observed pixel reflectance r_i and the reflectance for that pixel computed from the model. The individual fractions f_i must take values between 0 and 100%, and the fractions for any given mixed pixel must sum to 100%. Note that the number of end-members n must be less than the number of spectral bands m to be computable for the components of $\boldsymbol{r}$ ($= r_i$).

The estimation of lake-bottom cover is performed by an iterative fitting algorithm to adjust the bottom spectrum to the modelled bottom spectrum. The fit is performed using the complete spectral information of the retrieved bottom spectrum between 450 and 700 nm.

The unmixing is performed using downhill simplex minimisation (Heege, 2000):

$$\boldsymbol{r} = a_u f_u + a_s f_s + a_t f_t \tag{5.13}$$

where f_u, f_s, and f_h are the proportions of uncovered bottom sediments (u), small submerged vegetation (s) and tall submerged vegetation (t) within one image pixel. The classification is based on the relative contributions of these three pure bottom types (Figure 5.2). Furthermore, discrimination between tall (t) and short (s) growing vegetation is achieved by calculating the growth height of the macrophytes. This can be done by subtracting the absolute water depth Z from the calculated water column z on top of the plants. The absolute water depth Z is derived using a 3×3 digital elevation model, the subtracted water column z on top of the plants is iteratively calculated during the process of water column correction.
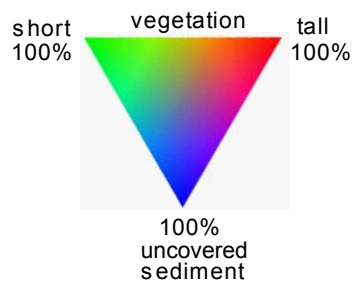
Figure 5.2: Diagrammatic presentation of percent cover distribution of tall growing macrophytes(t), short growing macrophytes (s), and sediment (u).

The information from the first bottom cover estimate is used in the subsequent analysis for species discrimination. Pixels having a bottom cover of less than 70 % vegetation were not included in the discrimination analysis, as the spectral information was not accurate enough to obtain meaningful conclusions. This second step involves a refinement of the classification with the goal to obtain a map of macrophyte species distribution. The final species distribution was obtained using spectral band combinations identified using the GALGO genetic algorithm and was applied to the HyMap remote sensing data. Distribution maps were derived to show the percent probability of one single species.

5.3.2   Validation of classification results

Pixels dominated by a specific species were identified on the scanner image using visual comparison of the image with field observations and GPS position records (Figure 7.1). The classification results were continuously validated with ground truth measurements at Lake Constance during and shortly after the flight campaigns and analysed by Geographic Information System (GIS) to test the plausibility of the data (Woithon et al., 2005). Figure 7.1 shows an example of how validation was performed at Lake Constance. GPS tracks (white lines) were recorded from the boat during field campaign to outline macrophyte patches, GPS data were compared to classified remote sensing data for correct identified patches.

The results were also compared to traditional aerial photography. Expert knowledge from Dr. D. Stelzer (TUM), Dr. K. Schmieder (Uni. Hohenheim), S. Wolfer (Uni. Constance), and A. Woithon (Uni. Hohenheim)[3] was applied for confirmation and validation of the remote sensing classification at Lake Starnberg and Lake Constance.
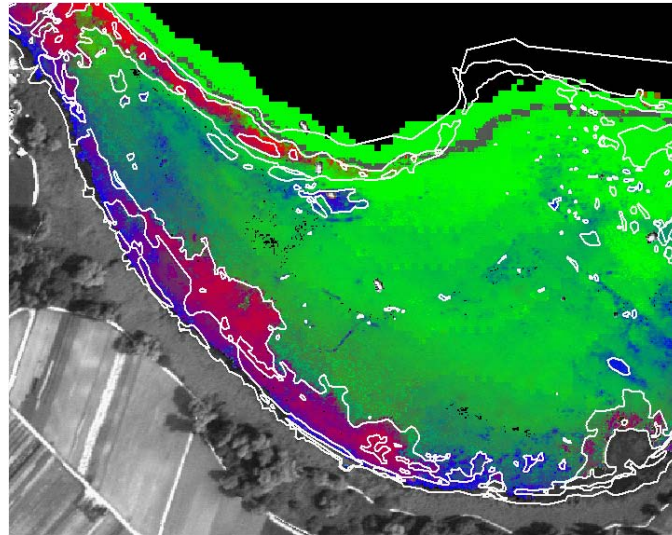
Figure 5.3: An example of validation of flight campaigns using GPS position records and GIS. The white lines in the image are GPS tracks recorded from the boat and were compared to remote sensing data classification result in GIS (Woithon et al., 2005)

---

[3] Institut für Landschafts-und Pflanzenökologie, Universität Hohenheim

Chapter 6

Results

In the following chapter, the results of statistical analyses are described, indicating the spectral difference of macrophyte species in certain wavelength regions. The classification results of hyperspectral airborne data are presented, showing the distribution of tall- and short-growing macrophytes as well as the species distribution of two selected areas in Lake Starnberg and Lake Constance.

The data set represents spectra of eight different macrophyte species: *Potamogeton pectinatus*, *P. perfoliatus*, *Chara contraria*, *C. intermedia*, *C. aspera*, *C. tomentosa*, *Najas marina*, and *Nitellopsis obtusa*. Six of the species were found at Lake Starnberg, where a juvenile and a senescent phase of the species *C. aspera*, *C. contraria* and *P. pectinatus* were also discriminated. Seven of the species were found at Lake Constance, whereas five species occurred at both of the test sites (Table 4.3).

6.1 Analysis of spectral data

A general description of the aquatic macrophytes spectra is presented first. Results of an unsupervised feature extraction technique, where PCA, derivative analysis, and the Jeffries–Matusita distance index were used, are subsequently presented. The classification potential, as determined by the degree of spectral discrimination between macrophytes species, is compared against the degree of spectral discrimination established through a supervised feature extraction technique.

6.1.1 Spectral difference between macrophyte species

Reflection spectra of the eight macrophyte species, measured directly above uniform patches, showed low VIS reflectance, caused by absorption by chlorophyll and other pigments, and high NIR reflectance due to multiple-scattering processes occurring within the leaf structure,
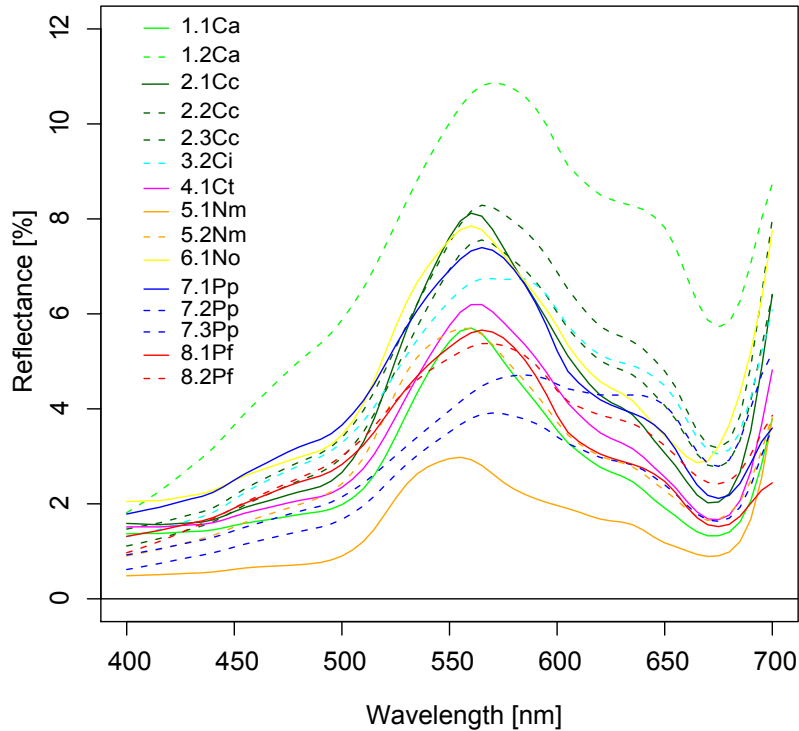
Figure 6.1: Mean irradiance reflectance spectra of eight macrophytes species measured *in situ* using a submersible RAMSES spectroradiometer. Codes for the macrophytes correspond to those used in Table 4.3. Dashed lines are spectra measured at Lake Starnberg, solid lines are spectra measured at Lake Constance.

both of which are typical vegetation reflectance patterns (Gausman, 1984). Reflectance values slowly increase from approximately 400 to 510 nm, where they rise sharply to a maximum around 550−570 nm, depending upon species. Reflectance in all spectra decrease between 550−640 nm (Figure 6.1 and 6.2); this trend at lower wavelengths is in sharp contrast with the reflectance of pure water, which is higher between 400−550 nm and drops rapidly at wavelengths greater than 600 nm (Figure 3.2). There was considerable variation in reflectance spectra between each species, particularly in the green to red (570−680 nm) portion of the visible spectrum. This region is influenced by chlorophyll absorption, and since pigment concentration and composition varies between species, so does their absorption and reflectance. Spectral reflectance of sediment (Figure 6.2, 9.2Ss) was notably higher than for macrophyte species in the visible wavelength. There was also an assumption that spectra of *Chara aspera*

(1.2Ca) were influenced by sediment (9.2Ss), as their spectra resemble the sediment more than other species.

Spectral reflectances of the macrophyte samples measured at Lake Starnberg were notably higher than those from Lake Constance (Figure 1.2). In Lake Starnberg, reflectance magnitude was highest in short-growing species, e.g. *C. aspera* (1.2Ca, 11 %) and *C. contraria* (2.2Cc, 7.5 %), and lowest in tall-growing species, e.g. *P. pectinatus* (7.2Pp, 4 %) and *P. perfoliatus* (8.2Pf, 5 %). Thus the maximum reflectance difference was about 7 %. In Lake Constance, macrophyte species had less variation in reflectance values, mostly ranged from 5 to 8 %, only *Najas marina* (5.1Nm) had a low reflectance of approximately 3 %. The maximum reflectance difference between all macrophytes was about 5 %. *Chara* species displayed a dominant reflectance peak in the green wavelengths (540−560 nm), whereas the main reflectance peak in *Potamogeton* species shifted towards longer wavelengths (570−580 nm). There were also small spectral shoulders at 650 nm present in *Potamogeton* species that were lacking in *Chara* species.

Spectral separability

The JM distance indices were calculated for all pairs of macrophytes species using the first and second principal components (Table 6.1). Sixty-one species pairs were spectrally separable, having a JM distances greater than the selected threshold value of 1.90. Thirty seven pairs were unseparable, having distances less than 1.90, and included some of the *Chara* species (2.1Cc, 3.2Ci, 4.1Ct) and some species found in Lake Constance (6.1No, 7.1Pp, 8.1Pf). Eight pairs of *Chara* species, namely *Chara aspera*, *C. contraria*, *C. intermedia*, and *C. tomentosa*, were unseparable. *Potamogeton pectinatus* (7.1Pp) was also generally unseparable from other macrophytes, based upon JM distance.

However some of the same species pairs between lakes were separable, e.g. 1.1Ca and 1.2Ca, 5.1Nm and 5.2Nm, and 8.1Pf and 8.2Pf, such that in the following analyses, the two lakes were examined separately.

6.1.2 Spectral differences within macrophyte species

The spectral reflectance curves measured over the same *P. pectinatus* patch show that reflectance increases rapidly at the beginning of the growing season, from late June (June 26th) to the middle of July (July 8th), coincident with a shift to longer wavelengths (Figure 6.3). After peak reflectance values in July, the curves show a second peak of reflectance at longer wavelengths (640−650 nm) towards the middle of August (August 12th, August 16th).

The same measurement procedure was carried out on a *C. contraria* patch in 1 m water
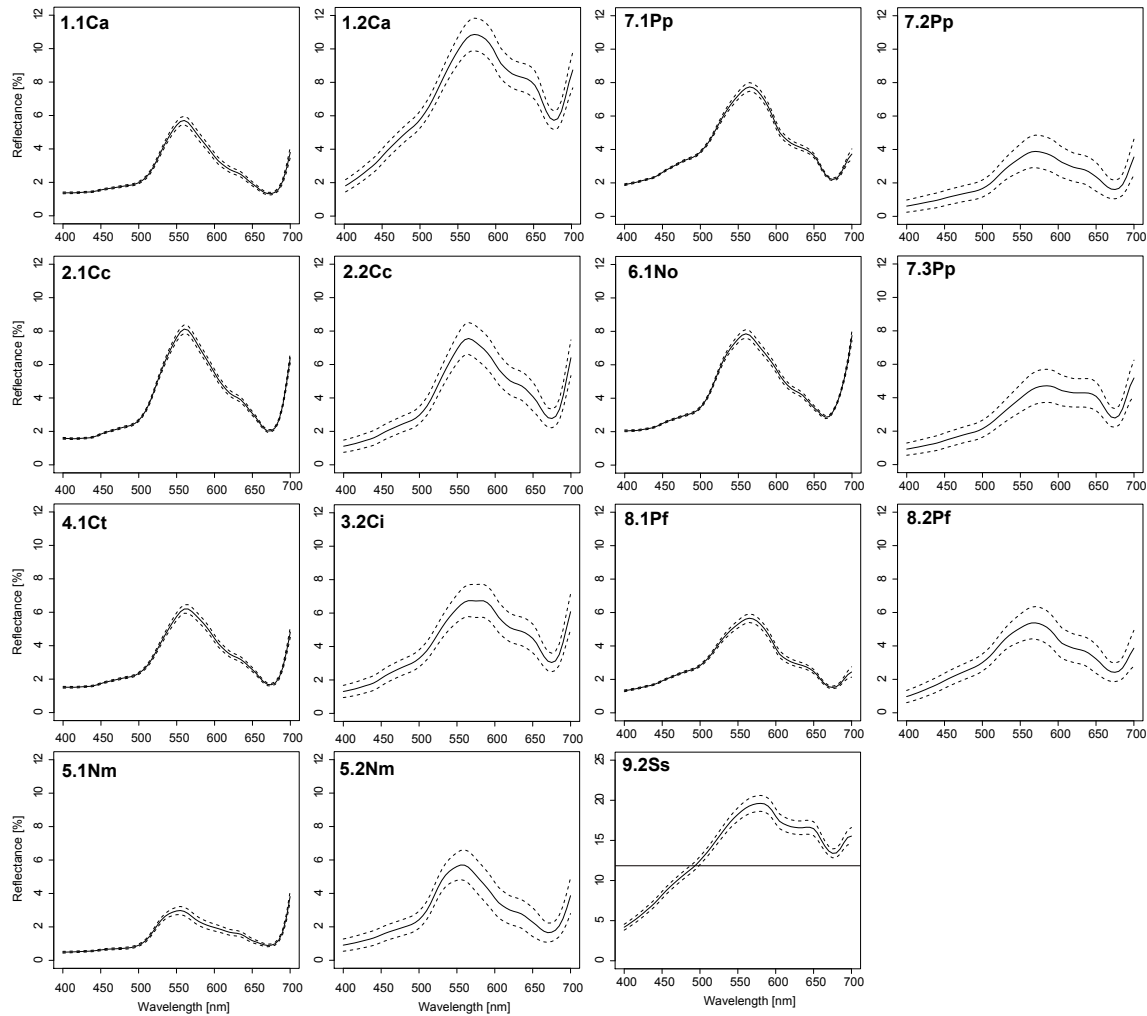
Figure 6.2: Mean and standard deviation of reflectance spectra from macrophyte species measured from Lake Constance (1) and Lake Starnberg (2 and 3). Codes for the macrophytes correspond to those used in Table 4.3(Ca=*C. aspera*, Cc=*C. contraria*, Ci=*Chara intermedia*, Ct=*Chara tomentosa*, Nm=*N. marina*, No=*N. obtusa*, Pp=*P. pectinatus*, Pf=*P. perfoliatus*, Ss=*Sediment*)

Table 6.1: Pair-wise distances between macrophyte species calculated using the first and second principal components. The values located on the upper part of the table, oriented to the right-hand side, are JM distance values and those shown on the lower portion, oriented to the left-hand side, are BH distances.

BH/JM	1.1Ca	1.2Ca	2.1Cc	2.2Cc	2.3Cc	3.2Ci	4.1Ct	5.1Nm	5.2Nm	6.1No	7.1Pp	7.2Pp	7.3Pp	8.1Pf	8.2Pf
1.1Ca		2.00	1.72	2.00	2.00	2.00	1.89	2.00	0.95	2.00	1.77	2.00	2.00	1.51	2.00
1.2Ca	13.17		1.91	1.93	1.86	1.88	2.00	2.00	2.00	1.98	1.95	2.00	2.00	2.00	2.00
2.1Cc	1.98	3.05		1.65	1.94	1.95	1.38	1.89	1.03	0.65	0.41	1.97	2.00	1.55	1.97
2.2Cc	14.74	3.38	1.75		1.16	0.99	1.88	1.95	2.00	1.04	1.40	1.92	1.97	2.00	1.79
2.3Cc	21.20	2.68	3.47	0.87		1.08	1.98	2.00	2.00	1.77	1.77	2.00	2.00	2.00	1.96
3.2Ci	9.07	2.83	3.68	0.68	0.78		1.80	1.75	1.98	1.67	1.57	1.86	1.97	1.99	1.75
4.1Ct	2.88	10.09	1.17	2.82	4.89	2.29		1.64	0.96	2.00	1.30	1.98	1.99	1.58	1.70
5.1Nm	38.78	7.01	2.86	3.62	6.23	2.10	1.73		1.97	1.88	1.43	0.63	2.00	1.97	2.00
5.2Nm	0.65	8.52	0.73	6.05	8.70	4.76	0.66	4.17		1.99	1.17	1.91	2.00	1.09	2.00
6.1No	47.18	4.47	0.39	0.74	2.18	1.81	12.47	2.84	4.96		0.72	2.00	2.00	2.00	1.99
7.1Pp	2.15	3.67	0.23	1.20	2.14	1.54	1.05	1.25	0.88	0.44		1.77	1.91	1.62	1.81
7.2Pp	6.85	14.83	4.36	3.23	8.47	2.64	4.66	0.38	3.14	7.94	2.15		1.04	2.00	1.98
7.3Pp	17.39	12.59	9.93	4.28	8.85	4.24	5.21	8.29	11.78	6.50	3.10	0.73		2.00	2.00
8.1Pf	1.41	12.07	1.50	7.81	9.48	5.35	1.55	4.23	0.79	65.32	1.66	6.79	10.96		6.59
8.2Pf	52.63	9.81	4.10	2.27	3.81	2.06	1.89	21.74	6.49	5.15	2.36	4.49	7.80	6.59	
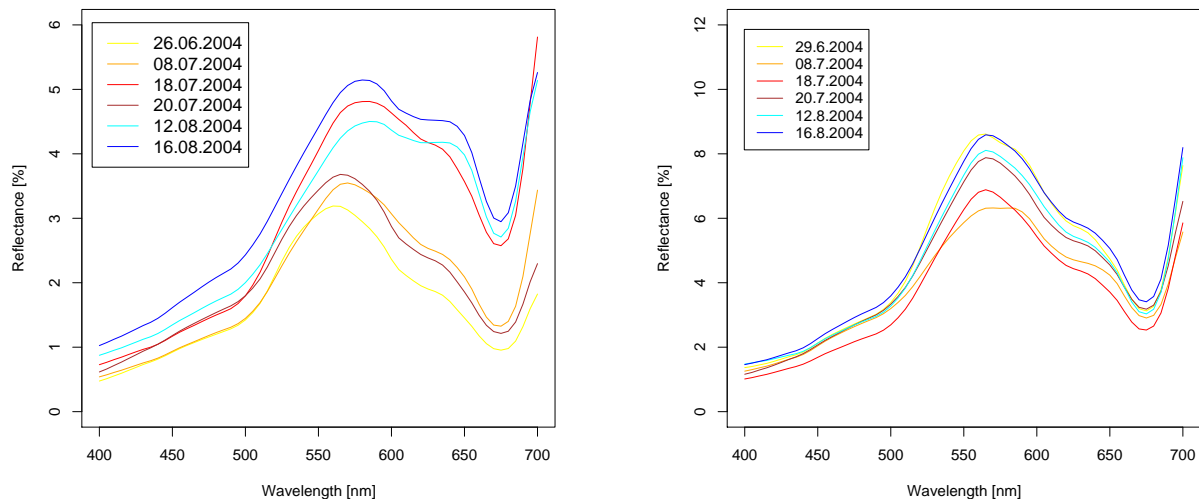
Figure 6.3: Mean reflectance spectra of *P. pectinatus* (left) and *C. contraria* (right) on six different days during the summer to show growth season variation in spectral reflectance for tall- and short-growing species.

depth (Figure 6.3). The reflectance curve for the 29th of June shows the highest reflectance, however subsequent curves show an increasing trend from the lowest reflectance on July 8th to the penultimate curve on August 16th. It is apparent that homogeneous bottom types, such as short-growing *Chara* species, show less variation in reflectance values and wavelengths than tall-growing species such as *P. pectinatus*. To investigate whether changes in sun angle contribute to differing spectral reflectance behaviour at the same plant species (e.g anisotropy effects (BRF[1]), measurements were taken at a *P. pectinatus* and a *C. contraria* patch at a constant sensor location, in nadir, on a cloud-free day every half hour from noon to late afternoon (Figure 6.4). The sun-zenith angle changed from 37.07° at noon to 57.34° in the late afternoon. Results indicate that difference in sun angle did influence spectral reflectance characteristics. This also shows that reflectance, as all AOPs, are dependent on incoming direction of the sunlight. Variation was about 1.5 % for *P. pectinatus* and 2.7 % for *C. contraria*, but differences can be considered as small compared to the large variation in sun angle. Principal components were calculated from the reflectance spectra from $400-675$ nm for all species. The total variance of all spectra explained 96.2 % of the variation, 86.1 % by the first axis and 10.1 % by axis two, thus most of the information contained in the data was able to be explained by two variables (Figure 6.5). The PCA revealed some separation

---

[1]   Bidirectional reflectance factor
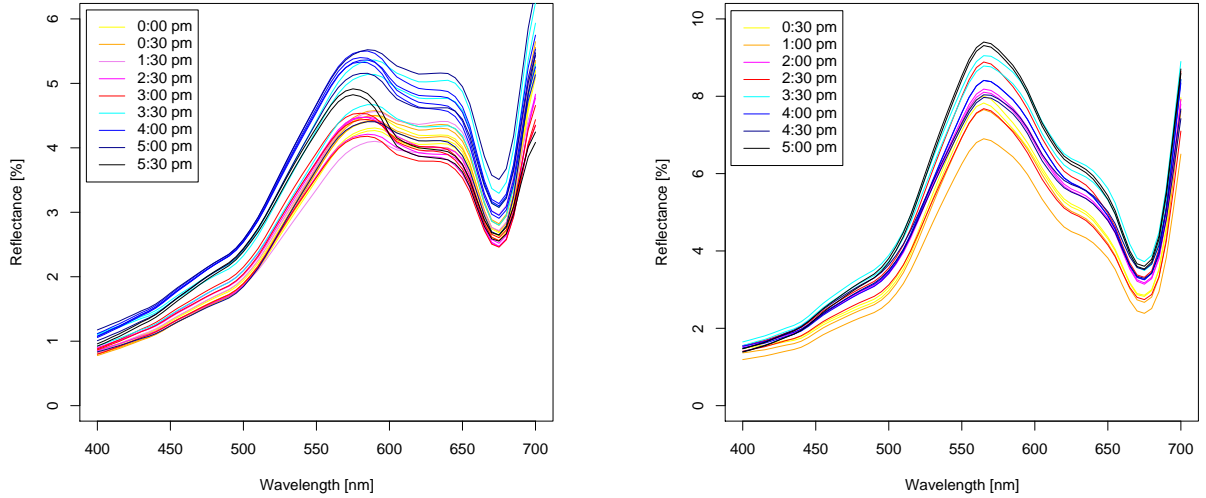
Figure 6.4: Reflectance spectra of *P. pectinatus* (left) and *C. contraria* (right) measured on August 12th 2004, every 30 minutes from 12 pm to 6 pm. Only selected curves are shown.

between two species groups, e.g. *P. pectinatus*, *C. contraria*, whereas other groups were less clearly separated.

An apparent difference in distribution occurred between the two lakes (Figure 6.5 B), with samples from Lake Constance lying above axis 1 and many of those from Lake Starnberg below this axis. A further distinction between tall-and short growing species is observed (Figure 6.5 C), likely due to the separation between *C. aspera* and *P. pectinatus*, and is more obvious in Lake Starnberg (Figure 6.5 B and C).

The variation in reflectance spectra between 2003 and 2004 appears equally distributed, such that no differences are considered to have occurred between years (Figure 6.5 D).

6.1.3 Wavelength selection for remote sensing of macrophyte species

The first, and second-order derivatives of mean reflectance spectra of macrophyte species show differences in shape and magnitude for both lakes (Figure 6.6), and provides a mean to quantify the exact wavelengths at which absorption troughs and inflection points occur in reflectance data. In all derivative calculations, the wavelength range at which macrophyte species exhibited noticeable difference was between 480 and 650 nm. The wavelengths where the greatest difference between the macrophyte species occurred in the reflectance spectra were at 485, 560, and 650 nm. In the first-order derivative, these wavelengths were 520, 545, 575, 600, and 665 nm. A greater number of absorption troughs and inflection points were

Figure 6.5: Principal component analysis of mean reflectance spectra for A: all macrophyte species, B: macrophytes in Lakes Starnberg and Constance, C: tall- and short-growing macrophytes, and D: all macrophytes measured in 2003 and 2004.

observed from the second-order derivative, occurring at 500, 560, 575, 600, 620, and 650 nm. The first-order derivative spectra appear to be less subject to noise than the second-order, suggesting that the first derivatives would be the best option in selecting wavelengths to distinguish between macrophyte species. Comparison of these wavelengths and published pigment absorption peaks confirms that the first-order derivative identified suitable wavelengths for subsequent analyses.
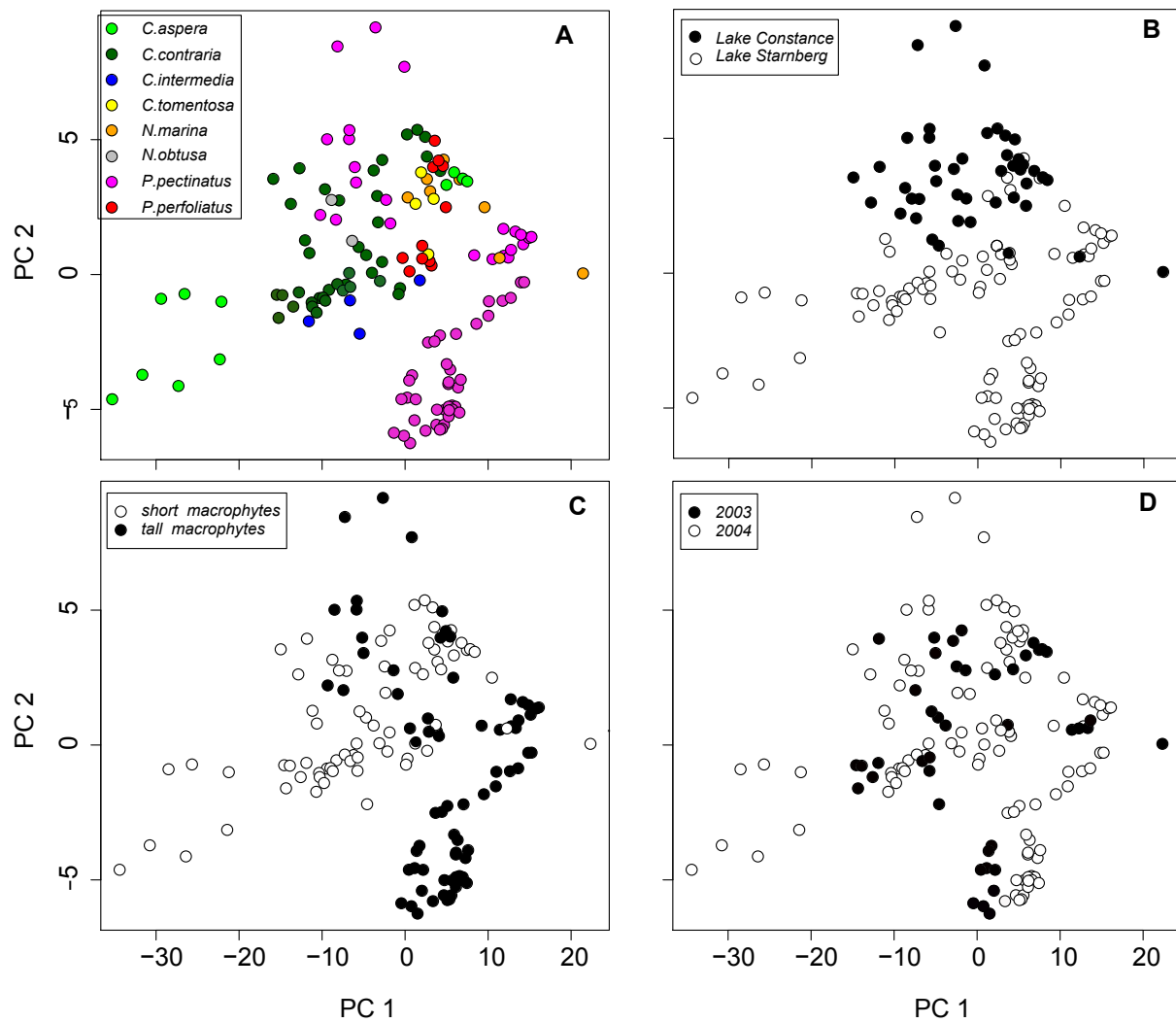
Principal component analysis was applied to reflectance spectra, first, and second-order derivative spectra. PC *loadings* (Figure 6.7) describe how closely a particular spectrum resembles the principal component. The higher the magnitude of the loading at a certain wavelength, the higher the correlation to the principal component at the same wavelength. These PC loadings thereby emphasise the significance of certain wavelength locations for macropyhte species discrimination and confirm important wavelengths location as found in derivative analysis.

Reflectance spectra were most correlated to the first PC (solid line) at about 560 nm, and most correlated to the second PC (dashed line) at about 550 and 650 nm. First-order derivatives for PC loadings showed the most correlation at $520-540$ nm and 565 nm for the first axis, and 520 and 585 nm for axis two. Second-order derivative spectra showed minor correlations at 510, 560, 575, 600 and 650 nm to axis one, and at 535, 600, 625, and 650 nm with axis two.

6.1.4 Automated feature selection using a Genetic Algorithm

Employment of the genetic algorithm to analyse the RAMSES data reveals an evolution of the maximum fitness across generations in searches (Figure 6.8). This test function returns the average test error in all validation (test) sets and computes the accuracy of a given variable combination. The point where the highest interval intersects the 'goal fitness' is the average number of generations needed to reach the fitness value.

Reflectance spectra reached a goal fitness of 90 %, whereas a combination of reflectance spectra and their first and second derivatives increased goal fitness to 98 % in both lakes. Derivatives were therefore included in following analyses. The average fitness for Lake Constance was 98 % and for Lake Starnberg was 99 %. The average fitness reached the goal fitness (98 %) after 65 generations for Lake Constance and after already after 5 generations for Lake Starnberg. The unfinished fitness average (the fitness of all searches that has not ended by a given generation and shows the average worst case expectation) was 97 % for both Lake Constance and Lake Starnberg. Thus the genetic algorithm performance was moderately better on Lake Starnberg spectra, but was considered acceptable for both lakes.
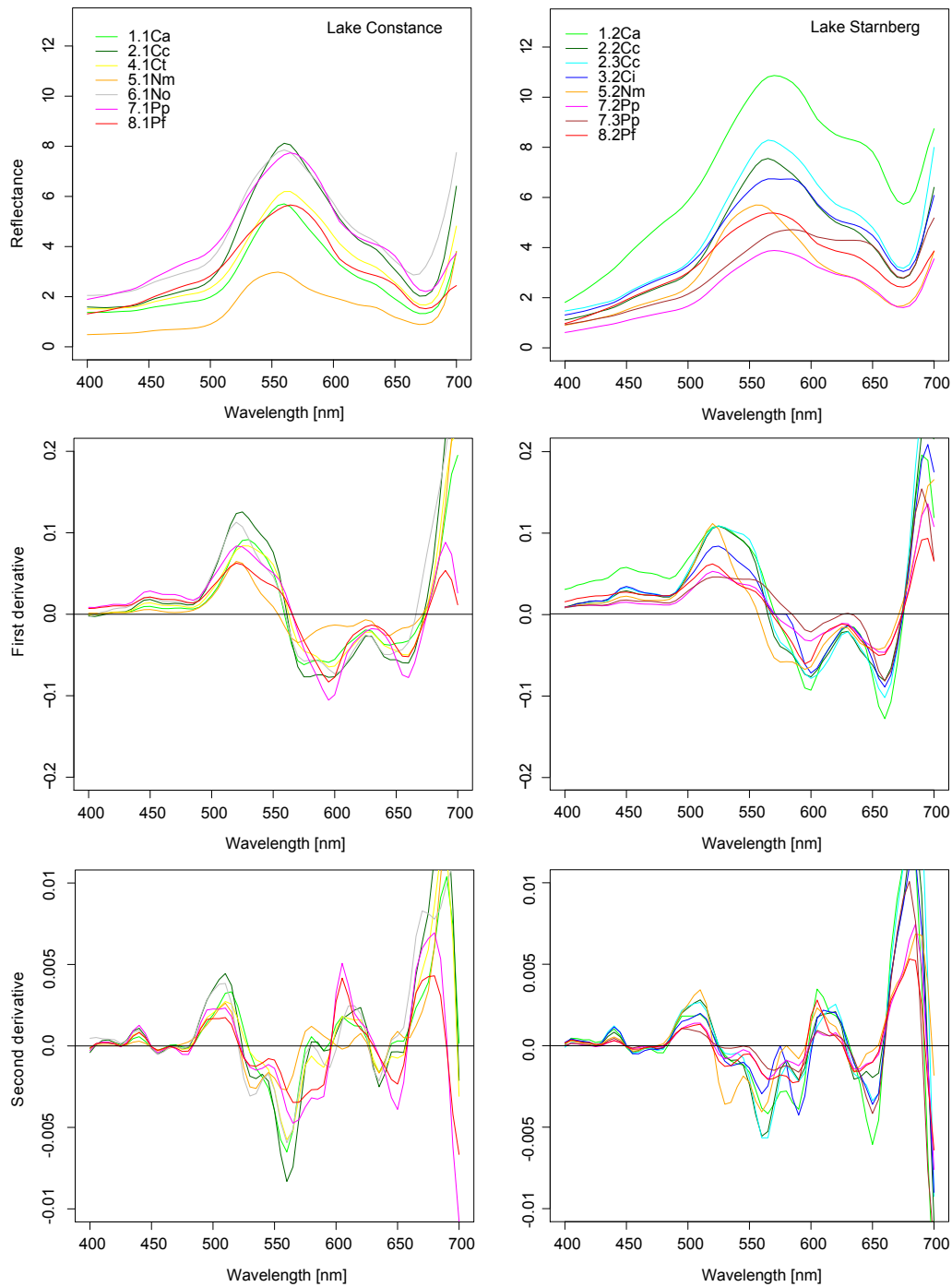
Figure 6.6: Average spectral reflectances, first, and second-order derivatives seven macro-phyte species measured at Lake Constance (left) and six species measured at Lake Starnberg (right)
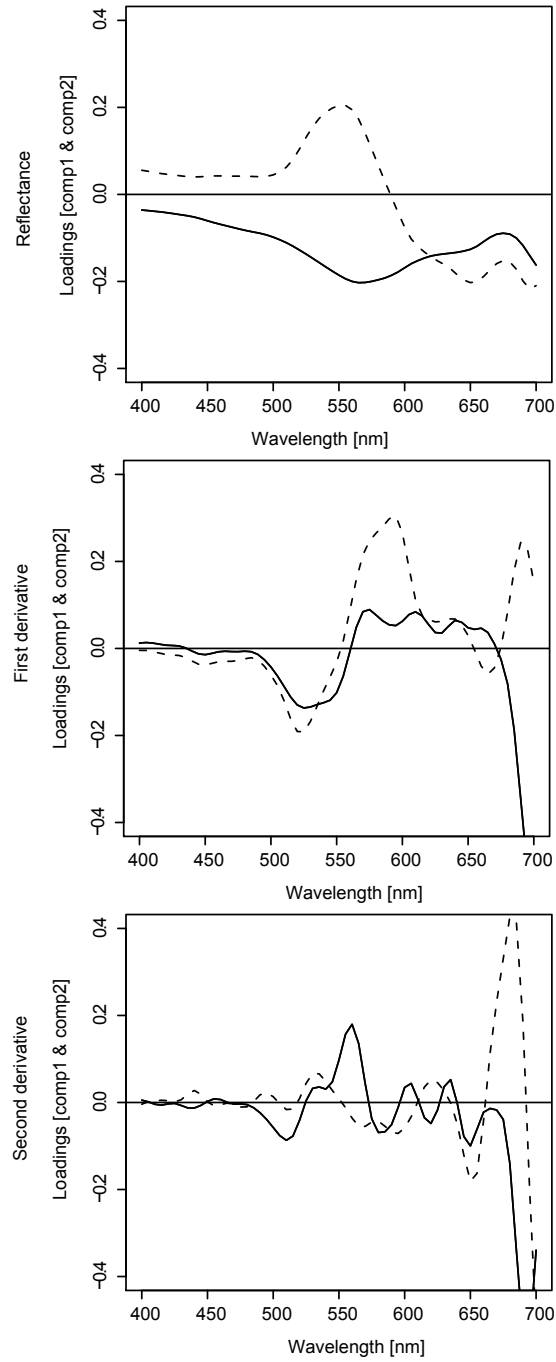
Figure 6.7: Reflectance (top), first-order (middle), and second-order (bottom) derivatives of PC loadings calculated for reflectance spectra shown in Figure 6.5. Axis one is shown as the solid line, axis two as the dashed line.
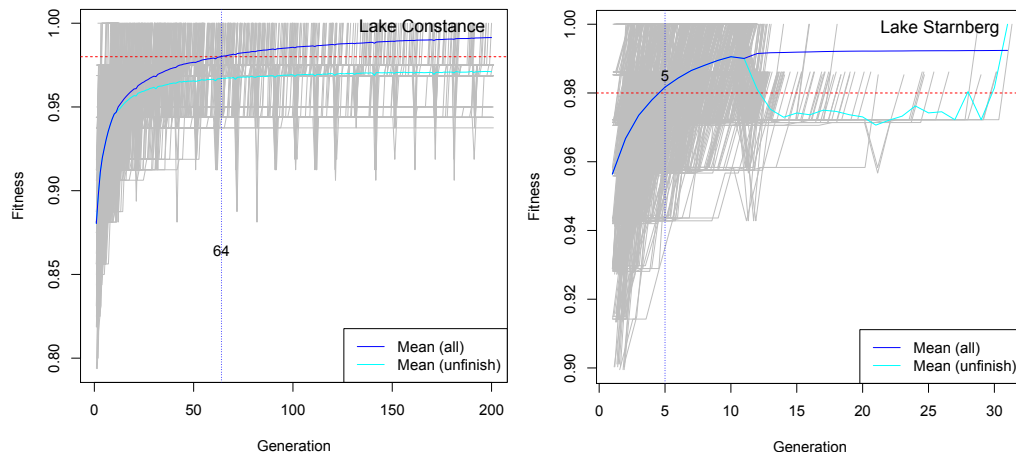
Figure 6.8: Fitness functions for Lake Constance (left) and Lake Starnberg (right). The generation in which the average fitness reaches the goal fitness of 98 %, shown in red, is indicated (64) and (5). Mean (all) fitness is the average fitness considering all searches and represents the expected frequency by generation. Mean (unfinish) fitness is the average fitness of all searches that has not ended by a given generation, and is intended to show the average worst-case expectation.

For Lake Constance and Lake Starnberg, four wavelength were chosen between $445 - 665$ nm. At Lake Constance, three were below 600 nm whereas for Lake Starnberg, features at longer wavelengths were selected which provided better separation between tall-growing species and senescent species. These selected wavelength for Lake Constance were 510 nm in reflectance, 530 nm and 625 nm in the 1st order, and 535 nm in the 2nd order derivative. For Lake Starnberg, somewhat different wavelength locations were selected: 445, 520, 625 and 665 nm in the 1st order. This confirmed the assumption that the two lakes should be treated separately.

Linear discriminant analysis, using the GALGO-selected spectral wavelengths, shows good discrimination between most species (Figure 6.9 and 6.10) in both Lake Constance and Lake Starnberg. Considerable between-species overlap occurs primarily with *Najas marina* (5.1Nm) in Lake Constance. In Lake Starnberg, less overlapping occurred, though *Chara contraria* (2.2Cc) had some overlap with *Najas marina*. For both lakes, a significant portion of macrophytes species could be discriminated based on wavelength selected by discriminant analysis. The magnitude of the discriminant coefficients can also be used to relate the importance of the wavelengths used for classification. A small coefficient implies that the selected wavelength is not that useful for discriminant analysis, while a large coefficient implies a robust wavelength.
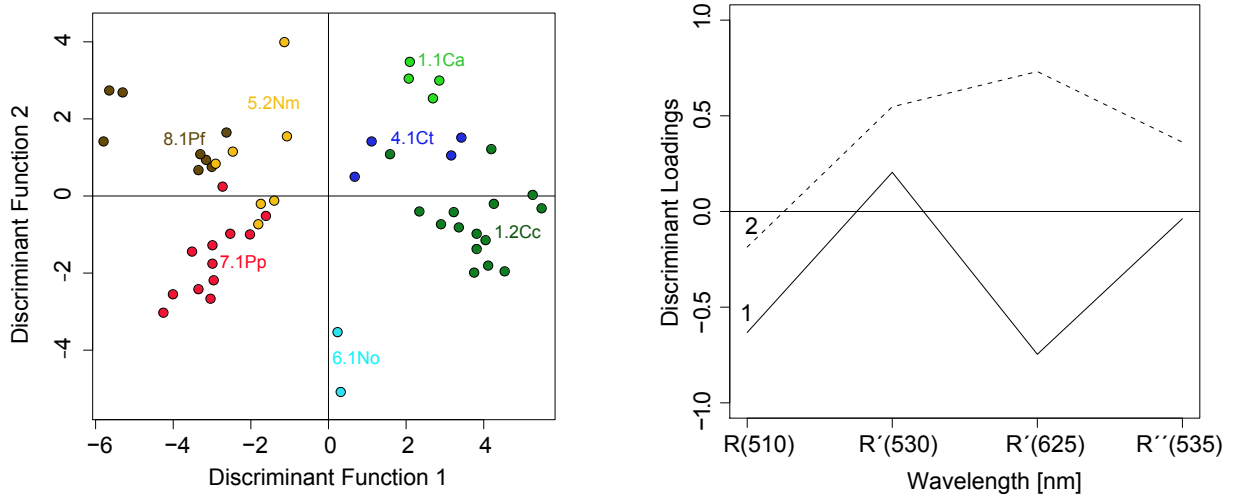
Figure 6.9: Discriminant analysis using GALGO-selected wavelengths for Lake Constance (left) and first and second discriminant loadings (right). Selected wavelengths for Lake Constance were 510 nm in reflectance, 530 and 625 nm in the first order derivative, and 535 nm in the second order derivative.
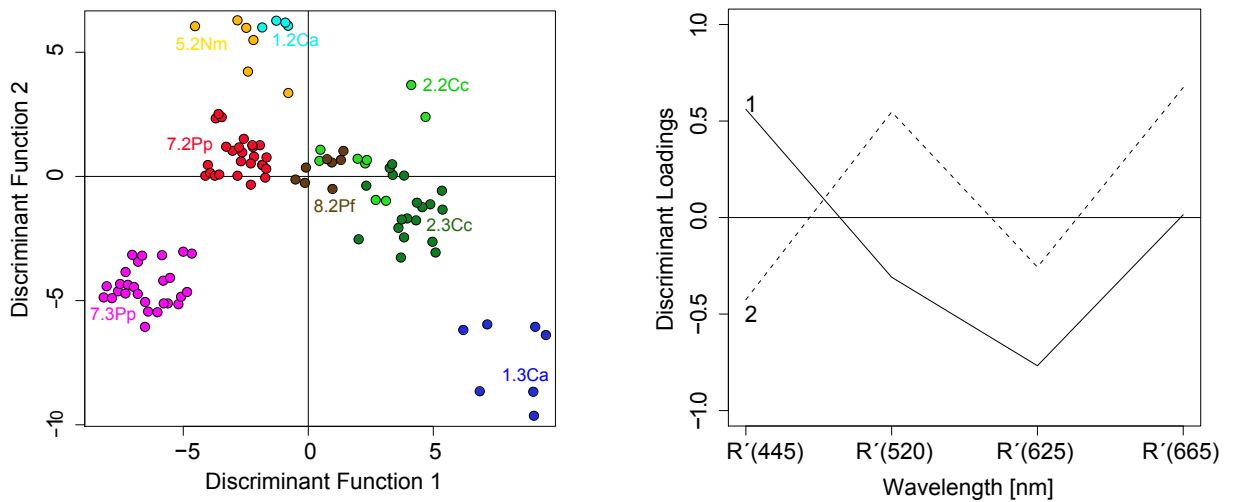
Figure 6.10: Discriminant analysis using GALGO-selected wavelengths for Lake Starnberg (left) and first and second discriminant loadings (right). The selected wavelengths for Lake Starnberg were 445, 520, 625, and 665 nm all in first order derivatives.

Analysis of model accuracy

A confusion matrix (Tables 6.2a and 6.2b) is a matrix that shows the various classifications and misclassifications of a model in a compact area and contains information about actual and predicted classifications. Each column of the matrix represents predicted classes from the classifier, while each row represents the true class values from the validation set. Correctly classified spectra therefore fall along the diagonal of the matrix.

The confusion matrix provides information on both the overall classification accuracy as well as the errors among specific species pairs of classes. The sensitivity (*Sensit*)[2] and specificity (*Specif*)[3] for all classes are given in horizontal axis, which indicates the percentage of true positive rate and true negative rate, respectively.

The accuracy of discrimination is shown by the probability that each species in the randomly-generated test set was identified correctly using a randomly-generated training set. From Lake Constance, 99.9 % of the species identified as *C. aspera* (bottom-most species on the vertical axis) were identified correctly, and 26.2 % of what was identified as *C. tomentosa* was actually *C. aspera* (Table 6.2a). Only 0.1 % of what was identified as *C. aspera* was in fact *C. tomentosa*.

Of the species identified as *C. contraria* (next species upwards on the vertical axis), 86.5 % were correctly identified, 1.6 and 2.9 % of what was identified as *C. tomentosa* and *N. obtusa*, respectively, was actually *C. contraria*. Only 0.7 % of what was identified as *C. contraria* was *C. aspera*. Similarly, 6.9, 3.4, and 2.0 % of what was identified as *C. tomentosa*, *N. marina*, and *N. obtusa*, respectively, was *C. contraria*. Of the species identified as *C. tomentosa* (third species upwards on the vertical axis), only 68.2 % were actually *C. tomentosa*, and 6.9 % of the algae identified as *C. contraria* were actually *C. tomentosa*.

Of the total species identified as *C. tomentosa*, 26.2 % were *C. aspera*, 1.6 % were *C. contraria*, and 2.9 % were *P. perfoliatus*. Of the species identified as *N. marina*, a total of 94.2 % were correctly identified, and 3.4 % of the species identified as *C. contraria* were in fact *N. marina*. False identifications were 1.5 % *C. aspera* and 4.0 % *P. perfoliatus*.

---

[2]   Sensitivity = true positives /(true positive + false negatives)
[3]   Specificity = true negatives /(true negatives + false positives)

Table 6.2a: Class confusion for Lake Constance using *in situ* spectra. Columns represent the true class value (*original class*), whereas rows represent the values assigned by the classification algorithm(*predicted class*). Correctly classified cases occur on the diagonal.

NA	0	0	0	0	0	0	0
8.1Pf	0	0.002	0.029	0.040	0	0.076	**0.982**
7.1Pp	0	0.003	0.007	0	0.009	**0.894**	0.002
6.1No	0	0.020	0.001	0.001	**0.958**	0.007	0
5.1Nm	0	0.034	0.002	**0.942**	0.002	0.002	0.003
4.1Ct	0.001	0.069	**0.682**	0.001	0.002	0.016	0.005
2.1Cc	0	**0.865**	0.016	0.001	0.029	0.001	0
1.1Ca	**0.999**	0.007	0.262	0.015	0	0.003	0.008

	1.1Ca	**2.1Cc**	**4.1Ct**	**5.1Nm**	**6.1No**	**7.1Pp**	**8.1Pf**
Samples	4	15	4	7	2	12	8
Sensit	**0.999**	**0.865**	**0.682**	**0.942**	**0.958**	**0.894**	**0.982**
Specif	**0.951**	**0.992**	**0.984**	**0.993**	**0.995**	**0.996**	**0.975**

Table 6.2b: Class confusion for Starnberg using *in situ* spectra. Columns represent the true class value (*original class*), whereas rows represent the values assigned by the classification algorithm (*predicted class*). Correctly classified cases occur on the diagonal.

NA	0	0	0	0	0	0	0	0
8.2Pf	0	0	0.021	0.04	0.009	0.010	0.001	**0.971**
7.3Pp	0	0	0.002	0.001	0.001	0.007	**0.996**	0.002
7.2Pp	0	0	0	0	0.008	**0.975**	0.003	0.013
5.2Nm	0	0	0.011	0	**0.952**	0.001	0	0.005
2.3Cc	0	0.002	0.061	**0.966**	0	0.001	0	0
2.2Cc	0	0	**0.901**	0.028	0.004	0.002	0.001	0.007
1.3Ca	0	**0.997**	0	0	0	0	0	
1.2Ca	1	0	0.003	0	0.026	0.003	0	0.002

	1.2Ca	**1.3Ca**	**2.2Ca**	**2.3Cc**	**5.2Nm**	**7.2Pp**	**7.3Pp**	**8.2Pf**
Samples	4	7	9	19	6	24	27	8
Sensit	**1**	**0.997**	**0.901**	**0.996**	**0.952**	**0.975**	**0.996**	**0.971**
Specif	**0.995**	**1**	**0.994**	**0.991**	**0.997**	**0.996**	**0.998**	**0.994**

Table 6.3a: Pair-wise distances calculated using four GALGO-selected wavelengths from Lake Constance (420 nm (R), 490 nm (R'), 620 nm (R'), and 530 nm (R'')). The values located on the upper part of the table, oriented to the right-hand side, are JM distance values and those shown on the lower portion, oriented to the left-hand side, are BH distances.

	1.1Ca	1.2Cc	4.1Ct	5.1Nm	6.1No	7.1Pp	8.1Pf
1.1Ca		1.99	1.94	2.00	2.00	1.98	2.00
2.1Cc	5.85		1.93	1.99	2.00	1.98	1.99
4.1Ct	3.60	3.38		2.00	1.99	1.81	1.99
5.1Nm	128.49	5.43	253.74		2.00	1.99	2.00
6.1No	285.59	15.64	7.76	41.69		1.97	1.99
7.1Pp	5.17	5.05	2.36	11.07	4.25		1.95
8.1Pf	23.98	6.44	6.47	23.93	8.97	3.83	

Identification accuracy for *N. obtusa* was 95.8 %, however 2.0 % of the species identified as *C. contraria* were actually *N. obtusa*, and 2.9 % of what was identified as *N. obtusa* was actually *C. contraria*. A total of 89.4 % of the species identified as *P. pectinatus* were correctly identified. Only minor percentages (< 1 %) of this species were identified as other species. However, 7.6 and 1.6 % of what was identified as *P. pectinatus* were actually *P. perfoliatus* and *C. tomentosa*, respectively. *P. perfoliatus* was identified correctly at 98.2 %, however 2.9 and 7.6 % of what were identified as *C. contraria* and *P. pectinatus* was actually *P. perfoliatus*.

Sensitivity was acceptable for all macrophyte classes except *C. tomentosa*, whereas specificity was acceptable in all classes. A NA class was added in the predicted class axis (vertical) for those classification methods that cannot produce a class prediction in any case. There were no cases where a classification could not be made. From Lake Starnberg (Table 6.2b, all species were correctly identified with an accuracy greater than 90 %. Sensitivity and specificity were acceptable in all classes. There were no cases were a classification could not be made.

The JM distance was calculated for GALGO-selected wavelengths of the macrophyte reflectance spectra from Lake Constance (Table 6.3a) and Lake Starnberg (Table 6.3b). All but one of the macrophyte species pairs were significantly different, exceeding the 1.90 threshold value. *Chara tomentosa* (4.1Ct) and *Potamogeton perfoliatus* (7.1Pf) at Lake Constance could not be separated, having a JM index less than 1.9.

Table 6.3b: Pair-wise distances between macrophyte species, calculated using GALGO-selected wavelengths from Lake Starnberg (485 nm (R), 440 nm (R'), 540 nm (R'), and 665 nm (R'')). The values located on the upper part of the table, oriented to the right-hand side, are JM distance values and those shown on the lower portion, oriented to the left-hand side, are BH distances.

	1.2Ca	1.3Ca	2.2Cc	2.3Cc	5.2Nm	7.2Pp	7.3Pp	8.2Pf
1.2Ca		2.00	2.00	2.00	2.00	2.00	2.00	2.00
1.3Ca	42.85		1.99	1.99	2.00	2.00	2.00	1.99
2.2Cc	32.81	12.91		1.95	1.99	1.99	1.99	1.99
2.3Cc	21.97	7.26	3.76		1.99	1.99	1.99	1.99
5.2Nm	36.84	19.63	9.41	12.85		1.99	1.99	1.99
7.2Pp	99.27	20.08	6.28	8.60	6.61		1.99	1.99
7.3Pp	219.66	19.77	12.06	6.83	12.73	6.31		1.99
8.2Pf	81.92	13.31	13.14	7.86	12.35	6.33	7.25	

Simulated HyMap spectral resolution

Optimal combinations of wavelengths were derived using GALGO based on a maximum likelihood discriminant function (MLHD) classifer and were calculated for different wavelength ranges: $400-700$ nm, $480-650$ nm, and $480-600$ nm, depending on usable spectral information in different water depths. Average JM distances for each species were derived and compared for variable selection performance in Lake Constance (Table 6.4a) and Lake Starnberg (Table 6.4b). For all variable combinations, JM distances were > 1.9, thus all species were significantly different. The selected wavelength combinations used for further analysis were in the $480-650$ nm wavelength range, providing maximal discrimination of species and usable spectral information for differing water depths after water column correction. The wavelengths used differed both between years and lakes (Table 6.4a).

The average fitness functions for HyMap resolution in 2003 and 2004 performed better for Lake Starnberg, reaching average fitnesses of 98 %, than in Lake Constance, where the average fitness was 96 % in 2003 and 95 % in 2004 (Figure 6.11b). The average unfinished fitness was 97 % for Lake Starnberg in 2003 and 2004, and 94 % and 92 % for 2003 and 2004, respectively, in Lake Constance. Thus the genetic algorithm performed better on Lake Starnberg spectra, showing more stable results independent of sensor resolution. The lower fitness values in Lake Constance for 2004 suggests some limitations in classification may occur. The HyMap resampled data showed, on average, a 2% lower fitness than with full-resolution RAMSES data (Figures 6.2a and 6.2b).

Linear discriminant analysis using the GALGO-selected wavelengths in resampled HyMap

Table 6.4a: Mean JM distances for GALGO-selected wavelengths from Lake Constance calculated independently for 2003 and 2004.

Species	mean JM 400-700 nm 2003	mean JM 400-700 nm 2004	mean JM 480-650 nm 2003	mean JM 480-650 nm 2004	mean JM 480-600 nm 2003	mean JM 480-600 nm 2004
1.1Ca	1.996	1.993	1.989	1.991	1.990	1.996
2.1Cc	1.967	1.995	1.979	1.956	1.998	1.998
4.1Ct	1.964	1.974	1.984	1.968	1.975	1.994
5.1Nm	1.992	2.000	1.999	1.975	1.999	1.999
6.1No	1.997	2.000	2.000	2.000	1.999	1.990
7.1Pp	1.982	1.974	1.982	1.977	1.985	1.984
8.1Pf	1.981	1.992	1.997	1.986	1.998	1.991

Table 6.4b: Mean JM distances for GALGO-selected wavelengths from Lake Starnberg calculated independently for 2003 and 2004.

Species	mean JM 400-700 nm 2003	mean JM 400-700 nm 2004	mean JM 480-650 nm 2003	mean JM 480-650 nm 2004	mean JM 480-600 nm 2003	mean JM 480-600 nm 2004
1.2Ca	2.000	2.000	2.000	1.999	1.988	2.000
1.3Ca	1.995	1.997	1.999	1.999	1.999	1.999
2.2Cc	1.971	1.978	1.949	1.923	1.738	1.826
2.3Cc	1.974	1.977	1.951	1.927	1.764	1.857
5.2Nm	1.999	1.999	1.999	1.970	1.960	1.998
7.2Pp	1.971	1.996	1.995	1.992	1.991	1.997
7.3Pp	1.999	1.999	1.998	1.994	1.990	1.998
8.2Pf	1.988	1.999	1.997	1.998	1.988	1.977

resolution show good discrimination between most species and between Lake Constance (Figure 6.12a) and Lake Starnberg (Figure 6.12b). For both data sets in Lake Constance (HyMap 2003 and 2004), species overlap occurs primarily with *Najas marina* (5.1Nm) and *Potamogeton pectinatus* (7.1Pp). Less overlap occurred in Lake Starnberg, though *Chara contraria* (2.2Cc) had some overlap with *Najas marina*. Lake Starnberg 2004 showed the best results, where only *Chara contraria* (2.2Cc) and *Chara contraria* senescent (sen.)(2.3Cc) could not be separated. Regardless of lake and HyMap resolution (2003 or 2004), both lakes showed that a significant portion of macrophytes species could be discriminated based on selected wavelengths by discriminant analysis.
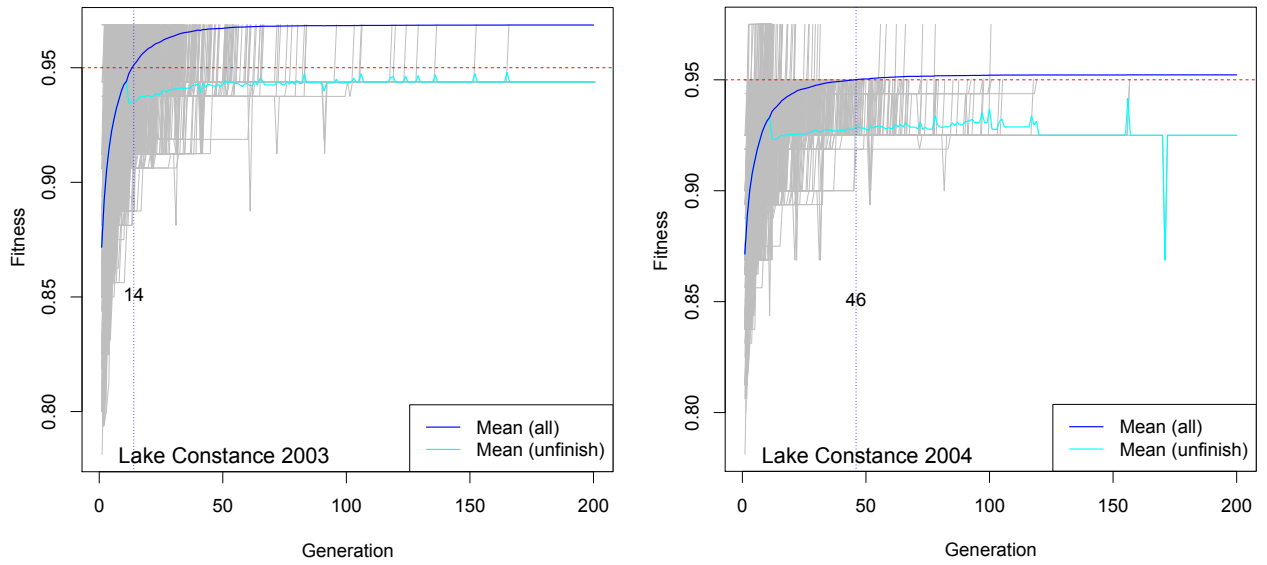
Figure 6.11a: Comparison of fitness evolution of different data sets for Lake Constance and Lake Starnberg, 2003 and 2004.
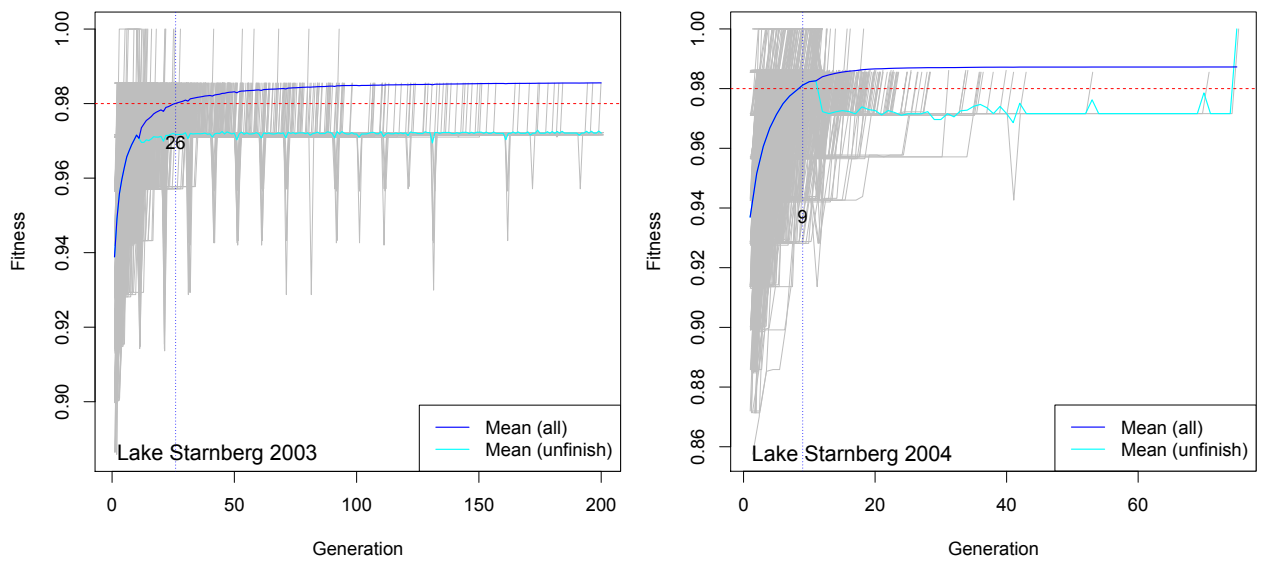

Figure 6.11b: Comparison of fitness evolution of different data sets Lake Starnberg 2003 and 2004.
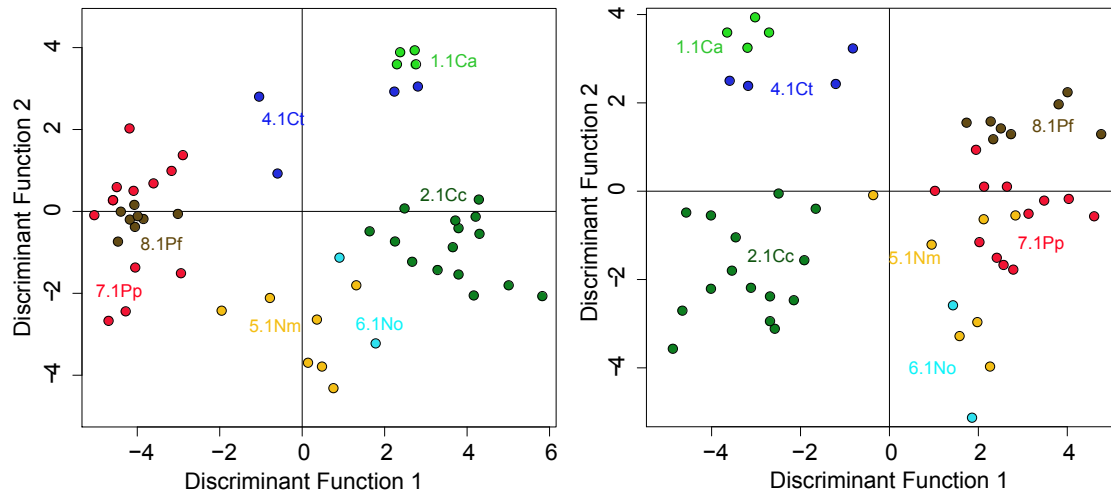
Figure 6.12a: Linear discriminant analysis using GALGO-selected wavebands for Lake Constance 2003 (left) and 2004 (right).
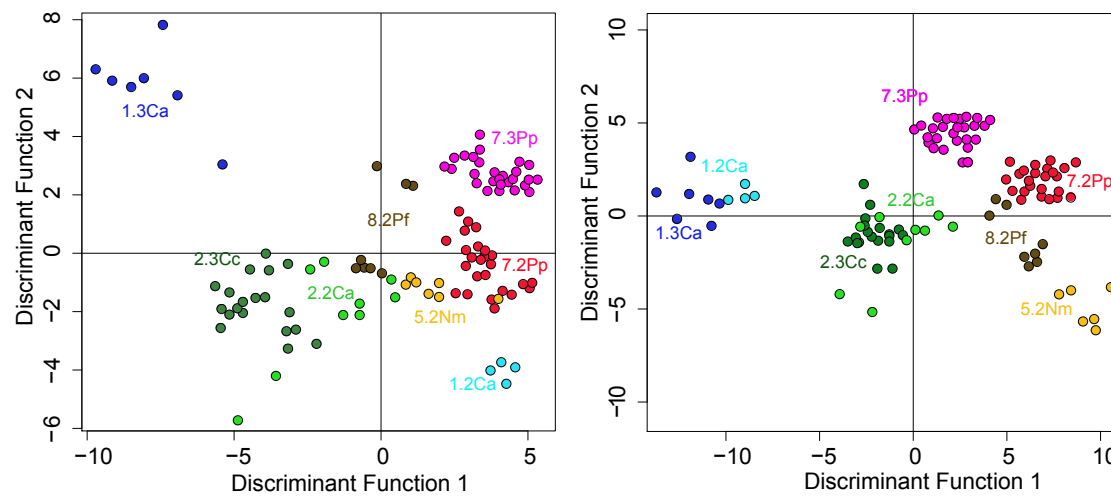

Figure 6.12b: Linear discriminant analysis using GALGO-selected wavebands for Lake Starnberg 2003 (left) and 2004 (right).

The accuracy of discrimination for Lake Constance 2003 data (Table 6.5a) reveals that *C. aspera* was 100 % correctly identified, though it was incorrectly classified as *C. tomentosa* 28.3 % of the time. *C. contraria* was 88.3 % correctly identified, but was also incorrectly classified as *P. pectinatus*. *C. tomentosa* was only 57.2 % correctly identified, as 28.3 % of what was classified as *C. tomentosa* was *C. aspera*. *N. marina* was correctly identified to 92 % and minor confusion existed with *N. obtusa*. *N. obtusa* was identified correctly 81.4 % of the time, where 6.7 % of what was classified as *N. obtusa* was actually *N. marina*. *P. pectinatus* was correctly classified to 84 %, however 6.2 and 6.3 % were actually *C. contraria* and *P. perfoliatus*, respectively. *P. perfoliatus* was classified to 99 % accuracy, and was also the best identifiable class with the highest sensitivity and specificity. Mean accuracy for all species was 86 %. *C. tomentosa* showed poor sensitivity (0.572), but in all cases identifications could be made, as no NA assignments occurred.

Class confusion at Lake Constance 2004 (Table 6.5b) showed an overall accuracy of 89 % for all classes, marginally better than in 2003. *C. aspera* was identified correctly to 100 %, but 26 % of what was classified as *C. tomentosa* was *C. aspera*. *C. contraria* was correctly identified to 84.3 %, but 15.8 % of what was incorrectly classified as *N. obtusa* was also *C. contraria*. *C. tomentosa* was identified slightly better than in 2003 at 72.5 %, but confusion with *C. aspera* still existed. *N. marina* was correctly identified to 98.1 %, whereas *N. obtusa* was correctly identified 76.5 % of the time. *P. pectinatus* was correctly classified to 93.7 %. *P. perfoliatus* was 99.6 % accurate, and was also the best identifiable class, having the highest sensitivity and specificity. The sensitivity was acceptable in all macrophyte classes except *C. tomentosa* and *N. obtusa*. Specificity was acceptable in all classes.

From Lake Starnberg (Tables 6.6a and 6.5b), all species except *C. contraria* and *C.contraria* senescent were correctly identified with an accuracy greater than 95 %. In 2003, *C. contraria* (2.2Cc) and *C. contraria* sen. (2.3Cc) had accuracies of 89.3 and 89.8 % respectively, whereas in 2004, *C. contraria* (2.2Cc) and *C. contraria* sen. (2.3Cc) had accuracies of 93.1 and 93.4 %, respectively. Sensitivity and specificity were acceptable in all classes in both years. No cases occurred where a classification could not be made.

Table 6.5a: Class confusion for Lake Constance 2003 using simulated HyMap spectra. Columns represent the true class value (*original class*), whereas rows represent the values assigned by the classification algorithm(*predicted class*). Correctly classified cases occur on the diagonal.

NA	0	0	0	0	0	0	0
8.1Pf	0	0.001	0.013	0.028	0.004	0.063	**0.995**
7.1Pp	0	0.026	0.007	0.001	0.057	**0.840**	0.005
6.1No	0	0.019	0.001	0.046	**0.814**	0.019	0
5.1Nm	0	0.029	0	**0.923**	0.067	0.003	0
4.1Ct	0	0.040	**0.572**	0.002	0	0.013	0
2.1Cc	0	**0.883**	0.008	0	0.058	0.062	0
1.1Ca	1	0.001	0.283	0.001	0	0	0
	1.1Ca	**2.1Cc**	**4.1Ct**	**5.1Nm**	**6.1No**	**7.1Pp**	**8.1Pf**
Samples	4	15	4	7	2	12	8
Sensit	**1**	**0.883**	**0.572**	**0.923**	**0.814**	**0.840**	**0.995**
Specif	**0.953**	**0.979**	**0.991**	**0.983**	**0.986**	**0.984**	**0.962**

Table 6.5b: Class confusion for Lake Constance 2004 using simulated HyMap spectra. Columns represent the true class value (*original class*), whereas rows represent the values assigned by the classification algorithm (*predicted class*). Correctly classified cases occur on the diagonal.

NA	0	0	0	0	0	0	0
8.1Pf	0	0.008	0.005	0.015	0.003	0.048	**0.996**
7.1Pp	0	0.015	0.003	0	0.054	**0.937**	0.003
6.1No	0	0.060	0.006	0.004	**0.765**	0.007	0
5.1Nm	0	0.034	0.001	**0.981**	0.015	0.003	0
4.1Ct	0	0.031	**0.725**	0	0.005	0.002	0
2.1Cc	0	**0.843**	0	0	0.158	0	0
1.1Ca	1	0.009	0.261	0.001	0	0.002	0
	1.1Ca	**2.1Cc**	**4.1Ct**	**5.1Nm**	**6.1No**	**7.1Pp**	**8.1Pf**
Samples	4	15	4	7	2	12	8
Sensit	**1**	**0.843**	**0.725**	**0.981**	**0.765**	**0.937**	**0.996**
Specif	**0.955**	**0.974**	**0.994**	**0.991**	**0.987**	**0.987**	**0.987**

Table 6.6a: Class confusion for Lake Starnberg 2003 using simulated HyMap spectra. Columns represent the true class value (*original class*), whereas rows represent the values assigned by the classification algorithm(*predicted class*). Correctly classified cases occur on the diagonal.

NA	0	0	0	0	0	0	0	0
8.2Pf	0	0.002	0	0.02	0.008	0.01	0.001	**0.988**
7.3Pp	0	0	0	0.001	0	0.021	**0.999**	0.002
7.2Pp	0	0	0.001	0.023	0	**0.963**	0	0.008
5.2Nm	0	0.015	0.001	0	**0.956**	0	0	0.001
2.3Cc	0	0.01	0.105	**0.898**	0	006	0	0
2.2Cc	0	0	**0.893**	0.059	0	0	0	0.001
1.3Ca	0	**0.971**	0	0	0.003	0	0	0
1.2Ca	1	0	0	0	0.033	0	0	0
	1.2Ca	**1.3Ca**	**2.2Ca**	**2.3Cc**	**5.2Nm**	**7.2Pp**	**7.3Pp**	**8.2Pf**
Samples	4	7	9	19	6	24	27	8
Sensit	**1**	**0.991**	**0.893**	**0.898**	**0.956**	**0.963**	**0.999**	**0.988**
Specif	**0.995**	**1**	**0.991**	**0.982**	**0.998**	**0.995**	**0.997**	**0.994**

Table 6.6b: Class confusion for Lake Starnberg 2004 using simulated HyMap spectra. Columns represent the true class value (*original class*), whereas rows represent the values assigned by the classification algorithm (*predicted class*). Correctly classified cases occur on the diagonal.

NA	0	0	0	0	0	0	0	0
8.2Pf	0	0	0.006	0.054	0	0.007	0	**0.986**
7.3Pp	0	0	0	0	0	0.004	1	0
7.2Pp	0	0	0.006	0.006	0	**0.989**	0	0.014
5.2Nm	0	0	0.001	0	1	0	0	0
2.3Cc	0	0	0.056	**0.934**	0	0	0	0
2.2Cc	0	0	**0.931**	0.006	0	0	0	0
1.3Ca	0	1	0	0	0	0	0	0
1.2Ca	1	0	0	0	0	0	0	0
	1.2Ca	**1.3Ca**	**2.2Ca**	**2.3Cc**	**5.2Nm**	**7.2Pp**	**7.3Pp**	**8.2Pf**
Samples	4	7	9	19	6	24	27	8
Sensit	**1**	**1**	**0.931**	**0.934**	**1**	**0.989**	**1**	**0.986**
Specif	**1**	**1**	**0.999**	**0.992**	**1**	**0.996**	**0.999**	**0.990**

Table 6.7a: Pair-wise distances for macrophyte species calculated using GALGO-selected wavelengths from Lake Constance 2003 (632 nm (R), 509 nm (R'), 524 nm (R'), 632 nm (R'')). The values located on the upper part of the table, oriented to the right-hand side, are JM distance values and those shown on the lower portion, oriented to the left-hand side, are BH distances.

	1.1Ca	1.2Cc	4.1Ct	5.1Nm	6.1No	7.1Pp	8.1Pf
1.1Ca		2.00	1.94	2.00	2.00	2.00	2.00
2.1Cc	27.41		1.99	1.99	1.99	1.99	1.99
4.1Ct	3.51	5.41		2.00	2.00	1.92	1.99
5.1Nm	121.44	6.99	59.81		2.00	1.99	2.00
6.1No	161.61	8.63	20.46	44.00		1.99	2.00
7.1Pp	18.95	9.57	3.23	6.35	9.43		1.99
8.1Pf	162.04	13.16	6.80	20.36	147.95	5.84	

Table 6.7b: Pair-wise distances for macrophyte species calculated using GALGO-selected wavelengths from Lake Constance 2004 (500 nm (R), 531 nm (R'), 623 nm (R'), 561 nm (R'')). The values located on the upper part of the table, oriented to the right-hand side, are JM distance values and those shown on the lower portion, oriented to the left-hand side, are BH distances.

	1.1Ca	1.2Cc	4.1Ct	5.1Nm	6.1No	7.1Pp	8.1Pf
1.1Ca		2.00	1.97	2.00	2.00	2.00	2.00
2.1Cc	56.18		1.99	1.99	1.99	1.99	1.99
4.1Ct	4.41	5.71		1.99	2.00	1.99	1.99
5.1Nm	32.22	9.18	10.20		2.00	1.99	1.99
6.1No	19.99	8.70	109.18	24.73		1.95	1.99
7.1Pp	18.22	6.47	10.28	9.93	3.72		1.95
8.1Pf	38.68	8.74	12.10	11.12	5.40	3.84	

Table 6.7c: Pair-wise distances for macrophyte species calculated using GALGO-selected wavelengths from Lake Starnberg 2003 (555 nm (R), 493 nm (R'), 585 nm (R'), 600 nm (R'')). The values located on the upper part of the table, oriented to the right-hand side, are JM distance values and those shown on the lower portion, oriented to the left-hand side, are BH distances.

	1.2Ca	1.3Ca	2.2Cc	2.3Cc	5.2Nm	7.2Pp	7.3Pp	8.2Pf
1.2Ca		1.99	2.00	1.99	2.00	2.00	2.00	2.00
1.3Ca	12.03		1.97	1.95	2.00	2.00	1.99	2.00
2.2Cc	49.21	4.55		1.20	2.00	1.96	1.93	1.99
2.3Cc	7.49	3.75	0.91		1.99	1.99	1.98	1.94
5.2Nm	18.75	26.52	19.63	12.00		1.99	2.00	1.99
7.2Pp	19.45	17.66	3.96	7.31	6.92		1.77	1.98
7.3Pp	44.69	14.43	3.40	4.82	37.24	2.16		1.99
8.2Pf	22.57	15.66	10.47	3.54	9.74	4.96	10.56	

Table 6.7d: Pair-wise distances for macrophyte species calculated using GALGO-selected wavelengths from Lake Starnberg 2004 (561 nm (R), 592 nm (R'), 607 nm (R'), 515 nm (R'')). The values located on the upper part of the table, oriented to the right-hand side, are JM distance values and those shown on the lower portion, oriented to the left-hand side, are BH distances.

	1.2Ca	1.3Ca	2.2Cc	2.3Cc	5.2Nm	7.2Pp	7.3Pp	8.2Pf
1.2Ca		2.00	2.00	2.00	2.00	2.00	2.00	2.00
1.3Ca	51.08		1.99	1.99	2.00	2.00	1.99	2.00
2.2Cc	63.31	15.54		0.83	1.99	1.98	1.96	1.87
2.3Cc	47.59	8.34	0.54		2.00	1.99	1.99	1.92
5.2Nm	30.03	74.15	9.41	21.11		1.99	2.00	1.99
7.2Pp	65.30	17.04	4.89	12.11	7.09		1.99	1.97
7.3Pp	242.38	12.22	3.82	6.06	30.90	5.81		1.99
8.2Pf	271.70	18.08	2.78	3.30	5.80	4.51	6.39	

The JM distance was calculated for GALGO-selected wavelengths of the 2003 and 2004 macrophyte spectra from Lake Constance (Table 6.7a and 6.7b) and Lake Starnberg (Table 6.7c and 6.7d). No single channel discriminates between all pairs of species, but genetic algorithm results were used in the selection of the four best discriminating wavelengths (variables). The JM distance between species at these wavelengths indicates the degree of separability, suggesting that the more spectrally distant species pairs have greater potential of being separated from other species in remotely sensed imagery. In both lakes from both years, all but two of the macrophyte species pairs were significantly different, exceeding the 1.90 threshold value. *Chara contraria* (2.2Cc) and *C. contraria* sen. (2.3Cc) from Lake Starnberg in both 2003 and 2004 could not be separated, having a JM index less than 1.9.

6.2   Remote sensing data classification

6.2.1   Lake Constance

A classification of shallow water macrophytes near Reichenau Island (Lake Constance) was established from HyMap data collected on 19th July 2003 and processed with the Modular Inversion & Processing System (MIP) (Figure 6.13). The results are presented as the main bottom-cover classes, including short-growing macrophytes such as the Characeae (in green - see colour triangle in Figure 5.2), tall-growing macrophytes, mainly *Potamogeton perfoliatus* and *P. pectinatus* (in red), and bottom sediments (in blue). Mixed picture elements contain more than one single class, e.g. Characeae and bottom sediment, and the sum of the bottom cover in each pixel is always 100 %. The Characeae and *Potamogeton* species could be separated based simply on their growth height alone. The bottom coverage could be mapped down to a depth of 4.5 m, the maximum depth to which plausible reflectance spectra have been derived after water depth correction.

At Lake Constance, macrophytes grow beyond this depth, and were not able to be detected with remote sensing techniques, and appear as dark (white) colour in the classification. All classified pixels exceeding 70 % vegetation cover were further classified to macrophytes species distribution in a second processing step using GALGO-selected wavelengths (Figure 6.14).

The algorithm was able to distinguish two tall growing species (*Potamogeton perfoliatus* and *P. pectinatus*) and four different short growing species (*C. aspera*, *C. contraria*, *C. tomentosa* and *N. marina*). The labelled classes are species with the highest probability, and classes such as *Nitellopsis obtusa* and *C. contraria* sen. were not differentiated in this classification. A validation result of a former classification at Lake Constance 2003 using visually selected wavelength reached a 77 % accuracy compared to ground-truth data. It is

Figure 6.13: Classification of hyperspectral airborne data at Lake Constance flown on 19th July 2003, 30th June 2004, and 29th July 2004. The major bottom classes are tall-growing macrophytes (red), short-growing macrophytes (green), and exposed sediment (blue). White colour pixels are either water > 4.5 m deep or unclassified pixels
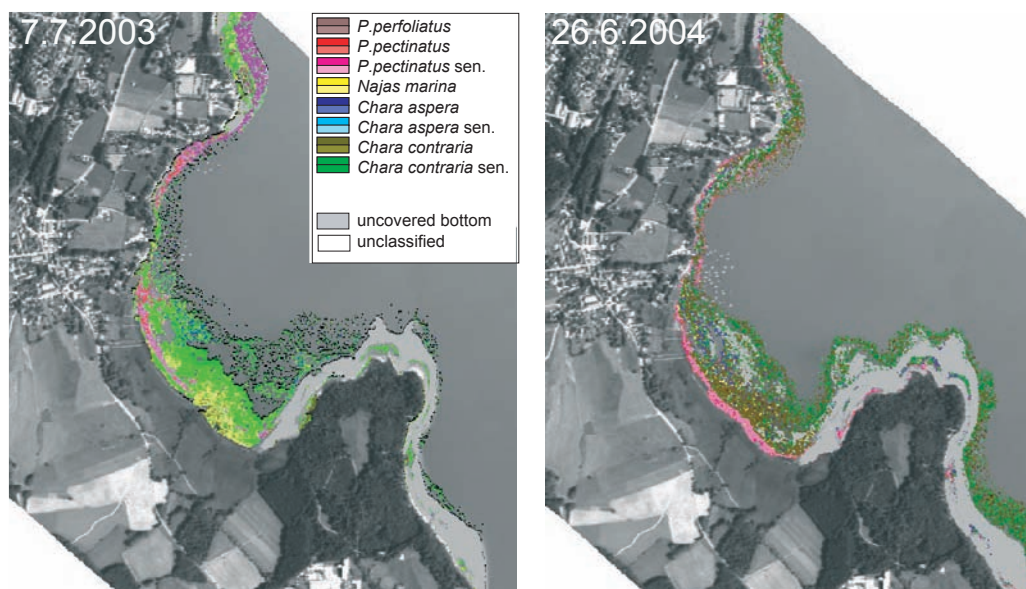
Figure 6.14: Macrophyte species distribution using GAIGO-selected wavelengths of hyperspectral airborne data at Lake Constance flown on 19th July 2003, 30th June 2004, and 29th July 2004.
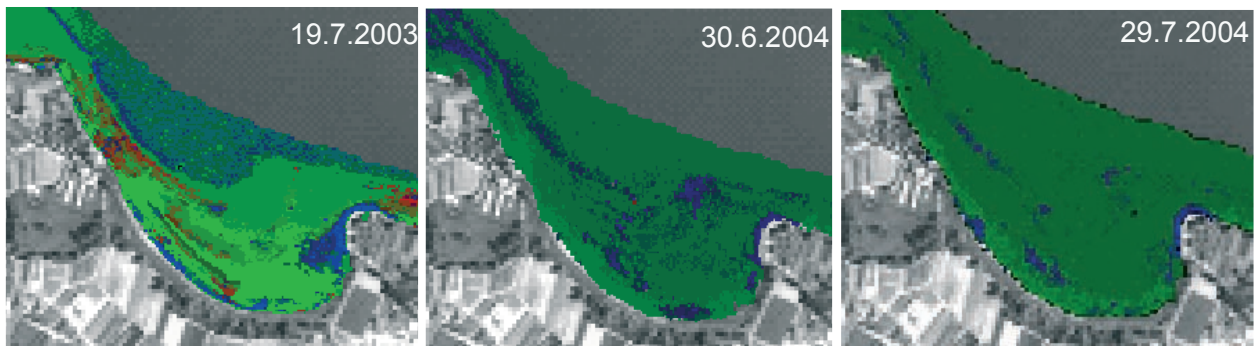
Figure 6.15: Classification of hyperspectral airborne data at Bauerhornbucht, Lake Constance (19th July 2003, 30th June, and 29th July 2004).
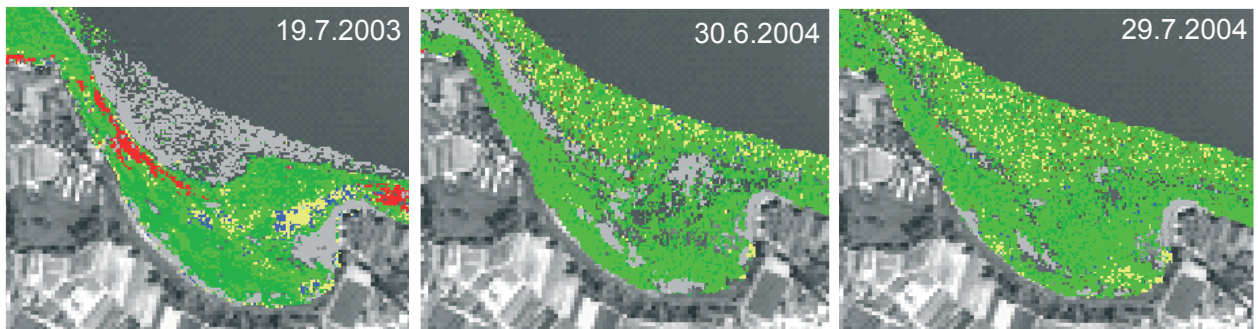
Figure 6.16: Macrophyte species distribution of hyperspectral airborne data at Bauerhornbucht, Lake Constance (19th July 2003, 30th June, and 29th July 2004).

anticipated, that recent classification results using the objective GA approach exceeds this validation result.

6.2.2 Lake Starnberg

A classification of shallow water macrophytes near Karpfenwinkel (Lake Starnberg) was established from HyMap data collected on 7th July 2003 and processed with the Modular Inversion & Processing System (MIP) (Figure 6.17). The results are presented as the main bottom-cover classes, including short-growing macrophytes such as the Characeae (in green), tall-growing macrophytes, mainly *Potamogeton perfoliatus* and *P. pectinatus* (in red), and bottom sediments (in blue). Mixed picture elements contain more than one single class, e.g. Characeae and bottom sediment, and the sum of the bottom cover in each pixel is always 100 %. The Characeae and *Potamogeton* species could be separated based simply on their growth height alone. The bottom coverage could be mapped down to a depth of 4.5 m, the maximum depth to which plausible reflectance spectra have been derived after water depth correction.
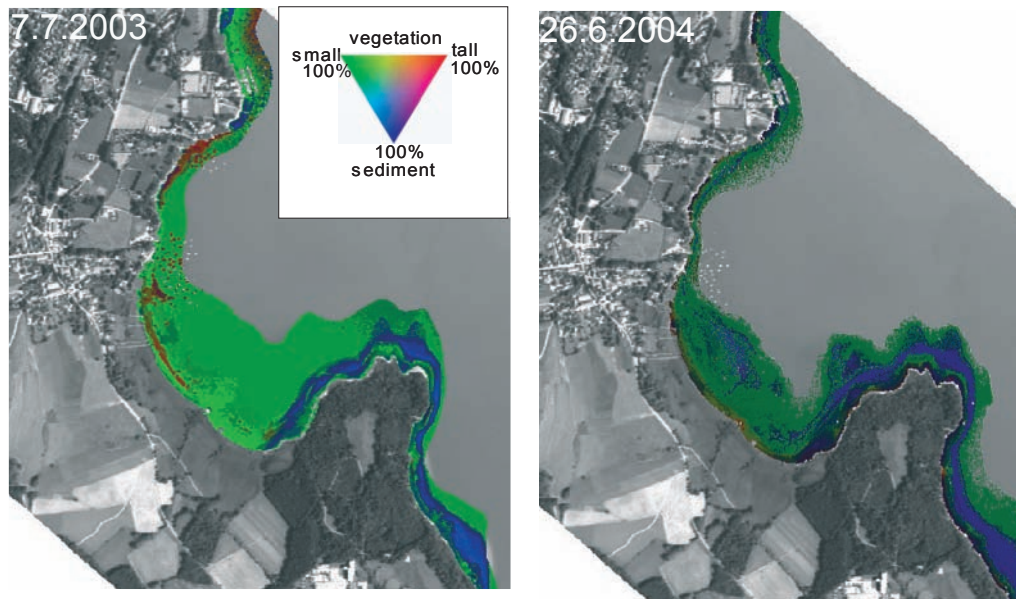
Figure 6.17: Classification of hyperspectral airborne data at Lake Starnberg flown on 7th July 2003 and 26th June 2004. The major bottom classes are tall-growing macrophytes (red), short-growing macrophytes (green), and exposed sediment (blue). White colour pixels are either water > 4.5 m deep or unclassified pixels.

Figure 6.18: Macrophyte species distribution using GAlGO-selected wavelengths of hyperspectral airborne data at Lake Starnberg flown on 7th July 2003 and 26th June 2004.

At Lake Starnberg, unlike at Lake Constance, macrophytes generally do not appear to grow, and thus the extent of the macrophytes was detected with remote sensing techniques, and is bounded by exposed sediment (blue colour) in the classification.

The classification of macrophyte species distribution was processed in the same manner as described in section 6.2.1 using GALGO-selected waveband derivatives (Figure 6.18) and was able to distinguish two tall growing species (*P. pectinatus* and *P. perfoliatus*) and three different short growing species (*C. aspera*, *C. contraria*, and *N. marina*). Distinction could be made between juvenile and senescent states of tall growing species (*P. pectinatus* and *P. pectinatus* sen.), and short growing species (*C. contraria* and *C. contraria* sen.). The labelled classes are species with the highest probability, and classes such as *Nitellopis obtusa*, and *C. tomentosa*, did not occur in this area and were therefore not differentiated in this classification.

6.3 Validation of remote sensing data

6.3.1 Model correction accuracy

Atmospheric and water column correction

HyMap at sensor radiance was corrected for atmospheric effects to subsurface reflectance $R(0-)$, as described in section 4.4.2 (Figure 4.7). Atmospheric correction accuracy of less than 0.5 % absolute reflectance difference could be achieved (T. Heege, pers.comm.). Modelled subsurface reflectance from HyMap were compared to *in situ* measured subsurface reflectance measured with RAMSES spectroradiometers (Figure 6.19). Atmospherically corrected HyMap spectra matched with *in situ* RAMSES measurements within its standard deviation of less than 0.2 %. There were minor difference in the blue wavelength region, caused by lower sensor signal-to-noise and higher scattering of the water column.

HyMap subsurface reflectances $R(0-)$ were further corrected for water column effects and water depth. The accuracy of water column correction is dependent on several signal influencing factors, such as water optical depths, wavelengths and brightness of substrate. The modelled bottom albedo spectra (A) were compared to *in situ* RAMSES bottom albedo spectra above a *Chara contraria* patch at Lake Starnberg in 1.70 m water. Despite the dominance of the water column optical properties in the surface reflectance signal, the inversion process using MIP resulted in obtaining benthic albedo spectra of up to 0.5 % absolute reflectance difference compared to *in situ* spectra for transmissions higher than 50 %, a result found to be acceptable for differentiating similar substrates, such as macrophyte species.

A transmittance curve plotted against the reflectance spectra shows the percentage of light

that reaches the water surface after being reflected from the substrate in 1.70 m water for different wavelengths. It shows how much light is lost on its way up to the water surface due to absorption and scattering in the water and what proportion of light can still be detected by the remote sensor. At 550 nm, 60 % of reflected light reaches the water surface, whereas at 620 nm, 40% and at 650 nm, only 20 % of the reflected light can be detected. Beyond 650 nm, more than 80 % of the light is absorbed by the water column, thus it can not be used in remote sensing. With increasing water depth, transmission decreases and in 4 m water depth, only spectral information between 480 nm and 600 nm can be used by remote sensors for spectral analysis.

6.3.2   Remote sensing data classification

To test the plausibility of the data at Lake Constance, the classification results were validated with extensive ground truth measurements during the flight campaigns, GIS analysis, and traditional aerial photographic interpretation. The tall- and short-growing macrophytes and exposed sediment results at Lake Constance from 2003 (Figure 6.13) and macrophyte species distributions (Figure 6.14) were compared to the ground truth data as a primary validation step to assess the success presented in hyperspectral processing methods. The results (Table 6.8) indicate a high correspondence (87.5 %) between short-growing vegetation and sediment (86.7 %), however tall-growing macrophytes were less correctly classified (64.2 %), as many were of them misidentified as short growing macrophytes that had not grown up to the water surface, but were covered with a water column of at least 2 m (Woithon et al., 2005). A plausibility control based on 216 ground truth measurements were statistically analysed and produced an overall accuracy of 73 %.

The ground-truthing results from a former classification at Lake Constance 2003 using visually selected wavelength (Pinnel et al., 2004) (Table 6.9) indicate that there was some spectral confusion with several macrophyte species, only *C. tomentosa* and *C. contraria/C. aspera* were 100 and 92.6 % accurate, respectively. However the species *C. contraria* and *C. aspera* could not be differentiated and showed a high degree of confusion. *Potamogeton perfoliatus* was identified correctly at 66.7 %, whereas *P. pectinatus* was correctly identified at 50.0 %. Using the measured spectra as a means of checking the accuracy of this second classification, it was determined that 92 % of tall-growing, 75 % of short-growing, and 80 % of *Chara* species would were correctly identified. It is anticipated, that recent classification results using the objective GA approach exceeds this former validation result.
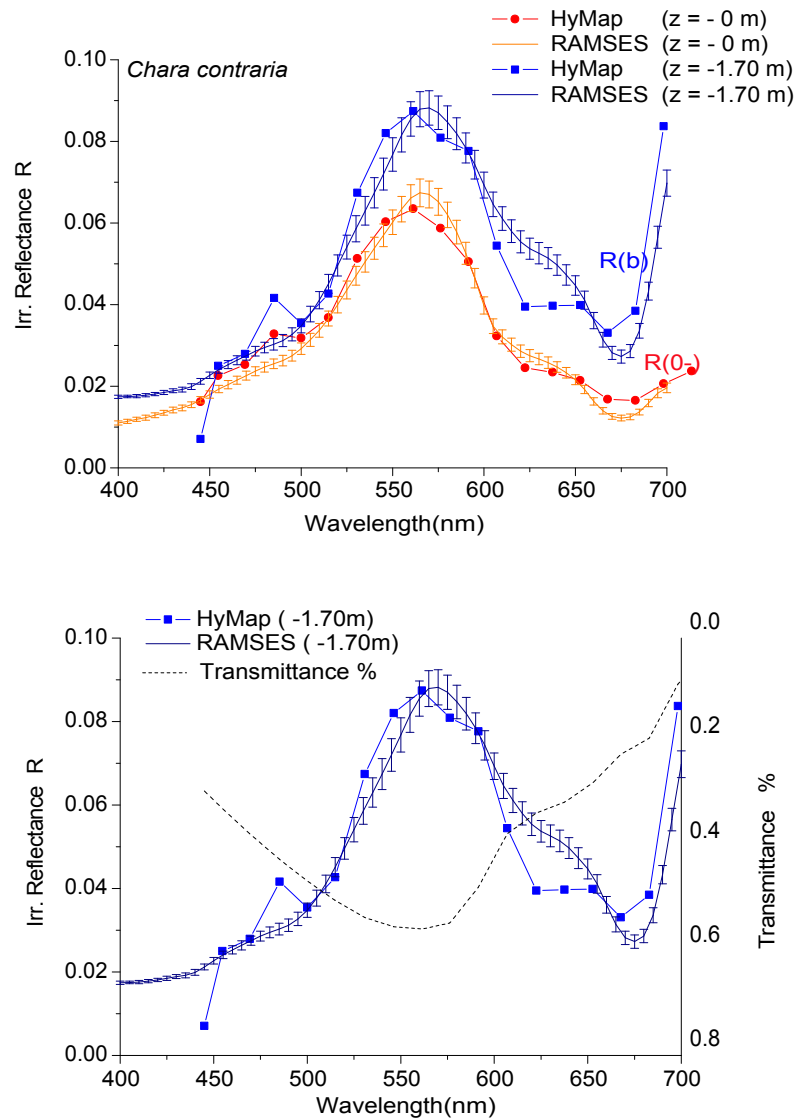
Figure 6.19: HyMap modelled reflectance compared to RAMSES *in situ* reflectance and standard deviation after atmospheric (red) and water column correction (blue) above a *C. contraria* patch in 1.70 m water (a). Bottom albedo spectra from HyMap and RAMSES compared to transmittance (%) in 1.70 m water (b).

Table 6.8: A non-GA HyMap classification of Lake Constance 2003 tall-growing macrophytes, short-growing macrophytes, and exposed sediments verified with ground truth measurements.

		Scanner Classification			
	Vegetation classes	short growing (s)	tall growing (t)	sediment (u)	User's Accuracy
Ground-Truth-Campaign	short growing (s)	56	8	0	87.5 %
	tall growing (t)	48	88	1	64.2 %
	sediment (u)	2	0	13	86.7 %
	Producer's Accuracy	52.8 %	91.7 %	92.9 %	**73 %**

Table 6.9: A non-GA HyMap classification macrophyte species of Lake Constance 2003 compared to ground truth validation.

		Scanner Classification				
	Macrophyte species	*Potamogeton perfoliatus*	*Potamogeton pectinatus*	*Chara contraria /C. aspera*	*Chara tomentosa*	
Ground-Truth-Campaign	*Potamogeton perfoliatus*	66.7 %	33.3 %	0 %	0 %	100 %
	Potamogeton pectinatus	35.7 %	50.0 %	14.3 %	0 %	100 %
	Chara contraria /C. aspera	0 %	3.7 %	92 .6%	3.7 %	100 %
	Chara tomentosa	0 %	0 %	0 %	100 %	100 %

Chapter 7

Discussion

In the following discussion, the results of this thesis will be placed into context, first by providing a direct explanation of each facet of the study as outlined in the research methodology. The identification and discrimination of *in situ* measurements of spectra will be evaluated, and possible reasons for intra-specific (within species) variation or error will be presented. Second, the results from a supervised feature extraction technique of choosing limited wavelength ranges will be examined. Effects of sensor choice will be discussed in terms of macrophyte discrimination effectiveness. Third, the macrophyte mapping results at Lake Constance and Lake Starnberg will be discussed in terms of accuracy, objectivity, and error. Application of this method for monitoring macrophytes to meet EU WFD guidelines will be proposed.

7.1 Analysis of *in situ* measurements

7.1.1 Spectral discrimination of macrophyte species

Monitoring macrophyte species is a meaningful, accurate, and relatively straightforward way to assess the water quality of littoral ecosystems (Dennison et al., 1993; Grasmück et al., 1995; Lehmann and Lachavanne, 1999; Melzer, 1999). Using remote sensing methods for discriminating macrophyte species can be a consistent and objective means in mapping large areas for monitoring purposes (Bostater et al., 2004), but only if the spectra of *in situ* species are distinct.

Spectra description

The first goal of this study was to determine whether underwater bottom reflectance measurements performed *in situ* close above patches of several macrophyte species contain useful information for discrimination to species level. To achieve this goal, a comprehensive spectral

library of several macrophyte species was produced, characterising the spectral signatures of each species and defining the levels of spectral variability associated with them over a range of natural growing conditions in Lake Constance and Lake Starnberg, Germany.

The reflectance spectra of the macrophyte species were found, as expected, to be optically quite similar because they display the absorption features characteristic of the spectral property of green plants that contain abundant chlorophyll. Differences in the spectral signatures of macrophytes, as shown in Figure 6.1, were quite limited, and may be in part based on small differences in pigments and their concentrations. For example, at the green reflectance peak ($540-560$ nm) and red absorption trough ($670-680$ nm), the macrophytes may possibly be separated on the basis of leaf chlorophyll content. The reflectance differences in the range from $600-650$ nm can be attributed mainly to different proportions of red, orange, yellow, and brown carotenoids (Merzlyak et al., 2003; Gitelson et al., 2002). In the blue region of the spectrum, absorption occurs from chlorophyll a and b and a range of carotenoids that extend absorption to shorter wavelengths of the visible spectrum (Table 2.2) (Blackburn, 1998). The influence of individual pigments on reflectance in the blue region cannot be observed in the spectral signatures of macrophytes. The observed differences in the visible spectral reflectance of macrophyte species are thus often attributed to consistent differences in the total and relative concentrations of chlorophyll, carotenoids and accessory pigments in their leaves.

Additional significant influences on macrophyte reflectance spectra are vegetation (patch) density, canopy openness, and the amount, form, and orientation of leaves. The discrimination of macrophytes using remote sensing relies upon differences in the magnitude of both pigment and structural characteristics as measured or seen in features of their absorption spectra (i.e. the depth and width of absorption troughs, or the height and shape of reflectance peaks). Lake Constance and Lake Starnberg both have macrophytes growing to $4-6$ m depth in fairly large, uniform patches (approx. $1-5$ m diameter), thus accurate discrimination based on the moderate differences observed was feasible in these lakes, at least for some species.

The effects of water-column absorption are most noticeable at wavelengths longer than 720 nm. Although NIR reflectances can be useful for mapping tall growing macrophyte species, especially those extending to the water surface, visible wavelengths ($400-700$ nm) are less attenuated by a water column and thus were used to remotely sense submerged aquatic vegetation.

Spectra discrimination

Results of the Jeffries Matusita distance analysis, presented in Table 6.1, suggests that several of the macrophytes are indeed spectrally sufficiently distinct for classification. The limited differentiation between some macrophyte species, e.g. *Chara contraria, C. intermedia, C. aspera, C. tomentosa*, indicates that with simple data-analysis techniques, they were confused with each other, but could be separated from other genera. The limited separation in the genus *Potamogeton* (*P. pectinatus, P. perfoliatus*) confirms this problem. However the separation between genera and many species pairs clearly indicates that it is possible to remotely detect and delineate areas of submerged macrophyte cover, and that the potential for separation using advanced data-analysis techniques exists.

Spectral differences between macrophyte species occurred primarily in their visible wavelengths (Figure 6.2), suggesting that either pigment concentrations or morphological differences, (e.g. cell wall thickness, airspace, leaf surface quality, and inter-specific leaf structure variability) play an important role in spectral discrimination (Carter et al., 1989).

7.1.2 Intraspecific variability in reflectance

The potential for within species variation on spatial and seasonal scales has to be considered when intending to compare measurements from different dates and lakes, as one would wish to do in a monitoring program. Spatial, depths and temporal variations in light intensity, nutrient availability, and temperature influences photosynthesis and growth, thereby altering the spectral reflectance. Furthermore, the differing ability of each macrophyte species to chromatically adapt and maintain photosynthetic ability under a range of different environmental conditions will affect the direction and degree of spectral change, and thus will also influence spectral reflectance. Environmental conditions will also determine the biomass and species composition of epibionts, such as diatoms, that contribute to spectral reflectance of macrophytes.

An additional reason spectral differences might be observed in macrophytes over different seasons, in consecutive years, or over different locations is the within species variation. Macrophytes themselves can influence the underwater light field affecting plant growth and leaf/thallus morphology. This in turn affects the spectral shape and magnitude of reflectance significantly, such that quantification of this phenomena is not feasible (Kirk, 1994).

Seasonal, temporal, and local variations in macrophyte reflectance were observed from both Lake Constance and Lake Starnberg. Additional sources of variation include species composition differences between lakes and macrophyte density. The difficulties in deriving

comparable spectra indicating a species–inherent optical signature due to these variations are outlined below, and implications to remote sensing are discussed.

Temporal variation

Variation in macrophyte characteristics, such as leaf volume, reproductive structures, and biomass, occurs over seasons and between years (Bueno and Bicudo, 2006). Leaf age is particularly important in remote sensing applications as it determines internal leaf architecture and chemical properties, as well as affecting the amount of time exposed to epiphylls and herbivory (Carter et al., 1989; Drake et al., 1999, 2003). Higher chlorophyll content in young leaves likely accounts for lower VIS reflectance (i.e. higher VIS absorption) in the blue (450 nm) and red (680 nm) regions (Gausman, 1984). As the leaf ages, lower concentrations of chlorophyll greatly reduce the amount of absorption throughout the VIS (chlorophyll breaks down rapidly whereas carotenoids persist longer, thereby increasing reflectance). This effect of senescence could be mainly observed in species which grew to the water surface, e.g. *P. pectinatus* and *P. perfoliatus* (Figure 6.3). Chromatic adaptation to light stress and acclimation to different water depths could not be observed in measured reflectance data (Ziegler, 2005), however morphological adaptation due to light stress has been documented for some species (Schneider et al., 2006).

First, seasonal variation has a tremendously large effect on remote sensing applications. It likely influences the efficacy of species discrimination, as macrophyte morphology and physiology changes significantly over the growth season. This has to be considered when comparing measurements from different dates of airborne data collection. It might be useless to collect data at the very beginning of the growing season as spectral differences are not yet discernible. At the end of the growing season spectral variation might also complicate species classification as epithetic growths and leaf senescence lead to increased variation in spectral reflectance characteristics. For example, in Lake Constance and Lake Starnberg, *C. tomentosa* was confused with *C. aspera* and *P. pectinatus* at the beginning of the growing season. Better separation might have been achieved at a later growth stage, when red carotenes (γ-carotene) responsible for the red colour, develop in the anteridia of vegetative *C. tomentosa* plants (Schagerl et al., 2003). This could ultimately lead to improved discrimination of *C. tomentosa* from other Characeae. Most macrophyte species at Lake Starnberg showed a distinct reflectance shoulder centred around 650 nm (not so apparent in spectra measured at Lake Constance) that might be related to spectral changes found in aging and diseased plants, leading to chlorophyll breakdown and subsequent unmasking of carotenoids and other leaf pigments (Gitelson et al., 2002).

Second, varying growth behaviours and sensitive adaptations to light and weather conditions make it difficult to compare data collected over different years. Different distribution and growth forms, and thus different reflectance spectra, occurred between 2003 and 2004, likely due to different water temperatures and nutrient conditions (Luterbacher et al., 2004)(DWD, 2006[1]). For example, during extreme hot summer in 2003 species developed 2-3 weeks earlier than those in 2004 likely due to faster degree-day accumulation (Best and Boyd, 2003; Pilon and Santamaría, 2002). Ideal growth conditions for macrophytes were apparent by the dense, homogenous macrophyte patches in both lakes in 2003, whereas in 2004, relatively cold temperatures may have been responsible for reduced macrophyte growth, as fewer macrophytes were observed, and those present grew in sparse patches. Structural differences between macrophytes may therefore play a more important role in the spectral discrimination than pigment concentration. Surprisingly, there was no observable spectral difference between years, as expected when comparing different growths forms. A spectral library of different growth forms might be a feasible means to quantify the spectral variation within one species. Reflectances spectra of young, mature and senescent macrophytes species could be an attempt to obtain valid spectra which can be transferred to different lakes and different seasons.

Third, illumination conditions also contribute to some within species differences. The angle of incidence (sun angle) varies significantly throughout the day and thus it may be logical that this will affect reflection, sunglint, and absorption processes. More importantly is the effect, that apparent optical properties (AOPs) are dependent on both the medium and the ambient light fields geometric directional structure. Thus upwelling and downwelling irradiance reflectances, as measured underwater, are dependent on sun angle changes and will ultimately be altered by illumination condition. Measurements in this study have shown that these influences are negligible in comparison to other parameters. Changing sun angle conditions did affect *in situ* measurements. An increase in reflectance and higher within species variability was observed in tall growing macrophytes, e.g. *P. pectinatus*, but only after 4 pm (sun-zenith of 40°). Short growing macrophytes, being a better lambertian target, showed less sun angle related reflectances (Figure 6.4). Increased reflectance in tall growing species was more obvious at lower sun-zenith angles, and can be explained by decreased downwelling irradiance with lower sun angle, as compared to upwelling irradiance, caused by anisotropic scattering. Optimal measuring time is therefore when sun-zenith angles between 25 - 40° occur (10 am to 4 pm). Investigation of anisotropy effects and reflectance properties

---

[1]   Deutscher Wetter Dienst, Monatswerte der Station 10962 Hohenpeissenberg und 10929 Konstanz,1996-2006, $http://www.dwd.de/de/FundE/Klima/KLIS/daten/online/nat/ausgabe\_monatswerte.htm$

of tall growing and short growing plants under water are a future challenge in remote sensing applications and would benefit from further investigation. It might give valuable additional information of understanding spectral reflectance properties of submerged aquatic plants when using *in situ* radiance reflectances (R_{rs}) instead of irradiance reflectances (R) and are therefore highly recommended in all future applications.

Spatial variation

Environmental conditions between lakes vary, often because of differing amounts and types of epithetic growth ('aufwuchs', incl. diatoms), community interactions (density effects, herbivory, allelopathy), nutrients, water temperature, or leaf/plant morphology. This has likely contributed to the greater variation in morphology, such as cell wall thickness, air space (Merzlyak et al., 2003), leaf surface qualities, and leaf internal structure (Binzer and Sand-Jensen, 2002; Peters, 2006), than found in terrestrial plants (Ronzhina and P'yankov, 2001; Schneider et al., 2006), so that exact identifications are often left to genetic analyses (Mannschreck, 2003; Bögle et al., subm).

The *in situ* measured macrophyte spectra difference between Lake Constance and Lake Starnberg, apparent in the PCA analysis (Figure 6.5), was likely influenced by a combination of the above parameters. However, the most influential factor was likely differing macrophyte species composition, as *C. tomentosa, N. obtusa* were only found in Lake Constance. The difference in reflectances of common species may be a function of patch density, as *C. aspera* in Lake Constance shows a distinct green reflectance spectrum, while *C. aspera* reflectance in Lake Starnberg resembles, to some extent, sediment reflectance (Figure 6.2). Macrophyte patches in Lake Starnberg were generally less dense, showing exposed sediment, and often mixed with other species. These results suggest that when comparing spectra (or macrophyte classifications) from different lakes with similar macrophyte taxa composition, homogeneity, density, and patch size may be critical. The differences in spectra between Lake Constance and Lake Starnberg provided additional impetus for separate treatments of each lake in subsequent analyses.

Epibiont response to nutrient availability may also result in partial masking of macrophyte leaf reflectance (Drake et al., 1999). For example, in some (mainly oligotrophic) waters, epibionts can insulate incoming macrophyte leaves from light up to 90 - 100 % (Goos, 2003), while contributing their own absorption and reflectance features to the measured signal. Diatoms, for example, have fucoxanthin (a carotenoid pigment) as the major light harvesting pigment, absorbing green visible wavelengths *in vivo* and reflect a broad range of green to near-red wavelengths (Rowan, 1989). Without a diatom film, these macrophyte species,

due to lutein (a xanthophyll pigment), would absorb mainly blue wavelengths while reflecting green wavelengths. Aquatic plants can also secrete substances that have direct, adverse effects on algal growth, a phenomenon known as allelopathy (Gross, 2003; Berger and Schagerl, 2003; Körner and Nicklisch, 2002). Non-uniform allelopathy between species may result in different epibiontic loading, and thus affect spectral signatures. The degree of allelopathic response may also be related to plant age and health.

In Lake Constance and Lake Starnberg, the spectral properties of macrophyte species were not uniformly affected by the epibionts, as short-growing *C. aspera* and *C. tomentosa* (Gross, 2003) were suspected to have less diatom biomass than the tall growing *P. pectinatus*, which have large leaf-surface areas. Epibiont effects were also not uniform between the lakes, as *P. pectinatus* reflected more light in Lake Constance than in Lake Starnberg over the whole visible wavelength range, whereas *P. perfoliatus* and *C. contraria* had similar reflectances in both lakes (Figure 6.2). Epibiont effects are not entirely negative from a remote sensing perspective as they can intensify some pigment related features, thus their presence/absence and abundance might contribute to species specific class separability (Fyfe, 2003). Epithetic growth was not quantified in this study, however.

Measurement error

Measuring under water is somewhat different to terrestrial applications, as the overlying water column is an obstacle to accurately producing a spectral library of aquatic vegetation and bottom types. Measurement errors likely contribute significantly to spectral variation.

The three RAMSES sensors were securely mounted on a frame such that their optical axes were parallel (Section 4.2.2). Instability caused by wave action and boat drift likely varied the distance between the sensors and the plants, changing measurement position and the field of view of the underwater sensors while altering the water column signal in the spectrum.

The most variable factor was the water column itself, as surface movements resulted in variable distances between sensors and macrophytes and variation in water column absorption. Observed distance variation was approximately $10-40$ cm, depending on state of water surface and water depth. The changing conditions were assumed to be negligible for data-processing purposes, but theoretically should not be ignored when measuring fine-scale features such as macrophytes.

Improved accuracy may be achieved by applying a water column correction on measured *in situ* spectra in the same manner as it was applied on the remote sensing data. This suggestion was not applied to this data set, however the water column correction on the *in situ* data could improve the quality and purity of the spectral signature of various macrophyte

species, and thus improve spectral species discrimination.

The sensitivity of apparent optical properties (AOPs) to illumination effects is also a factor which should be considered when measuring underwater substrates. Radiance reflectance measurements provide more information on ambient light field of underwater plants and might therefore contain useful information for species discrimination, which are not comprehensible when using irradiance reflectance measurements. Correction for sun angle effects on radiance reflectance spectra could provide comparable measurements regardless of time and date. This might be a feasible approach to produce a spectral library to be useful for an operational and transferable methodology.

Shading effects can also influence the measured reflectance signals. During *in situ* measuring campaigns, it was more convenient to collect the data above the patches, even for the tall growing plants. Tall plants, especially those growing to the water surface, present a particular challenge for underwater spectral measurements, as the only possible sensor position is inside the patch. Shading effects, specifically for the downwelling sensor, occurred. Shading by leaves produces increased reflectances, caused by a lower downwelling irradiance in comparison to the upwelling irradiance. The measured signal is easily mixed with other parameters, such as water constituents, stems of plants, or short *Chara* species growing on the bottom.

What is actually recorded by the spectrometer can also be somewhat different to what may have been observed by an individual. Monitoring an underwater video camera mounted next to the sensor's field of view or direct observations via SCUBA diving might result in a different interpretation than made from the spectrometer data. These problems mainly occur in sampling locations with sparse substrate cover, turbid water, or in small macrophyte patches. Thus underwater spectrometer measurements are most reliable with large and dense macrophyte cover, such as those found at Lake Constance.

Field measurements should be performed in order to produce a spectral library of comparable and suitable spectra, as their accuracy has a great influence of the validity of the classification results. A systematic approach is essential if they are to be compared between years and lakes, and should begin simply by obtaining more spectra, regardless of sample location and instruments. Inter-calibration with field instruments and airborne sensors (i.e. HyMap) would be useful if both spectra have to be compared at a later date. Inter-calibration of the field spectrometers (i.e. RAMSES) could also be done using a stable light source, especially for application in multi-temporal analyses.

Implications of temporal and spatial variation and measurement errors

Spectral differences between species were seen to exist between Lake Constance and Lake Starnberg, however consistent statistical spectral separation, regardless of season and location, could not be confirmed. Further measurements for these and other species and at other sampling locations over longer periods need to be performed to better understand spectral reflectance behaviour. To improve accuracy of remote sensing results, the field sampling should be completed on the same day of the remote sensing data collection (flight overpass) and independently derive an algorithm for each data set (location). This would also require the presence of field data acquisition with each flight campaign, somewhat contradicting Fyfe's (2004) suggestion of a universal, operational approach.

Further investigations of single-contributing components need to be done to be able to incorporate the macrophyte reflectance signal to the modelling procedure. Signal influences, such as epithetic growth, pigment concentration, water column effect, anisotropy effects, sun angle effects, weather condition and clouds, as well as sensor calibration and sensor signal-to-noise play certainly a significant role and contribute more or less to the measured signal. Once all macrophyte-signal influencing parameters found in nature are well understood, a model approach could probably replace extensive field work.

Measuring spectra in the laboratory (Schmidt and Skidmore, 2003) may reduce these effects by producing a 'purer' spectral library of endmembers. Each component could be investigated separately and deliver useful information about changing growth conditions, such as plant vigour or age, as found in nature. These parameters could be incorporated into a growth model, similar to terrestrial applications, e.g. (Verhoef and Bach, 2003), providing valuable information regarding aquatic plant development. Relating laboratory-based measurements to field conditions remains difficult for terrestrial environments, and is even more complex in aquatic habitats.

The remote sensing approach is therefore limited in its application and assumes previous knowledge of the sampling location and species present. Reflectance spectra of additional submerged aquatic species and at different locations should be collected to be able to make more accurate and precise estimates of water quality. This would also allow improved transferability to additional sampling locations and extend the monitoring season. Further research is also required into the high spectral resolution reflectance properties of aquatic macrophytes. Ground-truthing at the time of remote sensing data acquisition is still highly recommended, as no macrophyte species appeared to have consistent spectral features over the year. Over

the long term, field data could eventually be reduced, once the spectral behaviour of macrophytes in each lake is better understood. Although difficulty in differentiating *Chara* species is expected, as indicated by the low JM distance values, the results encourage further investigations into the application of on-board hyperspectral sensors in macrophyte discrimination.

7.1.3   Feature selection

The second goal of this study was to explore how the macrophyte species differ in their *in situ* reflectance characteristics at certain wavelength areas. This was a necessary step in determining the location and width of wavebands that can be quickly, objectively, and practically applied in the remote sensing of submerged aquatic vegetation. An automated feature selection strategy using a genetic algorithm found the best wavelength combinations from the first and second derivatives of reflectance. Derivatives have been proven valuable in identifying characteristic spectral features, where raw reflectance spectra can be affected by environmental conditions during spectral measurements, such as illumination condition and water column.

The initial derivative analysis recovered both spectral shape information, creating peaks in the derivative analysis, and magnitude information, reflected in the height of the derivative peaks, leaving the inherent properties in the data that can be related specifically to leaf physiology, biochemistry and morphology. A large spectral region between 500 and 590 nm was identified in the first derivative, and appears to provide good separation between substrate types. Depending on the spectral resolution of the remote sensor, an appropriate wavelength range could be selected from within this range to remotely identify macrophyte cover. A few narrow spectral bands, between 510 and 650 nm, were identified in the second derivative where macrophytes separation may also be possible, however there is some indication that this a noise artifact. The wavelengths identified are present in the visible spectrum, and have the ability to penetrate water, such that passive optical remote sensors can be employed for mapping the extent of macrophytes. The feature extraction technique also reduced the size of the hyperspectral data set (provided by RAMSES or HyMap sensors) and the sharp spectral information was an improvement over the pure reflectance spectra, allowing discrimination of fine-scale changes in spectral shape otherwise not observable.

Subsequent automatisation of feature selection of reflectance spectra and their derivatives was achieved using a genetic algorithm, which has the distinct advantage in selecting combinations of wavelength ranges. For example, two features chosen separately may produce less favourable results than two features chosen in combination. Selection of specific wavelength features by hand could also work, but is a labour intensive process and does not provide the

objectivity in searching for combinations of bands to maximise separation of known classes. The only assumption necessary for the genetic algorithm to operate was that a certain number of measured spectra should be provided by the user for statistically meaningful performance. *C. intermedia* was excluded from the analysis because of insufficient measurements, however *N. obtusa* with only four spectral measurements, which would normally be considered insufficient, was included because it was the only member of its genus present in the analysis. The separability of *N. obtusa* from other species should therefore be interpreted with caution.

The results show that the application of feature selection strategies in finding the best separable wavelength provided superior performance, compared to ordinary classification rules, where the over supply of variables likely caused a substantial deterioration in the classification performance. The genetic algorithm selected wavebands were distributed equally throughout the visible wavelength range, with the optimal discrimination wavelength between 510-625 nm for both lakes. They were also conveniently located below 625 nm, where less water column absorption occurs, suggesting that spectra discrimination might also be possible in 2.0-4.5 m of water, corresponding to the depth of the littoral zone.

The GA selected wavelengths were consistent with visually selected wavebands from derivative analyses and coincide with major peaks of reflectance and troughs of absorption for the macrophyte photosynthetic and accessory pigments, e.g. centred at 445 and 665 nm, or were selected near the shoulders of wide peaks or troughs, which give more information for the green peaks at around 530 and 625 nm. The red wavelengths also penetrate shallow water sufficiently to allow detection of chlorophyll absorption features, between 650 and 665 nm, of different species. Selected wavelengths above 600 nm were most suitable in discriminating tall growing species. Thus the selected wavelengths targeted absorption and reflectance features that characterised each species. A band in NIR could have been improved discrimination of tall growing macrophytes, but was intentionally excluded because of water column effects. Cross-validation of the discriminant analysis confirmed that the *in situ* reflectances could be used to discriminate between seven of the eight measured species with > 98 % overall accuracy using as few as four optimally-positioned bands. These selected wavelengths for Lake Constance were 510 nm in reflectance, 530 nm and 625 nm in the 1st order, and 535 nm in the 2nd order derivative of reflectance. For Lake Starnberg somewhat different wavelengths were seelcted: 445, 520, 625 and 665 nm in the 1st derivative.

Feature selection using the GALGO genetic algorithm technique was able to provide stable and consistent results, when a large number of iterations (=1000) was performed. It has to be considered that there is not just one solution (one set of ideal band sets) that can be

used to separate the species, especially when working with different spectra and spectral resolutions. Additional statistical tests, such as unsupervised classifications (PCA) or distance measure (JM) indices, were used to validate the selected feature result and they confirmed the improvement in macrophyte species classification. At Lake Constance classification accuracy ranged from 68.2 % (*Chara tomentosa*) to 98.2 % (*Potamogeton perfoliatus*), whereas species at Lake Starnberg could be correctly classified between 90.1 % (*Chara contraria*) and 99.6 % (*Potamogeton pectinatus*). The results of this study demonstrate that it is possible to accurately detect and delineate submerged macrophytes using a hyperspectral remote sensing technique, and that the potential for species separation using advanced data-analysis techniques exists.

The highest goal of the final classification step is to obtain biological meaningful classes of substrates using objective statistical methods. In the case of the genetic algorithm applied in this study, the analysis indicated that only a few optimised wavelengths were necessary for the identification of macrophytes, although a different set of wavelength was derived for each data set separately. This certainly showed some limitation in the automatisation approach, however with increased knowledge of spectral behaviour of macrophyte reflectances a more general approach might be feasible. More detailed studies are needed to test whether remote sensing on the basis of specific spectral band sets will routinely provide meaningful classifications prior to its acceptance as a method for mapping and monitoring macrophyte species distributions.

7.1.4   Simulation of sensor spectral resolutions

Discriminant analysis demonstrated that RAMSES resolution *in situ* spectra provide good spectral separation of macrophyte species. Achieving the fitness goal of 98 % for both lakes was a highly encouraging result for all future applications in remote sensing of water quality. Different classification performance in these lakes might have been due to the different number of spectra included in the analysis, as only one third of the measurements were used in Lake Constance compared to Lake Starnberg.

Analysis of sensor-specific spectra showed that hyperspectral and narrowband multi-spectral sensors have the ability to discriminate between some macrophyte species and sediment across many levels of mixing, while broadband multi-spectral sensors do not. Although the full resolution (5 nm) RAMSES spectra of *in situ* macrophytes performed better class separations than simulated HyMap spectra (15 nm). The somewhat weaker performance of simulated HyMap resolution spectra compared to RAMSES field spectra can be explained by the lower spectral resolution (15 nm) masking out small spectral differences in the spectra.

Very narrow spectral bands as provided by the RAMSES spectroradiometer (5 nm) proofed to be advantageous in spectral discrimination of macrophyte species. The classification accuracy of simulate HyMap resolution spectra was still high (95-96%) and showed great potential in species discrimination. The spectral resolution of the HyMap sensor was therefore similar to the field spectrometer, demonstrating that derivative spectroscopy is an appropriate means of interpreting remotely sensed images. The actual number and width of the bands may not be critical. Bands should not be wider than any peak or trough they represent and must not overlap with the spectral information provided by other features. This approach would allow different substrate classes to be remotely identified and monitored over time.

7.2 Remote sensing data classification

Although it appears that the macrophyte species could be discriminated based on their visible reflectance of *in situ* measurements alone, the signals sensed from an aeroplane or satellite contain different information from that collected by ground spectrometers. This will mainly be due to scattering and absorption of light in the atmosphere and water column, reflectance of light from the water surface, mixing of signals in image pixels, the density and geometry of the macrophyte canopy, and background effects of the substrata.

Despite the dominance of the water column optical properties in the surface reflectance of optically shallow Case2 waters, inversion using MIP resulted in obtaining reasonable values for benthic albedo spectra. The model results indicated mixed substrate composition with a single dominant component, which is more realistic than a result of 100% coverage due to the complex ecology of benthic substrata.

The remote sensing data classification of 5 m spatial resolution HyMap data showed a somewhat different result than anticipated by linear discriminant analysis of *in situ* spectra. There was a remarkable difference in classification performance between 2003 and 2004. In 2003, tall and short growing species were accurately classified (Figure 6.13), but in 2004, tall growing species could not be classified in the image data from neither overflight (30th June and 29th July). What actually can be determined by image analysis may be dependent upon the relative scales of the image and the patch size. At Lake Constance, the 2003 species classification (Figure 6.14) correctly distinguished between *P. pectinatus* and *P. perfoliatus*, both tall growing species, and some short growing species such as *N. marina* and *C. tomentosa*. *C. aspera* were confused with *C. contraria*, the most abundant species. The 2004 classification was not able to correctly distinguish any species except the abundant *C. aspera/C. contraria* group. Similar results were obtained from Lake Starnberg, which showed good correlation

between classification and field data in 2003 and poorer performance in 2004. Obviously, the results for 2004 were disappointing as better classifications were expected. These results may be explained in part by sparse macrophyte cover throughout the growing season in 2004, such that dense, homogenous patches may be a prerequisite in achieving accurate classification and generating valid macrophyte distribution maps.

There are several strategies that could be attempted to improve classification. Applying specific waveband combinations for classifying short and tall growing species separately and maximising 'optimal' spectral features to species and water depth might improve separability and needs investigation. Separation of tall and short growing macrophytes based on their growth height alone simplifies the classification, but it also requires that the digital elevation model implemented in the water column correction step must be accurate. Differentiation of tall and short growing species must be reliable to avoid multiplicative errors in subsequent species classifications. Separating tall and short growing macrophytes based on spectral information might also be achievable, but would complicate species discrimination. A combination of both approaches would probably be the best solution. Additional, object-oriented classification strategies might also improve differentiation, such as including expert knowledge of macrophyte spatial distribution in relation to water depth and species composition.

There are further challenges for researchers in scaling the spectral reflectance of field measured leaf samples up to real mapping situations. The discrimination of aquatic macrophytes species by digital image processing methods is highly dependent on species diversity, composition, and variations in density in the given area. The effect of the lake bottom on the total reflectance of aquatic macrophytes was found to be more problematic than the effect of water quality, since the lake bottom effect changed with water depth. Nevertheless, the observations presented in this study are encouraging because the spectral differences between macrophyte species are rather subtle.

7.2.1   Classification error sources

Classifying macrophyte species is confounded by such technical factors as model accuracy and performance, water column correction influences, measurements errors, and calibration and signal-to-noise performance of the sensor. These are in addition to the highly variable nature of substrata which are spectrally mixed with several other materials. The relative low reflectances of aquatic macrophytes (usually $< 12\ \%$ of the magnitude of the green reflectance peak) generally presents a bottleneck for remote sensing, as less quantisation levels can be distinguished by the remote sensor. Thus, the signal-to-noise performance for the remote sensor must be higher for aquatic ecosystems than in terrestrial applications.

In developing a hyperspectral remote sensing-based detection and monitoring method, species discrimination is dependent on the accuracy for which the atmosphere, the air-water interface, and the water column effects are accounted. The remote sensing approach therefore involves accurate simulation of substrate reflectance at the bottom through the water column, the air-water interface, and the atmosphere to a remote sensor, based on radiative transfer principles. The accuracy of the inversion algorithm needs to be assessed and quantified when making prediction of data quality. Water depth is one of most limiting factors when applying remote sensing instruments in shallow littoral areas.

Except for some mechanical and automatic processing steps, it can be conclusively stated that remote sensing products in shallow littoral environments depend very much on field conditions and classification accuracy might be limited by:

- water depth. The deeper the water, the more difficult it is to differentiate species, because of the limited number of available spectral bands for discrimination.

- water clarity. This factor is highly correlated to optical depth, the depth to which plants reach 1% of light depends on water optical properties.

- density of macrophyte patches.

- homogeneity of the patches and distribution of species within the littoral zone.

- growth height. The higher the plants grow up to water surface, the easier it is to detect their spectral signatures. Growth height is influenced by water depth and turbidity.

- variability or amount of different species found in one area.

- species richness. Some species can easily be separated from each other while other species simply cannot.

- quality of spectral library. The quality and quantity of *in situ* measurements significantly influences the statistical analyses and needs to be strategically and systematically collected.

The accuracy of the remote sensing result is thus dependent upon these conditions which can vary over space and time. However some error sources can be avoided when sufficient attention is applied beforehand, such as ensuring sensor stability, choosing an appropriate day with respect to weather conditions for the flight campaign, and sensor alignment relative to sun angle.

7.2.2   Applicability of remote sensing and the WFD

Transfer of this method to different lakes or even other environments, such as wetlands and coastal environments, is theoretically possible as shown by Heege et al. (2006). The underlying premise is that substrata of interest are known and can be distinguished from each other. An extensive spectral library might facilitate future applications and reduce new field data acquisition. The application should always take into consideration the interests and accuracy needed, particularly with respect to choosing the sensor's spectral and spatial resolution. The user should be thoroughly informed about the sensor's capabilities and limitations, as well as quality of the data required, and how they might be used for future investigations. Distribution maps of submerged aquatic vegetation and their percentage cover can then be achieved with a reasonably high accuracy, even with limited or no ground-truth measurements, provided the area is known.

The distribution of tall and short growing macrophytes to 4.5 m water depth in turbid waters can be achieved with high accuracy over large areas. This may be an interesting product for limnologists who wish to know the extent of uniform communities, such as invasive or alien species, particularly if there are only one or two species present. High density cover of macrophyte growth facilitates remote sensing applications, as the returned signal from the water bottom is not mixed or deteriorated by other substrates.

Differentiation of macrophyte species and mapping their abundance and distribution according to the monitoring requirements for macrophytes within the Water Framework Directive (Melzer, 1999) was the ultimate goal for this study. The results showed that remote sensing has great potential for monitoring several macrophyte species and eventual incorporation into a WFD assessment strategy. However, the eight macrophyte species investigated in this study are only a small fraction compared to e.g. the 45 species found in the macrophyte index list (MI) (Melzer, 1999). Only the dominant species (*Potamogeton pectinatus*, *P. perfoliatus*, *Nitellopsis obtusa*, *Najas marina*, *Chara tomentosa*, *C. intermedia*, *C. contraria*, and *C. aspera*) at the study sites were investigated, since any other species could not be discriminated or detected by remote sensing instruments. This was primarily because of the spectral overlap with other species groups, (e.g., *Chara aspera*, *C. contraria*) or a lack of field data (e.g., *C. intermedia*, *Nitellopsis obtusa*).

Eventual incorporation into an automated, objective method should consider a variety of factors. Seasonal variation should be taken into account when applying remote sensing data to submerged vegetation communities, as some species change significantly with season, whereas other species have only minor changes. The occurrence of the growth season would

depend upon climate and degree days, thus scheduling overflights would have to be done according to annual variations. Temporal and spatial information could be used in remote sensing to improve species classification and ensure accuracy of classification. A combination of object-oriented classification methods (Andresen, 2004; Mott, 2005) could also contribute to the approach of an automated and operational remote sensing application.

Remote sensing data acquisition applied twice (or several times) during the growing season might be able to reveal spectral groups and classes which were otherwise not discernible. For example, *P. pectinatus* and *P. perfoliatus* were less discernable at the beginning of the growing season, whereas during senescence their spectral shape changed significantly and could be separated to 99 % accuracy. Remote sensing could use this seasonal and spatial information and detect species according to seasonal variability. Investigation of other dominant species in other locations is absolutely necessary prior to any further application of this method.

Size of vegetation patches should also be at least the size of sensor resolution, (preferably 3×3) the size of a sensor pixel (0.8-4 m pixels). Here lies possibly one of the limiting factors for remote sensing in limnological applications. Only in larger lakes, such as Lake Constance, do such growth conditions occur. The littoral zone of smaller lakes would be too complex for current remote sensor resolution, restricting current remote sensing applications to large-lake littoral zones. A similar situation will occur with turbid or deep waters. Until increased resolution sensors are developed and commercially available, this limitation will always exist.

Successful results of a semi-automated, remote-sensing approach for mapping the distribution of submerged aquatic vegetation in littoral zones has been presented. This approach forms the basis for future developments in precise automated methods. However, further research needs to be done to stabilise and improve the retrieval procedures (e.g. to improve algorithms for species recognition in shallow waters and derivation of growth height of aquatic plants from remote sensing data as an indicator for biomass). Consequently, remote sensing could become an economical monitoring technology for inland waters, with respect to managing and monitoring natural ecosystem restoration, rehabilitation, and conservation.

By use of physical-based algorithms, a general transferability of data to different water types and seasons is possible, showing promising potential for further research in the field of airborne remote sensing over shallow water targets. A previous application of a remote sensing approach to assess water quality using macrophytes at Lake Constance in 2003 (Woithon et al., 2005) resulted in the classification of sufficient species to produce a distribution map of ecological states (Figure 6.16). Some locations, seen as red pixels, are suspected to have unsatisfactory - bad water quality and may be related to areas of very frequent public use.
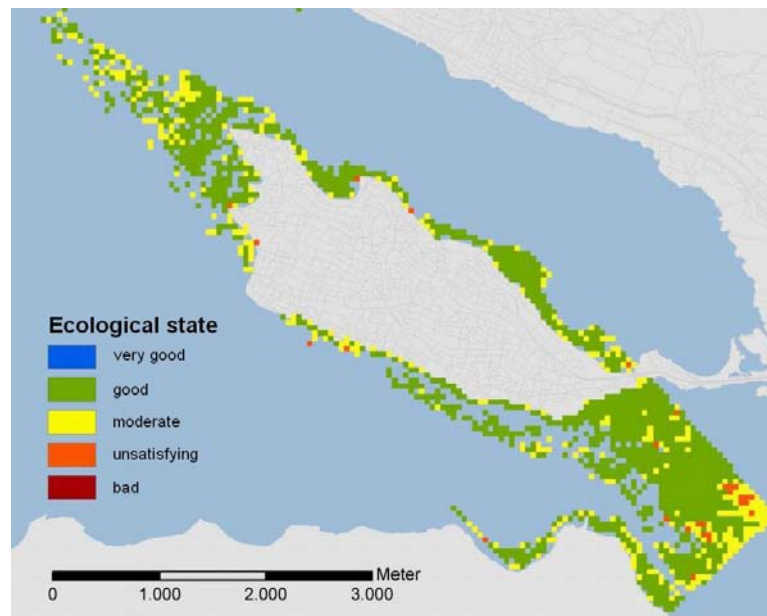
Figure 7.1: Pixel-based reference index calculation after Schaumburg (2004), based on the 2003 remote sensing macrophyte species classification at Lake Constance (Figure 6.16) adapted from Woithon et al. (2005)

Their pioneering attempt established first, the potential for this type application and second, the need for improved sensor resolution and species classification. This study is an attempt to meet these needs.

Bibliography

Aas, E. (1987). Two-stream irradiance model for deep waters. *Applied Optics*, 26:2095–2101.

Ackleson, S. and Klemas, V. (1987). Remote sensing of submerged aquatic vegetation in Lower Chesapeake Bay - a comparison of Landsat MSS to TM imagery. *Remote Sensing of Environment*, 22(2):235–248.

Alberotanza, L., Brando, V., Ravagnan, G., and Zandonella, A. (1999). Hyperspectral aerial images. A valuable tool for submerged vegetation recognition in the Orbetello Lagoons, Italy. *International Journal of Remote Sensing*, 20(3):523–533.

Albert, A. (2004). *Inversion technique for optical remote sensing in shallow water*. PhD Thesis, Institut für Methodik der Fernerkundung, Deutsches Zentrum für Luft und Raumfahrt, Oberpfaffenhofen.

Albert, A. and Gege, P. (2006). Inversion of irradiance and remote sensing reflectance in shallow water between 400 and 800 nm for calculations of water and bottom properties. *Applied Optics*, 45(10):2331–2343.

Albert, A. and Mobley, C. (2003). An analytical model for subsurface irradiance and remote sensing reflectance in deep and shallow case-2 waters. *Optics Express*, 11(22):2873 –2890.

Alefs, J. (1997). *Feinstratigraphie und Diatomeensukzession in den Profundalsedimenten des Ammersees und Starnberger Sees (Oberbayern)*. PhD Thesis, Institut für Angewandte Geologie und Mineralogie, Fakultät für Chemie, Biologie und Geowissenschaften, Technische Universität München.

Andrefouet, S., Hochberg, E., Payri, C., Atkinson, M., Müller-Karger, F., and Ripley, H. (2003a). Multi-scale remote sensing of microbial mats in an atoll environment. *International Journal of Remote Sensing*, 24(13):2661–2682.

Andrefouet, S., Müller-Karger, F., Hochberg, E., Hu, C., and Carder, K. (2001). Change detection in shallow coral reef environments using Landsat 7 ETM+ data. *Remote Sensing of Environment*, 79:150–162.

Andrefouet, S., Payri, C., Hochberg, E., Che, L., and Atkinson, M. (2003b). Airborne hyperspectral detection of microbial mat pigmentation in Rangiroa Atoll (French Polynesia). *Limnology and Oceanography, Light in shallow water*, 48(1, part 2):426–430.

Andresen, T. (2004). *Strategien zur wissensbasierten Bildanalyse hoch auflösender Fernerkundungsdatensätze für das Monitoring gewässernaher Feuchtgebiete*. PhD Thesis, Wissenschaftszentrum Weihenstephan für Ernährung, Landnutzung und Umwelt, Department für Ökologie, Fachgebiet für Limnologie, Technische Universität München.

Anstee, J., Dekker, A., Brando, V., Pinnel, N., Byrne, G., Daniel, P., and Held, A. (2001). Hyperspectral imaging for benthic species recognition in shallow coastal waters. In *IEEE2001 International Geoscience and Remote Sensing Symposium*, pages 1051–1061, Sydney, Australia.

Anstee, J., Dekker, A., Byrne, G., Daniel, P., Held, A., and Miller, J. (2000). Use of hyperspectral imaging for benthic species mapping in South Australian coastal waters. In *10th Australasian Remote Sensing and Photogrammetry Conference*, volume CD-ROM, pages 1051–1061, Adelaide, Australia.

Anstee, J., Jupp, D., and Byrne, G. (1997). The shallow benthic cover map and optical water quality of Port Philip Bay. In *4th International Conference of Remote Sensing for Marine and Coastal Environment*, pages 1–19, Orlando, Florida, USA.

Armstrong, R. (1993). Remote sensing of submerged vegetation canopies for biomass estimation. *International Journal of Remote Sensing*, 14(3):621–627.

Artigas, F. and Yang, J. (2005). Hyperspectral remote sensing of marsh species and plant vigour gradient in the New Jersey Meadowlands. *International Journal of Remote Sensing*, 26(23):5209–5220.

Asner, G. (1998). Biophysical and biochemical sources of variability in canopy reflectance. *Remote Sensing of Environment*, 64:234–253.

Bajjouk, T., Guillaumont, B., and Populus, J. (1996). Application of airborne imaging spectrometry system data to intertidal seaweed classification and mapping. *Hydrobiologia*, 327:463–471.

Bajjouk, T., Populus, J., and Guillaumont, B. (1998). Quantification of subpixel cover fractions using principal component analysis and a linear programming method: application to the coastal zone of Roscoff (France). *Remote Sensing of Environment*, 64(2):153–165.

Bäuerle, E. and Gaedke, U. (1998). Lake Constance: Characterisation of an ecosystem in transition. In *Archiv für Hydrobiologie, Special issues: Advances in Limnology*, volume 53.

Berger, J. and Schagerl, M. (2003). Allelopathic activity of *Chara aspera*. *Hydrobiologia*, 501:109–115.

Best, E. and Boyd, W. (2003). Aquatic plant control research program. Simulation model for growth of the submersed aquatic macrophyte Sago Pondweed (*Potamogeton pectinatus* L.). Technical report, Environmental Laboratory, U.S. Army Corps of Engineers.

Binzer, T. and Sand-Jensen, K. (2002). Production in aquatic macrophyte communities: A theoretical and empirical study of the influence of spatial light distribution. *Limnology and Oceanography*, 47(6):1742–1750.

Blackburn, G. (1998). Quantifying chlorophylls and carotenoids at leaf and canopy scales. An evaluation of some hyperspectral approaches. *Remote Sensing of Environment*, 66(3):273–285.

Bögle, M., Schneider, S., Mannschreck, B., and Melzer, A. (subm). Differentiation of *Chara intermedia* and *C. baltica* compared to *C. hispida* based on morphology and amplified fragment length polymorphism. *Hydrobiologia*.

Bogner, A. (2003). *Prozessekette zur Kartierung submerser Makrophyten mit dem Multi-spektralscanner DAEDALUS*. Msc Thesis, Vermessungswesen und Karthographie, Fach-hochschule München.

Bostater, C., Ghir, T., Bassetti, L., Hall, C., Reyeier, E., Lowers, L., Holloway-Adkins, K., and Virnstein, R. (2004). Hyperspectral remote sensing protocol development for submerged aquatic vegetation in shallow waters. In *Remote Sensing of the Ocean and Sea Ice 2003*, volume 5233 of *Proceedings of SPIE*, pages 199–215.

Bostater, C., Ma, W., McNally, T., and Keller, M. (1997). Hyperspectral remote sensing of coastal and estuarine waters: A comparison between modeled and measured reflectance spectra. In *4th International Conference on Remote Sensing for Marine and Coastal Environments*, Orlando, Florida.

Brando, V. and Dekker, A. (2003). Satellite hyperspectral remote sensing for estimating estuarine and coastal water quality. *IEEE Transaction on Geoscience and Remote Sensing*, 41(6):1376–1387.

Bricaud, A., Morel, A., and Prieur, L. (1981). Absorption by dissolved organic matter of the sea (yellow substance) in the UV and visible domains. *Limnology and Oceanography*, 26(1):43–53.

Bricaud, A. and Stramski, D. (1990). Spectral absorption coefficients of living phytoplankton and nonalgal biogenous matter: A comparison between the Peru upwelling area and the Sargasso Sea. *Limnology and Oceanography*, 35(3):562–582.

Bueno, N. and Bicudo, C. (2006). Temporal variation of *Nitella furcata* subsp. *mucronata* var. *mucronata* f. *oligospira* (Charophyceae) in the Ninféias pond, São Paulo State, southeast Brazil. *Acta Botanica Brasilia*, 20(1):1–11.

Buiteveld, H., Hakvoort, J., and Donze, M. (1994). Optical properties of pure water. In Jaffe, J., editor, *Ocean Optics XII*, pages 174–183, Bellingham, Washington, USA.

Bulgarelli, B., Kisselev, V., and Roberti, L. (1999). Radiative transfer in the atmosphere ocean system: the Finite-Element Method. *Applied Optics*, 38(9):1530–1542.

Butler, W. and Hopkins, D. (1970). Higher derivative analysis of complex absorption spectra. *Photochemistry and Photobiology*, 12:439–450.

Call, K., Hardy, J., and Wallin, D. (2003). Coral reef habitat discrimination using multivariate spectral analysis and satellite remote sensing. *International Journal of Remote Sensing*, 24(13):2627–2639.

Carder, K., Steward, R., Harvey, G., and Ortner, P. (1989). Marine humic and fulvic acids: Their effects on remote sensing of ocean chlorophyll. *Limnology and Oceanography*, 34(2):68–81.

Carter, G. and Knapp, A. (2001). Leaf optical properties in higher plants: linking spectral characteristics to stress and chlorophyll concentration. *American Journal of Botany*, 4:677–684.

Carter, G., Paliwal, K., Pathre, U., Green, T., Mitchell, R., and Gjerstad, G. (1989). Effect of competition and leaf age on visible and infrared reflectance in pine foliage. *Plant, Cell and Environment*, 12:309–315.

Chauvaud, S., Bouchon, C., and Maniere, R. (1998). Remote sensing techniques adapted to high resolution mapping of tropical coastal marine ecosystems (coral reefs, seagrass beds and mangroves). *International Journal of Remote Sensing*, 19(18):3625–3639.

Chipchase, C. and Leach, J. (2000). Methods of identifying *Hormosira banksii* on the intertidal platforms using low altitude aerial photography. Technical report, Department of Geomatics, University of Melbourne.

Clark, C., Mumby, P., Chisholm, J., Jaubert, J., and Andrefouet, S. (2000). Spectral discrimination of coral mortality states following a severe bleaching event. *International Journal of Remote Sensing*, 21(11):2321–2327.

Clark, M., Roberts, D., and Clark, D. (2005). Hyperspectral discrimination of tropical rain forest tree species at leaf to crown scales. *Remote Sensing of Environment*, 96:375–398.

Cochrane, M. (2000). Using vegetation reflectance variability for species level classification of hyperspectral data. *International Journal of Remote Sensing*, 21(10):2075–2087.

Curran, P. (1989). Remote sensing of foliar chemistry. *Remote Sensing of Environment*, 30(3):271–278.

Dekker, A. (1993). *Detection of optical water quality parameters for eutrophic waters by high resolution remote sensing*. PhD Thesis, Vrije Universiteit Amsterdam, Amsterdam.

Dekker, A., Brando, E., and Anstee, J. (2005). Retrospective seagrass change detection in a shallow coastal tidal Australian lake. *Remote Sensing of Environment*, 97:415–433.

Dekker, A., Brando, V., Anstee, J., Fyfe, S., Malthus, T., and Karpouzli, E. (2006). Remote sensing of seagrass ecosystems: Use of spaceborne and airborne sensors. In Larkum, A., Orth, B., and Duarte, C., editors, *Seagrass Biology, Ecology and Conservation*, chapter 15, page 630. Springer.

Dekker, A., Brando, V., Anstee, J., Pinnel, N., Kutser, T., Hoogenboom, H., Pasterkamp, R., Peters, S., Vos, R., Olbert, C., and Malthus, T. (2001). Applications of imaging spectrometry in inland, estuarine, coastal and ocean waters. In *Imaging Spectrometry: Basic principles and prospective applications*, volume IV of *Remote Sensing and Digital Image Processing*. Kluwer Academic Publishers, Dordrecht.

Dekker, A., Hoogenboom, H., Goddijn, L., and Malthus, T. (1997). The relationship between inherent optical properties and reflectance spectra in turbid inland waters. *Remote Sensing Reviews*, 15:59–74.

Dekker, A. and Jordan, A. (in press). Satellite and airborne imagery including aerial photograpy. In *Marine benthic habitat mapping special publication*. Geological Association of Canada and GeoHab Geological and Benthic Habitat Mapping.

Dekker, A., Malthus, T., and Hoogenboom, H. (1995). The remote sensing of inland water quality. In Danson, F. and Plummer, S., editors, *Advances in Environmental Remote Sensing*, pages 123–142. John Wiley and Sons, UK.

Demetriades-Shah, T., Steven, M., and Clark, J. (1990). High resolution derivative spectra in remote sensing. *Remote Sensing of Environment*, 33:55–64.

Dennison, W., Orth, R., Moore, K., Stevenson, J., Carter, V., Kollar, S., Bergstrom, P., and Batiuk, R. (1993). Assessing water quality with submersed aquatic vegetation. Habitat requirements as barometers of Chesapeake Bay health. *Bioscience*, 43(2):86–94.

Dierssen, H., Zimmermann, R., Leathers, R., Downes, T., and Davis, C. (2003). Ocean color remote sensing of seagrass and bathymetry in the Bahamas Banks by high-resolution airborne imagery. *Limnology and Oceanography, Light in shallow water*, 48(1, part 2):444–455.

Doerffer, R. (1992). Imaging spectroscopy for detection of chlorophyll and suspended matter. In Toselli, F. and Bodechtel, J., editors, *Imaging spectroscopy: Fundamentals and prospective applications*, EuroCourses Remote Sensing, pages 215–257. Kluwer Academic Publishers, Dordrecht.

Doerffer, R. and Schiller, H. (1994). Inverse modelling for retrieval of ocean color parameters in case II coastal waters: An analysis of the minimum error. In Jaffe, J., editor, *Ocean Optics XII*, volume 2258, pages 887–893, Bellingham, Washington, USA.

Donald, D., Coomans, D., Everingham, Y., Cozzolino, D., Gishen, M., and Hancock, T. (2006). Adaptive wavelet modelling of a nested 3 factor experimental design in NIR chemometrics. *Chemometrics and Intelligent Laboratory Systems*, 82:122–129.

Drake, L., Dobbs, F., and Zimmermann, R. (2003). Effects of epiphyte load on optical properties and photosynthetic potential of seagrasses *Thalassia testudinum* Banks ex König and *Zostera marina* L. *Limnology and Oceanography, Light in shallow water*, 48(1, part 2):456–463.

Drake, L., Zimmermann, R., Cummings, M., and Dobbs, F. (1999). Epiphyte load on seagrass leaves: effects of leaf age and influence on inherent optical properties. In *American Society of Limnology and Oceanography*, Santa Fe.

Duarte, C. (1991). Seagrass depth limits. *Aquatic Botany*, 40:363–377.

Dunk, I. and Lewis, M. (1999). Seagrass and shallow water feature discrimination using Hymap imagery. In *10th Australian Remote Sensing and Photogrammetry Conference*, pages 1092–1108, University of Adelaide, Australia.

Durand, D., Bijaoui, J., and Cauneau, F. (2000). Optical remote sensing of shallow-water environmental parameters. *Remote Sensing of Environment*, 73(2):152–161.

EG-Europäische Gemeinschaft (2000). Richtlinie 2000/60/EG des Europäischen Parlamentes und des Rates vom 23. Oktober 2000 zur Schaffung eines Ordnungsrahmens für Manahmen der Gemeinschaft im Bereich der Wasserpolitik. *Amtsblatt der Europischen Union*, *L*327/1:72.

Einstein, A. (1910). Theorie der Opaleszenz von homogenen Flüssigkeiten und Flüssigkeitsgemischen in der Nähe des kritischen Zustandes. *Annalen der Physik*, 33:1275–1298.

Everitt, B. (2005). *An R and S-Plus companion to multivariate analysis*. Springer Texts in Statistics. Springer, London,UK.

Everitt, J., Yang, C., Escobar, D., Webster, C., Lonard, R., and Davis, M. (1999). Using remote sensing and spatial information technologies to detect and map two aquatic macrophytes. *Journal of Aquatic Plant Management*, 37:71–80.

Fariña, J., Salazar, S., Wallem, K., Witman, J., and Ellis, J. (2003). Nutrient exchanges between marine and terrestrial ecosystems: The case of the Galapagos sea lion *Zalophus wollebaecki*. *Journal of Animal Ecology*, 72:873–887.

Fennessy, M., Cronk, J., and Mitsch, W. (1994). Macrophyte productivity and community development in created freshwater wetlands under experimental hydrological conditions. *Ecological Engineering*, 3:469–484.

Ferguson, R. and Korfmacher, K. (1997). Remote sensing and GIS analysis of seagrass meadows in North Carolina, USA. *Aquatic Botany*, 58:241–258.

Ferguson, R., Wood, L., and Graham, D. (1993). Monitoring spatial change in seagrass habitat with aerial-photography. *Photogrammetric Engineering and Remote Sensing*, 59(6):1033–1038.

Fischer, J., Doerffer, R., and Grassl, H. (1986). Factor analysis of multispectral radiances over coastal and open ocean waters based on radiative transfer calculations. *Applied Optics*, 25(3):448–456.

Förster, C. (2006). Lichtabsorptions- und Streuungseigenschaften verschiedener Komponenten des Periphytons. Diplomarbeit, Wissenschaftszentrum Weihenstephan für Ernährung, Landnutzung und Umwelt, Department für Ökologie, Technische Universität München.

Fraser, R. (1998). Hyperspectral remote sensing of turbidity and chlorophyll a among Nebraska Sand Hills lakes. *International Journal of Remote Sensing*, 19(8):1579–1589.

Fyfe, S. (2003). Spatial and temporal variation in spectral reflectance: Are seagrass species spectrally distinct? *Limnology and Oceanography, Light in shallow water*, 48(1, part 2):464–479.

Fyfe, S. (2004). *Hyperspectral studies of New South Wales seagrasses with particular emphasis on the detection of light stress in eelgrass Zostera capricorni.* PhD Thesis, University of Woolongong.

Galvão, L., Formaggio, A., and Tisot, D. (2005). Discrimination of sugarcane varieties in Southeastern Brazil with EO-1 Hyperion data. *Remote Sensing of Environment*, 94:523–534.

Gausman, H. (1977). Reflectance of leaf components. *Remote Sensing of Environment*, 6:1–7.

Gausman, H. (1984). Evaluation of factors causing reflectance differences between sun and shade leaves. *Remote Sensing of Environment*, 15:177–181.

Gausman, H. and Allen, W. (1973). Optical parameters of leaves of 30 plant species. *Plant Physiology*, 52:57–62.

Gege, P. (1994). *Gewässeranalyse mit passiver Fernerkundung: Ein Modell zur Interpretation optischer Spektralmessungen.* PhD Thesis, Institut für Optoelektronik, Deutsche Forschungsanstalt für Luft-und Raumfahrt, Oberpfaffenhofen.

Gege, P. (2000). Gaussian model for yellow substance absorption spectra. In *Ocean Opitics XV*, Monaco.

Gege, P. (2001). The water colour simulator WASI: A software tool for forward and inverse modeling of optical in-situ spectra. In *IEEE 2001 International Geoscience and Remote Sensing Symposium*, Sydney, Australia.

Gege, P. (2004). Improved method for measuring gelbstoff absorption spectra. In *Ocean Optics XVII*, Fremantle, West Australia.

Gentleman, R., Carey, V., Huber, W., Irizarry, R., and Dudoit, S. (2005). *Bioinformatics and computational biology solutions using R and bioconductor*. Statistics for Biology and Health. Springer Science and Business Media, USA, 1 edition. 473p.

Gitelson, A., Zur, Y., Chivkunova, O., and Merzlyak, M. (2002). Assessing carotenoid content in plant leaves with reflectance spectroscopy. *Photochemistry and Photobiology*, 75(3):272–281.

Goetz, A., Vane, G., Solomon, J., and Rock, B. (1985). Imaging spectrometry for earth remote sensing. *Science*, 228:1147–1153.

Gong, P., Pu, R., and Yu, B. (1997). Conifer species recognition: An exploratory analysis of in situ hyperspectral data. *Remote Sensing of Environment*, 62:189–200.

Goos, C. (2003). *Einfluß des Periphytons auf das Lichtklima submerser Makrophyten*. PhD Thesis, Wissenschaftszentrum Weihenstephan für Ernährung, Landnutzung und Umwelt, Department für Ökologie, Fachgebiet für Limnologie, Technische Universität München.

Gordon, H., Brown, O., and Jacobs, M. (1975). Computed relationships between the inherent and apparent optical properties of a flat homogeneous ocean. *Applied Optics*, 14(2):417–427.

Gordon, H. and Clark, D. (1995). Atmospheric effects in the remote sensing of phytoplankton pigments. *Boundary-Layer Meteorology*, 18(3):299–313.

Gordon, H. and Morel, A. (1983). *Remote assessment of ocean color for interpretation of satellite visible imagery: a review*. Lecture Notes on Coastal and Estuarine Studies 4. Springer, New York.

Grasmück, N., Haury, J., Léglize, L., and Muller, S. (1995). Assessment of the bio-indicator capacity of aquatic macrophytes using multivariate analysis. *Hydrobiologia*, 300-301:115–122.

Green, E., Mumby, P., Edwards, A., and Clark, C. (2000). *Remote sensing handbook for tropical coastal management*. UNESCO.

Green, E., Mumby, P., Edwards, P., and Clark, C. (1996). A review of remote-sensing for the assessment and management of tropical coastal resources. *Coastal Management*, 24:1–40.

Green, R., Conel, J., Carrere, V., Bruegge, C., Margolis, J., Rast, M., and Hoover, G. (1991). Determination of the in-flight spectral and radiometric characteristics of the Airborne Visible/Infrared Imaging spectrometer (AVIRIS). In *Physical Measurements and Signatures in Remote Sensing*, pages 19–28.

Gross, E. M. (2003). Allelopathy of aquatic autotrophs. *Critical Reviews in Plant Science*, 22(3&4):313–339.

Hakvoort, J. (1994). *Absorption of light by surface water*. PhD Thesis, Delft University of Technology.

Häse, C., Gaedke, U., Seifried, A., Beese, B., and Tilzer, M. (1998). Phytoplankton response to re-oligotrophication in large and deep Lake Constance: Photosynthetic rates and chlorophyll concentration. In *Archiv für Hydrobiologie, Special issues: Advances in Limnology*, volume 53, pages 159–178.

Hastie, T., Buja, A., and Tibshirani, R. (1995). Penalized discriminant analysis. *Annals of Statistics*, 23(1):73–102.

Heege, T. (2000). *Flugzeuggestützte Fernerkundung von Wasserinhaltstoffen im Bodensee*. PhD Thesis, Institut für Methodik der Fernerkundung, Deutsches Zentrum für Luft und Raumfahrt, Oberpfaffenhofen.

Heege, T., Bogner, A., and Pinnel, N. (2003a). Mapping of submerged aquatic vegetation with a physically based processing chain. In Kramer, E., editor, *SPIE-The International Society for Optical Engineering*, volume 5233, Barcelona, Spain.

Heege, T. and Fischer, J. (2004). Mapping of water constitutents in Lake Constance using multispectral airborne scanner data and a physically based processing scheme. *Canadian Journal of Remote Sensing*, 30(1):77–86.

Heege, T., Häse, C., Bogner, A., and Pinnel, N. (2003b). Airborne multi-spectral remote sensing in shallow and deep waters. *Backscatter*, 14(1):17–19.

Heege, T., Hausknecht, P., and Kobryn, H. (2006). Hyperspectral seafloor mapping and direct bathymetry calculation using HyMap data from the Ningaloo reef and Rottnest Island areas in Western Australia. In *13th Australasian Remote Sensing and Photogrammetry Conference*, page 7, Camberra, Australia.

Heege, T., van der Piepen, H., Fischer, J., and Amann, V. (1998). Gewässerfernerkundung am Bodensee: Verfahren und Anwendungsbeispiele. DLR-Forschungsbericht 98-22, Institut für Optoelektronik, Deutsches Zentrum für Luft- und Raumfahrt, Oberpfaffenhofen.

Held, A., Byrne, G., Anstee, J., Williams, N., and Field, C. (1997). Monitoring of sensitive coastal ecosystems with the CASI (Compact Airborne Spectrographic Imager). In *3rd International Airnorne Remote Sensing Conference and Exhibition*, pages 134–141, Copenhagen, Denmark.

Hernández, O., Fraga, J., Jiménez, A., and Arias, J. (2005). Characterization of honey from the Canary Islands: determination of the mineral content by atomic absorption spectrophotometry. *Food Chemistry*, 93:449–458.

Hilton, J., Rigg, E., and Jaworski, G. (1989). Algal identification using in vivo fluorescence spectra. *Journal of Plankton Research*, 11(1):65–74.

Hochberg, E. and Atkinson, M. (2000). Spectral discrimination of coral reef benthic communities. *Coral Reefs*, 19:164–171.

Hochberg, E. and Atkinson, M. (2003). Capabilities of remote sensors to classify coral, algae, and sand as pure and mixed spectra. *Remote Sensing of Environment*, 85:174–189.

Hoge, F. and Lyon, P. (1996). Satellite retrieval of inherent optical properties by linear matrix inversion of oceanic radiance models - an analysis of model and radiance measurement errors. *Journal of Geophysical Research-Oceans*, 101(C7):16631–16648.

Holden, H. and LeDrew, E. (1997). Spectral discrimination of bleached and healthy submerged corals based on principal component analysis. In *4th International Conference on Remote Sensing for Marine Coastal Environments*, pages 177–185, Orlando, Florida.

Holden, H. and LeDrew, E. (1998). Spectral discrimination of healthy and non-healthy corals based on cluster analysis, principal components analysis, and derivative spectroscopy. *Remote Sensing of Environment*, 65:217–224.

Holden, H. and Ledrew, E. (1999). Hyperspectral identification of coral reef features. *International Journal of Remote Sensing*, 20:2545–2563.

Holden, H. and LeDrew, E. (2000). Accuracy assessment of hyperspectral classification of coral reef features. *Geocarto International*, 15:5–11.

Hoogenboom, H., Dekker, A., and De Haan, J. (1998). Retrieval of chlorophyll and suspended matter in inland waters from CASI data by matrix inversion. *Canadian Journal of Remote Sensing*, 24(2):144–152.

IGKB (2002). Limnologischer Zustand des Bodensees-Jahresbericht Januar 2001 bis März 2002. Technical Report 29, International Gewässerschutzkommission für den Bodensee.

Jäger, P. and Dumfarth, E. (2004). A method of mapping macrphytes in large lakes with regard to the Water Framework Directive. *Limnologica*, 34(1-2):140–146.

Jakubauskas, M., Kindscher, K., Fraser, A., Debinski, D., and Price, K. (2000). Close-range remote sensing of aquatic macrophyte vegetation cover. *International Journal of Remote Sensing*, 21(18):3533–3538.

Jarvis, R. and Goodacre, R. (2005). Genetic algorithm optimization for pre-processing and variable selection of spectroscopic data. *Bioinformatics*, 21(7):860–868.

Jensen, J., Hodgson, M., Christensen, E., Mackey, H., Tinney, L., and Sharitz, R. (1986). Remote sensing inland wetlands: A multispectral approach. *Photogrammetric Engineering and Remote Sensing*, 52:87–100.

Jensen, J., Narumalani, S., Weatherbee, O., and Mackey, H. (1993). Measurement of seasonal and yearly cattail and waterlily changes using multidate SPOT panchromatic data. *Photogrammetric Engineering and Remote Sensing*, 59(4):519–525.

Jensen, J., Rutchey, K., Koch, M., and Narumalani, S. (1995). Inland wetland change detection in the Everglades Water Conservation area 2A using a time series of normalized remotely sensed data. *Photogrammetric Engineering and Remote Sensing*, 61(2):199–209.

Jernakoff, P. and Hick, P. (1994). Spectral measurement of marine habitat: simultaneous field measurements and CASI data. In *7th Australasian Remote Sensing Conference*, pages 706–713, Melbourne, Australia.

Jolliffe, I. (1986). *Principal component analysis*. Springer, New York.

Jonckheere, I., Muys, B., and Coppin, P. (2005). Derivative analysis for in situ high dynamic range hemispherical photography and its application in forest stands. *IEEE Geoscience and Remote Sensing Letters*, 2(3):296–300.

Joyce, K. and Phinn, S. (2003). Hyperspectral analysis of chlorophyll content and photosynthetic capacity of coral reef substrates. *Limnology and Oceanography, Light in shallow water*, 48(1, part 2):489–496.

Jupp, D., Byrne, G., Anstee, J., McDonald, E., McVicar, T., Kirk, J., Hurlstone, C., and Chidgey, S. (1996). Port Philip Bay benthic habitat mapping project. Technical Report Task G2.2, CSIRO Land and Water.

Jupp, D., Mayo, K., Kuchler, D., Claassen, T., Kenchington, R., and Guerin, P. (1985). Remote sensing for planning and managing the Great Barrier Reef of Australia. *Photogrammetria*, 40:21–42.

Kailath, T. (1967). The divergence and Bhattacharyya Distance measures in signal selection. *IEEE Transaction on Geoscience and Remote Sensing*, 15(1):52–60.

Keller, P. (2001). *Imaging spectroscopy of lake water quality parameters*. PhD Thesis, Remote Sensing Laboratories, Department of Geography, University of Zurich.

Kirk, J. (1976). Yellow substance (gelbstoff) and its contribution to the attenuation of photosynthetically active radiation in some inland and coastal south-east Australian waters. *Australian Journal of Marine and Freshwater Research*, 27:61–71.

Kirk, J. (1989). The upwelling light stream in natural waters. *Limnology and Oceanography*, 34(8):1410–1425.

Kirk, J. (1991). Volume scattering function, average cosines, and the underwater light field. *Limnology and Oceanography*, 36(3):455–467.

Kirk, J. (1994). *Light and photosynthesis in aquatic ecosystems*. University Press, Cambridge, UK, 2 edition.

Kisselev, S., Heege, T., and Miksa, S.and Pinnel, N. (2005). A physically based technology for processing of water basin remote sensing data. In *31st International Symposium on Remote Sensing Environment*, Proceedings of ISRSE, St. Petersburg.

Kisselev, V. and Bulgarelli, B. (2004). Reflection of light from a rough water surface in numerical methods for solving the radiative transfer equation. *Journal of quantitative spectroscopy and radiative transfer*, 85(3-4):419–435.

Kisselev, V., Roberti, L., and Perona, G. (1995). Finite-element algorithm for radiative transfer in vertically inhomogeneous media: numerical scheme and applications. *Applied Optics*, 34(36):8460–8471.

Kondratyev, K., Pozdnyakov, D., and Pettersson, L. (1998). Water quality remote sensing in the visible spectrum. *International Journal of Remote Sensing*, 19(5):957–979.

Körner, S. and Nicklisch, A. (2002). Allelopathic growth inhibition of selected phytoplankton species by submerged macrophytes. *Journal of phycology*, 38:862–871.

Krawczyk, H. and Hetscher, M. (1997). Principal Component Inversion algorithm for the retrieval of water constituents and its application. In Neumann, A., editor, *1st International Workshop on MOS-IRS and Ocean Colour*, Deutsches Zentrum für Luft und Raumfahrt, Berlin.

Kruse, F., Richardson, L., and Ambrosia, V. (1997). Techniques developed for geological analysis of hyperspectral data applied to near-shore hyperspectral ocean data. In *Fourth International Conference on Remote Sensing and Coastal Environments*, Orlando, Florida,.

Krzanowski, W. (2000). *Principles of multivariate analysis. A user's perspective*. Number 22 in Oxford Statistical Science Series. Oxford University Press Inc., New York, USA, 2nd edition.

Kutser, T., Dekker, A., and Skirving, W. (2003). Modeling spectral discrimination of Great Barrier Reef benthic communities by remote sensing instruments. *Limnology and Oceanography, Light in shallow water*, 48(1, part 2):497–510.

Lamb, D. and O'Donnell, J. (1996). Airborne video for assessment of water quality in Australian inland rivers. *Australian Journal of Soil and Water Conservation*, 9(1):14–20.

Landres, P., Morgan, P., and Swanson, F. (1999). Overview of the use of natural variability concepts in managing ecological systems. *Ecological Applications*, 9:1179–1188.

LAWA (1985). *Seen in der Bundesrepublik Deutschland*. Länderarbeitsgemeinschaft Wasser.

Leathers, R. and McCormick, N. (1999). Algorithms for ocean-bottom albedo determination from in-water natural-light measurements. *Applied Optics*, 38(15):3199–3205.

Lee, Z., Carder, K., Mobley, C., Steward, R., and Patch, J. (1998a). Hyperspectral remote sensing for shallow waters. I. A semianalytical model. *Applied Optics*, 37:6329–6338.

Lee, Z., Carder, K., Mobley, C., Steward, R., and Patch, J. (1999). Hyperspectral remote sensing for shallow waters: II. Deriving bottom depths and water properties by optimization. *Applied Optics*, 38(18):3831–3843.

Lee, Z., Carder, K., Steward, R., Peacock, T., Davis, C., and Patch, J. (1998b). An empirical algorithm for light absorption by ocean water. *Journal of Geophysical Research*, 103(C12):27,967–27,978.

Lefsky, M., Cohen, W., Acker, S., Parker, G., Spies, T., and Harding, D. (1999). LIDAR remote rensing of the canopy structure and biophysical properties of Douglas-Fir Western Hemlock forests. *Remote Sensing of Environment*, 70:339–361.

Lehmann, A., Jaquet, J., and Lachavanne, J. (1997). A GIS approach of aquatic plant spatial heterogeneity in relation to sediment and depth gradients, Lake Geneva, Switzerland. *Aquatic Botany*, 58:347–361.

Lehmann, A. and Lachavanne, J. (1999). Changes in the water quality of Lake Geneva indicated by submerged macrophytes. *Freshwater Biology*, 42(3):457–466.

Lennon, P. and Luck, P. (1990). Seagrass mapping using Landsat TM data: a case study in southern Queensland. *Asian-Pacific Remote Sensing Journal*, 2(2):6.

Liceaga-Correa, M. and Euan-Avila, J. (2002). Assessment of coral reef bathymetric mapping using visible Landsat Thematic Mapper data. *International Journal of Remote Sensing*, 23(1):3–14.

Lichtenthaler, H. and Babani, F. (2000). Detection of photosynthetic activity and water stress by imaging the red chlorophyll fluorescence. *Plant physiology and biochemistry*, 38:889–895.

Lillesand, T. and Kiefer, R. (2000). *Remote sensing and image interpretation*. John Wiley and Sons, New York, 4 edition.

Lindell, L., Pierson, D., Premazzi, G., Zillioli, E., and et.al. (1999). *Manual for monitoring European lakes using remote sensing techniques*. European Communities, Luxembourg.

Logan, P. and Furse, M. (2002). Preparing for the European Water Framework Directive - making the links between habitat and aquatic biota. *Aquatic Conservation: Marine and Freshwater Ecosystems*, 12:425–437.

Louchard, E., Reid, R., and Stephens, C. (2000). Classification of sediment types and estimation of water depth using spectral libraries. In *Ocean Optics XV*, page 13, Monaco.

Louchard, E., Reid, R., Stephens, C., Davis, C., Leathers, R., and Downes, T. (2002). Derivative analysis of absorption features in hyperspectral remote sensing data of carbonate sediment. *Optics Express*, 10(26):1573–1584.

Louchard, E., Reid, R., Stephens, F., Davis, C., Leather, R., and Downes, T. (2003). Optical remote sensing of benthic habitats and bathymetry in coastal environments at Lee Stocking Island, Bahamas: A comparative spectral classification approach. *Limnology and Oceanography, Light in shallow water*, 48(1, part 2):511–521.

Lubin, D., Dustan, P., Mazel, C., and Stannes, K. (2001). Spectral signatures of coral reefs: features from space. *Remote Sensing of Environment*, 75:127–137.

Luczkovich, J., Wagner, T., Michalek, J., and Stoffle, R. (1993). Discrimination of coral reefs, seagrass meadows, and sand bottom types from space; a Dominican Republic case study. *Photogrammetric Engineering and Remote Sensing*, 59(3):385–386.

Luterbacher, J., Dietrich, D., Xoplaki, E., Grosjean, M., and Wanner, H. (2004). European seasonal and annual temperature variability, trends, and extremes since 1500. *Science*, 303(5663):1499–1503.

Lyzenga, D. (1978). Passive remote sensing techniques for mapping water depth and bottom features. *Applied Optics*, 17:379–383.

Maeder, J., Narumalani, S., Rundquist, D., Perk, R., Schalles, J., Hutchins, K., and Keck, J. (2002). Classifying and mapping general coral-reef structure using IKONOS data. *Photogrammetric Engineering and Remote Sensing*, 68:1297–1305.

Maffione, R. and Dana, D. (1997). Recent measurements of the spectral backward-scattering coefficient in coastal waters. In *Ocean optics XIII*, pages 154–157, Bellingham, USA.

Maindonald, J. and Burden, C. (2005). Selection bias in plots of microarray or other data that have been sampled from a high-dimensional space. *Anziam Journal*, 46:C59–C74.

Mallet, Y., Coomans, D., and de Vel, O. (1996). Recent developments in discriminant analysis on high dimensional spectral data. *Chemometrics and Intelligent Laboratory Systems*, 35:157–173.

Malthus, T., Best, E., and Dekker, A. (1990). An assessment of the importance of emergent and floating-leaved macrophytes to trophic status in the Loosdrecht lakes (The Netherlands). *Hydrobiologia*, 191:257–263.

Malthus, T., Ciraolo, G., La Loggia, G., Clark, C., Plummer, S., Calvo, S., and Tomasello, A. (1997). Can biophysical properties of submersed macrophytes be determined by remote sensing? In *Fourth International Conference on Remote Sensing for Marine and Coastal Environments*, volume 1, pages 562–571, Orlando, Florida.

Malthus, T. and George, D. (1997). Airborne remote sensing of macrophytes in Cefni Reservoir, Anglesey, UK. *Aquatic Botany*, 58(3-4):317–332.

Malthus, T. and Karpouzli, E. (2003). Integrating field and high spatial resolution satellite-based methods for monitoring shallow submersed aquatic habitats in the Sound of Eriskay, Scotland, UK. *International Journal of Remote Sensing*, 24(13):2585–2593.

Mannschreck, B. (2003). *Genetische und morphologische Differenzierung ausgewählter Arten der Gattung Chara*. PhD Thesis, Wissenschaftszentrum Weihenstephan für Ernährung, Landnutzung und Umwelt, Department für Ökologie, Fachgebiet für Limnologie, Technische Universität München.

Maritorena, S. (1996). Remote sensing of water attenuation in coral reefs: case study in French Polynesia. *International Journal of Remote Sensing*, 17(1):155–166.

Maritorena, S., Morel, A., and Gentili, B. (1994). Diffuse reflectance of oceanic shallow waters: influence of water depth and bottom albedo. *Limnology and Oceanography*, 39(7):1689–1703.

Marshall, T. and Lee, P. (1994). Mapping aquatic macrophytes through digital image-analysis of aerial photographs - an assessment. *Journal of Aquatic Plant Management*, 32:61–66.

Mather, P. (1999). *Computer processing of remotely-sensed images - An introduction*. John Wiley and Sons, New York, 2. edition.

Mathewson, D., Hocking, M., and Reimchen, T. (2003). Nitrogen uptake in riparian plant communities across a sharp ecological boundary of salmon density. *BMC Ecology*, 3:4.

McLachlan, G. (1992). *Discriminant analysis and statistical pattern recognition*. Applied probability and statistics. John Wiley and Sons, New York.

Meilinger, P., Schneider, S., and Melzer, A. (2005). The Reference Index Method for the macrophyte-based assessment of rivers - a contribution to the implementation of the European Water Framework Directive in Germany. *International Review of Hydrobiology*, 90(3):322–342.

Melzer, A. (1988). *Der Macrophytenindex - eine biologische Methode zur Ermittlung der Nährstoffbelastung von Seen*. Habil. Thesis, Fakultät für Chemie, Biologie und Geowissenschaften, Technische Universität München.

Melzer, A. (1999). Aquatic macrophytes as tools for lake management. *Hydrobiologia*, 395/396:181–190.

Merton, R. and Cochrane, G. (1995). Imaging spectroscopy: a new tool for the physical sciences. In *New Zealand Geographical Society Anniversary Conference 1995*. University of Canterbury, Christchurch, New Zealand.

Merzlyak, M., Gitelson, A., Chivkunova, O., Solovchenko, A., and Pogosyan, S. (2003). Application of reflectance spectroscopy for analysis of higher plant pigments. *Russian Journal of Plant Physiology*, 50(5):704–710.

Meulstee, C., Nienhuis, P., and van Stokkom, H. (1986). Biomass assessment of estuarine macrophytobenthos using aerial photography. *Marine Biology*, 91:331–5.

Miksa, S., Heege, T., Gege, P., and Kisselev, V. (2004). Coupled aerosol and water constituent retrieval algorithm for hyperspectral remote sensing sensors over case II water Lake Constance. In *Ocean Optics XVII*, page 11, Fremantle, West Australia.

Miksa, S., Heege, T., Kisselev, V., and Gege, P. (2005). Mapping water constituents in Lake Constance using Chris/Proba. In *Proceeding of the 3rd ESA Chris/Proba Workshop*, Frascati, Italy.

Mobley, C. (1994). *Light and water-Radiative transfer in natural waters*. Academic Press, London.

Mobley, C., Gentili, B., Gordon, H., Jin, Z., Kattawar, G., Morel, A., Reinersman, P., Stamnes, K., and Stavn, R. (1993). Comparison of numerical models for computing underwater light fields. *Applied Optics*, 32(36):7484–7504.

Mobley, C. and Sundman, L. (2000). Hydrolight 4.1 technical documentation. Technical report, Sequoia Scientific, Inc.

Mott, C. (2005). *Objektorientierte Klassifikationsstrategien zur Erfassung der Landnutzung aus hochauflösenden Fernerkundungsdaten*. PhD Thesis, Department für Ökosystem- und Landschaftsmanagement, Technische Universität München.

Müller, R., Lehner, M., Reinartz, P., Schröder, M., and Vollmer, B. (2002). A program for direct georeferencing of airborne and spaceborne line scanner images. In Morain, S. and Budge, A., editors, *Proceedings of the ISPRS Commission I Symposium: Integrating Remote Sensing at the Global, Regional and Local Scale*, volume 34, pages 148–153, Denver.

Mumby, P., Chrisholm, J., Clark, C., Hedley, J., and Jaubert, J. (2001). A bird's-eye view of the health of coral reefs. *Nature*, 413:36.

Mumby, P., Clark, C., Green, E., and Edwards, A. (1998). Benefits of water column correction and contextual editing for mapping coral reefs. *International Journal of Remote Sensing*, 19(1):203–210.

Mumby, P., Green, E., Edwards, A., and Clark, C. (1997). Measurement of seagrass standing crop using satellite and digital airborne remote sensing. *Marine Ecology-Progress Series*, 159:51–60.

Mutanga, O., Skidmore, A., and van Wieren, S. (2003). Discriminating tropical grass (*Cenchrus ciliarus*) canopies grown under different nitrogen treatments using spectroradiometry. *Photogrammetric Engineering and Remote Sensing*, 57:263–272.

Myers, M., Hardy, J., Mazel, C., and Dustan, P. (1999). Optical spectra and pigmentation of Caribbean reef corals and macroalgae. *Coral Reefs*, 18:179–186.

Nielsen, S. and Sand-Jensen, K. (1991). Variation in growth rates of submerged rooted macrophytes. *Aquatic Botany*, 39:109–120.

Norris, J., Wyllie-Echeverria, S., Mumford, T., Bailey, A., and Turner, T. (1997). Estimating basal area coverage of subtidal seagrass beds using underwater videography. *Aquatic Botany*, 58:269–286.

Nusch, E. (1980). Comparison of different methods for chlorophyll and phaeopigment determination. In *Archiv für Hydrobiologie, Special issues: Advances in Limnology*, volume 14, pages 14–36.

O'Haver, T. and Green, G. (1976). Numerical error analysis of derivative spectrometry for the quantitative analysis of mixtures. *Analytical Chemistry*, 48(2):312.

Ostendorp, W. (2004). New approach to integrated quality assessment of lakeshores. *Limnologica*, 34(1-2):160–166.

Pasqualini, V., Pergent-Martini, C., and Fernandez, C. (1997). The use of airborne remote sensing for benthic cartography: advantages and reliability. *International Journal of Remote Sensing*, 18(5):1167–1177.

Penuelas, J., Gamon, J., Griffin, K., and Field, C. (1993). Assessing community type, plant biomass, pigment composition, and photosynthetic efficiency of aquatic vegetation from spectral reflectance. *Remote Sensing of Environment*, 46(2):110–118.

Peters, K. (2006). Welche Anpassungen zeigen Characeen an Salz- und Lichtstress. Diplomarbeit, Wissenschaftszentrum Weihenstephan für Ernährung, Landnutzung und Umwelt, Department für Ökologie, Fachbereich für Biologie, Technische Universität München.

Philpot, W. (1987). Radiative transfer in stratified waters: a single-scattering approximation for irradiance. *Applied Optics*, 26(19):4123–4132.

Picchiotti, A., Casacchia, R., and Salvatori, R. (1997). Multitemporal Principal Component Analysis of spectral and spatial features of the Venice Lagoon. *International Journal of Remote Sensing*, 18(1):183–196.

Pilon, J. and Santamaría, L. (2002). Clonal variation in the thermal response of the submerged aquatic macrophyte *Potamogeton pectinatus*. *Journal of Ecology*, 90:141–152.

Pinnel, N., Heege, T., and Zimmermann, S. (2004). Spectral discrimination of submerged macrophytes in lakes using hyperspectral remote sensing data. In *Ocean Optics XVII*, page 11, Fremantle, West Australia.

Pope, R. and Fry, E. (1997). Absorption spectrum (380-700 nm) of pure water. II. Integrating cavity measurements. *Applied Optics*, 36(33):8710–8723.

Prieur, L. and Sathyendranath, S. (1981). An optical classification of coastal and oceanic waters based on the spectral absorption curves of phytoplankton pigments, dissolved organic matter and other particulate materials. *Limnology and Oceanography*, 26(4):671–689.

Procter, A. and Sherwood, M. (1982). Data analysis techniques in X-ray photoelectron spectroscopy. *Analytical Chemistry*, 54:13–19.

R Development Core Team (2005). *R: A language and environment for statistical computing.* R Foundation for Statistical Computing, Vienna, Austria.

Raitala, J. and Lampinen, J. (1985). A Landsat study of the aquatic vegetation of the Lake Luodonjarvi Reservoir, Western Finland. *Aquatic Botany*, 21:325–346.

Richards, J. (1993). *Remote sensing digital image analysis: An introduction.* Springer, Berlin, 2nd edition.

Richardson, L. (1996). Remote sensing of algal bloom dynamics. *Bioscience*, 46(7):492–501.

Ronzhina, D. and P'yankov (2001). Structure of the photosynthetic apparatus in leaves of freshwater hydrophytes : 1. General characteristics of the leaf mesophyll and a comparison with terrestrial plants. *Journal Russian Journal of Plant Physiology*, 48(5):567–575.

Rowan, K. (1989). *Photosynthetic pigments of algae.* Cambridge University Press, UK.

Russell, L. and Waters, D. (2002). Green algae and land plants - an answer at last? *Journal of Phycology*, 38:237–240.

Rutchey, K. and Vilchek, L. (1999). Air photointerpretation and satellite imagery analysis techniques for mapping cattail coverage in a northern Everglades impoundment. *Photogrammetric Engineering and Remote Sensing*, 65(2):185–191.

Sathyendranath, S. (2000). Remote sensing of ocean colour in coastal and other optically complex waters. Technical Report 3, International Ocean Colour Coordination Group (IOCCG).

Savitzky, A. and Golay, M. (1964). Smoothing and differentiation of data by simplified least squares procedures. *Analytical Chemistry*, 36(8):1627–1639.

Schagerl, M. and Pichler, C. (2000). Pigment composition of freshwater charophyceae. *Aquatic Botany*, 67:117–129.

Schagerl, M., Pichler, C., and Donabaum, K. (2003). Pattern of major photosynthetic pigments in freshwater algae. 2. Dinophyta, Euglenophyta, Chlorophyceae and Charales. *Annales de Limnologie*, 39(1):49–62.

Schaumburg, J. (1996). *Seen in Bayern*. Number 1/96. Bayrisches Landesamt für Wasserwirtschaft.

Schaumburg, J. (2004). Macrophytes and phytobenthos as indicators of ecological status in German lakes - a contribution to the implementation of the Water Framework Directive. *Limnologica*, 34:302–314.

Schiller, H. and Doerffer, R. (1999). Neural network for emulation of an inverse model - operational derivation of case2 water properties from MERIS data. *International Journal of Remote Sensing*, 20:1735–1746.

Schmidt, K. and Skidmore, A. (2003). Spectral discrimination of vegetation types in a coastal wetland. *Remote Sensing of Environment*, 85:92–108.

Schmieder, K. (2004). European lake shores in danger - Concepts for sustainable development. *Limnologica*, 34(1-2):3–14.

Schneider, S. (2000). *Entwicklung eines Macrophytenindex zur Trophieindikation in Fliessgewässern*. PhD Thesis, Institut für Landespflege und Botanik, Technische Universität München.

Schneider, S. (2004). *Indikatoreigenschaften und Ökologie aquatischer Makrophyten in stehenden und fliessenden Gewässern*. Habil Thesis, Wissenschaftszentrum Weihenstephan für Ernährung, Landnutzung und Umwelt, Department für Ökologie, Fachgebiet für Limnologie, Technische Universität München.

Schneider, S. and Melzer, A. (2003). The trophic index of macrophytes (TIM) a new tool for indicating the trophic state of running waters. *International Review of Hydrobiology*, 88(1):49–67.

Schneider, S. and Melzer, A. (2004). Sediment and water nutrient characteristics in patches of submerged macrophytes in running waters. *Hydrobiologia*, 527:195–207.

Schneider, S., Ziegler, C., and Melzer, A. (2006). Growth towards light as an adaptation to high light conditions in *Chara* branches. *New Phytologist*, 172:83–91.

Smith, R. and Baker, K. (1981). Optical properties of the clearest natural waters (200-800 nm). *Applied Optics*, 20(2):177–184.

Stelzer, D. (2003). *Makrophyten als Bioindikatoren zur leitbildbezogenen Seenbewertung - Ein Beitrag zur Umsetzung der Wasserrahmenrichtlinie in Deutschland*. PhD Thesis, Wissenschaftszentrum Weihenstephan für Ernährung, Landnutzung und Umwelt, Department für Ökologie, Fachgebiet für Limnologie, Technische Universität München.

Stelzer, D., Schneider, S., and Melzer, A. (2005). Macrophyte-based assessment of lakes - a contribution to the implementation of the European Water Framework Directive in Germany. *International Review of Hydrobiology*, 90(2):223–237.

Stephens, C., Louchard, E., Reid, P., and Maffione, R. (2003). Effects of micoralgal communities on reflectance spectra of carbonate sediments in subtidal optically shallow marine environments. *Limnology and Oceanography, Light in shallow water*, 48(1, part 2):535–546.

Tilzer, M. (1983). The importance of fractional light absorption by photosynthetic pigments for phytoplankton productivity in Lake Constance. *Limnology and Oceanography*, 28:833–846.

Trevino, V. and Falciani, F. (2006). GALGO: An R package for multivariate variable selection using genetic algorithms. *Bioinformatics Advance Access*.

Tsai, F. and Philpot, W. (1998). Derivative analysis of hyperspectral data. *Remote Sensing of Environment*, 66:41–51.

Vaiphasa, C., Ongsomwang, S., Vaiphasa, T., and Skidmore, A. (2005). Tropical mangrove species discrimination using hyperspectral data: A laboratory study. *Estuarine, Coastal and Shelf Science*, 65:371–379.

Valley, K., Drake, M., and Anderson, C. (2005). Evaluation of alternative interpolation techniques for the mapping of remotely-sensed submerged vegetation abundance. *Aquatic Botany*, 81:12–25.

Valta-Hulkkonen, K., Pellikka, P., Tanskanen, H., Ustinov, A., and Sandman, O. (2003). Digital false colour aerial photographs for discrimination of aquatic macrophyte species. *Aquatic Botany*, 75:71–88.

Van der Piepen, H., Doerffer, R., and Gierloff-Emden, H. (1987). Kartierung von Substanzen im Meer mit Flugzeugen und Satelliten. In *Münchner Geographische Abhandlungen*, volume A 37. Institut für Geographie der Universität München.

van Dijk, G. and van Vierssen, W. (1991). Survival of a *Potamogeton pectinatus* L. population under various light conditions in a shallow eutrophic lake (Lake Veluwe) in The Netherlands. *Aquatic Botany*, 39:121–129.

Vane, G., Duval, J., and Wellman, J. (1993). *Remote geochemical analyses: Elemental and mineralogical composition*, chapter Imaging spectroscopy of the earth and other solar system bodies, pages 121–144. Cambridge University Press, UK.

Venables, W. and Ripley, B. (2002). *Modern Applied Statistics with S. Fourth Edition.* Springer, New York.

Venanzi, G., Pasqualini, S., Pocceschi, N., and Antonielli, M. (1988). Comparison of some photosynthetic characteristics during the growth of three aquatic macrophytes in Transimeno Lake. *Riv. Idrobiol.*, 27(1):59–71.

Verhoef, W. and Bach, H. (2003). Simulation of hyperspectral and directional radiance images using coupled biophysical and atmospheric radiative transfer models. *Remote Sensing of Environment*, 87(1):23–41.

Vestergaard, G. and Sand-Jensen, K. (2000). Aquatic macrophyte richness in Danish lakes in relation to alkalinity, transparency, and lake area. *Canadian Journal of Fisheries and Aquatic Sciences*, 57:2022–2031.

Vis, C., Hudon, C., and Carignan, R. (2003). An evaluation of approach used to determine the distribution and biomass of emergent and submerged aquatic macrophytes over large spatial scales. *Aquatic Botany*, 77:187–201.

von Grafenstein, U., Erlenkeuser, H., Müller, J., and Kleinmann-Eisenmann, A. (1992). Oxygen isotope resords of benthic ostracods in bavarian lake sediments. *Naturwissenschaften*, 79:145–152.

Voss, K., Mobley, C., Sundman, L., Ivey, J., and Mazel, C. (2003). The spectral upwelling radiance distribution in optically shallow waters. *Limnology and Oceanography, Light in shallow water*, 48(1, part 2):364–373.

Walker, R. (1994). *Marine light field statistics*. Wiley series in pure and applied optics. Wiley, New York.

Werdell, P. and Roesler, C. (2003). Remote assessment of benthic substrate composition in shallow waters using multispectral reflectance. *Limnology and Oceanography, Light in shallow water*, 48(1, part 2):557–567.

Wettle, M., Phinn, S., Dekker, A., Brando, V., Clementson, L., Roelfsema, C., and Oubelkheir, K. (2004). Deriving bleached coral substrate maps from space-borne hyperspectral data. In *Ocean Optics XVII*, page 14, Fremantle, West Australia.

Wetzel, R. (2001). *Limnology - Lake and River Ecosystems*. Academic Press, New York, USA, 3rd edition.

Wiegleb, G. and Brux, H. (1991). Comparison of life history characters of broad-leaved species of the genus *Potamogeton* L. I. general characterization of morphology and reproductive strategies. *Aquatic Botany*, 39:131–146.

Williams, D., Rybicki, N., Lombana, A., O'Brien, T., and Gomez, R. (2003). Preliminary investigation of submerged aquatic vegetation mapping using hyperspectral remote sensing. *Environmental Monitoring and Assessment*, 81:383–392.

Wittlinger, S. and Zimmermann, R. (2000). Hyperspectral remote sensing of subtidal macroalgal assemblages in optically shallow waters. In Ackleson, S., editor, *Ocean Optics XV*, page 6, Monaco.

Woithon, A., Heege, T., and Schmieder, K. (2005). Entwicklung von automatisierbaren Fernerkundungsverfahren zur effektiven Unterstützung von Planungsprozessen in der Uferzone von Seen - EFPLUS. Forschungsbericht FZKA-BWPLUS, Institut für Landschafts-und Pflanzenökologie, Universität Hohenheim.

Wolter, P., Johnston, C., and Niemi, G. (2005). Mapping submerged aquatic vegetation in the US Great Lakes using Quickbird satellite data. *International Journal of Remote Sensing*, 26(23):5255–5274.

Yu, B., Ostland, M., Gong, P., and Pu, R. (1999). Penalized discriminant analysis of *in situ* hyperspectral data for conifer species recognition. *IEEE Transaction on Geoscience and Remote Sensing*, 37(5):2569–2577.

Zhang, X. (1998). On the estimation of biomass of submerged vegetation using Landsat thematic mapper (TM) imagery: a case study of the Honghu Lake, PR China. *International Journal of Remote Sensing*, 19(1):11–20.

Ziegler, C. (2005). Einfluss der Lichtintensität auf die Morphologie und das Reflexionsspektrum von Characeen. Diplomarbeit, Fachbereich Umweltschutz, Fachhochschule Bingen.

Acknowledgements

Curriculum Vitae

Nicole Pinnel

Date of birth   16.07.1974, Dachau, Germany

education

1981-1985	Primary school in Weichs
1986-1994	Abitur (High school intrance qualification),
	Städt. Luisengymnasium in Munich
1995-1996	Study in social geography at the Technical University of Munich
1996-2002	Study in physical geography, geology and remote sensing
	at the Ludwig-Maximilians-University of Munich
	Thesis:'Seagrass mapping in coastal shallow waters
	using hyperspectral remote sensing data from CASI'
2003	Scientific diver certification
2002-2006	PhD thesis at the Limnological Institute
	of Technical University of Munich

job experience

1999	Practical training at German Aerospace Center (DLR),
	Institute of Optoelectronic, Oberpfaffenhofen, Germany
2000-2001	Practical training and Diploma thesis at CSIRO, Land and Water,
	Remote sensing research group, Canberra, Australia
2001-2002	Research assistant at CSIRO, Land and Water,
	Remote sensing research group, Canberra, Australia